PhD thesis

Multifunctional Layered Double Hydroxide (LDH) Based Epoxy Nanocomposites

Author:

Ehsan Naderi Kalali

Supervisor:

Prof. Dr. De-Yi Wang

A dissertation submitted for the degree of Doctor of Philosophy at the

Department of Materials Science and Engineering and Chemical

Engineering

Universidad Carlos III de Madrid

Leganés, September 2015

TESIS DOCTORAL

Multifunctional Layered Double Hydroxide (LDH) Based Epoxy Nanocomposites

Autor: **Ehsan Naderi Kalali**

Directores: **Prof. Dr. DeYi Wang**

Firma del Tribunal Calificador:

Firma

Presidente: Prof. Juan Baselga Llido

Vocal: Dr. Santiago Gomes Ruiz

Secretario: Dr. ……

Calificación:

Leganés ….. de ………. de 2015

"Science is based on experiment; on a willingness to challenge old dogma; on an openness to see the universe as it really is. Accordingly, science sometimes requires courage - at the very least the courage to question the conventional wisdom"

Carl Sagan

List of schemes

List of figures

treatment on a reduced graphene oxide contaminated with KOH salts (1 wt%).

List of tables

List of abbreviations

°C: Centigrade degree

APP: Ammonium polyphosphate

ASTM: American Society for Testing and Materials

ATH: Aluminium hydroxide

ATR: Attenuated total reflection

BA: Boric acid

BET: Brunauer-Emmett-Teller

BO: Boric oxide

BJH: Barrett-Joyner-Halenda

BP: Boron phosphate

C: Colemanite

CCT: Cone calorimeter test

CD: Cyclodextrin

CD: β-cyclodextrin

CDBS: β- cyclodextrin butane sultone

CGT'ase: Cyclodextrin gluconotransferase

c-LDH: Calcinated layered double hydroxide

CNT: Carbon nanotube

CNT-PR: Functionalized MWCNTs

CoAl LDH: Cobalt aluminum layered double hydroxide

Cp: Specific heat

DBS: Dodecylbenzenesulfonate

DDS: Diamino diphenyl sulfone

DGEBA: Diglycidyl ether of bisphenol A

DIC: Digital image correlation

DMA: Dynamic mechanical analysis

DOPO: 9,10-dihydro-9-oxa-10-phosphaphenanthrene 10-oxide

DPPES: 2-(diphenylphosphino) ethyltriethoxy silane

EDX: Energy-dispersive X-ray spectroscopy

EP: Epoxy resin

EVA: Ethylene vinylacetate

fCD: Functionalized sCD

Fe_3O_4: Iron III oxide

$FeCl_2$: Iron II chloride

$FeCl_3$: Iron III chloride

FIGRA: Fire growth rate indexFTIR: Fourier transform infrared spectroscopy

GB: Guanidinium nonaborate

GO: Graphene oxide

HCl: Hydrochloric acid

HP-β-CD: Hydroxypropyl-β- cyclodextrin

HRR: Heat release rate

ISO: International Organization for Standardization

kV: kilo volt

LDH: Layered double hydroxide

LOI: Limiting oxygen index

MB: Melamine borate

MDH: Magnesium hydroxide

Mel: Melamine

Mg-Al–LDH: Magnesium-aluminum- layered double hydroxide

mm: Millimeter

MMT: Montmorillonite

Mo-PR: Molybdenum-phenolic resin

m-SiO$_2$:

MWNT: Multiwalled carbon nanotubes

N: Normal

N$_2$: Nitrogen

nm: Nano meter

NO$_3$-LDH: Un-modified layered double hydroxide

OapPOSS: Octa(aminophenyl)-silsesquioxane

OMMT: Organo-modified montmorillonite

PER: Pentaerythritol

Ph: Phytic acid

pHRR: Peak of heat release rate

PMLR: Peak mass loss rate

PMMA: Poly(methyl methacrylate)

POSS: Polyhedral oligomeric silsesquioxanes

PP: Polypropylene

PPA: Polyphosphamide

PS: Polystyrene

RoHS : Restriction of Hazardous Substances Directive

RP: Red phosphorus

SAED: Selected area electron diffraction

sCD: Hydroxypropyl-sulfobutyl-beta-cyclodextrin

sCD: Hydroxypropyl-sulfobutyl-beta-cyclodextrin

SDBS: Sodium dodecylbenzenesulfonate

SEM: Scanning electron microscopy

SWNT: Single-walled carbon nanotubes

T: Taurine

$T_{5\%}$: The temperature at which the mass loss is 5%

TED: Transmission Electron Diffraction

TEM: Transmission electron microscopy

T_g: Glass transition temperature

TGA: Thermogravimetric analysis

TGPSO: Triglycidyl phenyl silane oxide

THE: Total heat evolved

THR: Total heat release

T_{max}: Tthe temperature at which the maximum mass loss rate occurs

TSP: Total smoke production

TTI: Time-to-ignition

U: Ulexite

UL-94: Standard for Safety of Flammability of Plastic Materials for Parts in Devices and Appliances testing

UV: Ultraviolet

V-0: Burning stops within 10 seconds on a vertical specimen; drips of particles allowed as long as they are not inflamed.

V-2: Burning stops within 30 seconds on a vertical specimen; drips of flaming particles are allowed.

VTES: Vinyltriethoxysilane

WAXS: Wide angle X-ray scattering

WEEE: Waste Electrical and Electronic Equipment

wt: Weight percent

XRD: X-ray diffraction

ZnB: Zinc borate

α- CD: α- cyclodextrin

β- CD: β- cyclodextrin

γ-CD: γ-cyclodextrin

Abstract

As one of the most important thermosetting polymers, epoxy resin (EP) has acquired wide application in the fields of coating, adhesive, electronic/electrical insulation, carbon fiber composites and etc. EP possesses many outstanding advantages, such as low shrinkage, high thermal and mechanical stabilities and excellent solvent and chemical resistance. However, like most of polymeric materials, high flammability of EP is its main fatal drawback, which has severely restricted the application fields required a remarkable flame-retardant standards. Thus, the flame retardancy of epoxy resins continues to remain as a very important area of research for polymer chemists and material engineers. Such research is also highly encouraged by the polymer industries because of huge economic and sociological casualties involved each year in fire accidents. Among the various methods of improving flame retardancy of polymeric materials, incorporation of flame retardants is a very commonly used one.

The present work and the relevant reporting involve the investigation of a relatively new fascinating nano-filler, known as layered double hydroxide (LDH) as potential flame retardant for polymers composites. The basic reason for selecting LDH or more specifically magnesium-aluminum based LDH (Mg-Al–LDH) is their typical metal hydroxide-like chemistry and conventional clay-like layered crystalline structure.

The current desertation containing:

- Functionalization of LDH;

  Multi-modifiers' systems composed by bio-based modifiers such as

hydroxypropyl-sulfobutyl-beta-cyclodextrin sodium (sCD) and its hybridized form with chalcone species (fCD), taurine (T), phytic acid (Ph), and dodecylbenzenesulfonate (DBS) were fabricated in this thesis, each designed for specified feature, aiming at developing high performance fire retardant epoxy nanocomposites.

- Preparation and characterization of functionalized LDH based epoxy nanocomposites;

Based on these functionalized LDHs, bisphenol A epoxy resin and diamino diphenyl sulfone (DDS), and utilizing multi step mixing method followed by appropriate curing process, series functionalized LDH/Epoxy nanocomposites have been developed.

- Structural Properties relationship;

The structural morphology of LDH/epoxy nanocomposites was investigated by transmission electron microscopy (TEM) and wide-angle X-ray scattering (WAXS), revealing that multi-modified LDH based epoxy nanocomposites showed much better dispersion state than the epoxy composites containing un-modified LDH or single modifier modified LDH. In contrast to conventional LDHs based epoxy composites, the functionalized LDH based epoxy nanocomposites show significantly improvement on both flame retardancy, such as passing UL94 V0 rating and significant reduction of peak of heat release rate, total heat release, total smoke, etc. and well maintenance

on impact, flexural, micro-mechanical and anti-UV properties. Such multifunctional nano-hybrid will provide a promising solution to develop various functional epoxy-based composites for advanced applications.

Resumen

Como uno de los polímeros termoestables más importantes, resina epoxi (EP) ha adquirido una amplia aplicación en los campos de recubrimiento, adhesivos, aislamiento eléctrico / electrónico, materiales compuestos de fibra de carbono y etc. EP posee muchas ventajas excepcionales, tales como baja contracción, alta térmica y estabilidades mecánicas y excelente disolvente y resistencia química. Sin embargo, como la mayoría de los materiales poliméricos, alta inflamabilidad de EP es su principal inconveniente fatal, que ha restringido severamente la aplicación campos requieren un notable estándares ignífugos. Por lo tanto, la resistencia a la llama de resinas epoxi sigue siendo como un área muy importante de la investigación para los químicos de polímeros e ingenieros de materiales. Este tipo de investigación es también muy animado por las industrias de polímeros debido a enormes bajas económicas y sociológicas que participan cada año en accidentes de fuego. Entre los diversos métodos para mejorar llama retardancia de materiales poliméricos, la incorporación de los retardantes de la llama es muy comúnmente usada.

El presente trabajo y el informe correspondiente implican la investigación de un nuevo y fascinante nano-relleno relativamente, conocido como de doble capa de hidróxido (LDH) como potencial retardante de llama para polímeros compuestos. La razón básica para la selección de LDH o LDH más basada en específicamente de magnesio-aluminio (Mg-Al-LDH) es su química típica hidróxido como el metal y la estructura cristalina capas similar a la arcilla convencional.

El desertation actual que contiene:

• La funcionalización de la LDH;

Los sistemas Multi-modificadores 'compuestas por modificadores de origen biológico, tales como hidroxipropil-sulfobutil-beta-ciclodextrina de sodio (SCD) y su forma hibridado con especies chalcona (FCD), taurina (T), el ácido fítico (Ph) y dodecilbencenosulfonato (DBS) fueron fabricados en esta tesis, cada uno diseñado para la función especificada, con el objetivo de desarrollar de alto rendimiento nanocompuestos epoxi retardante de fuego.

• Preparación y caracterización de nanocompuestos epoxi funcionalizados LDH basada;

En base a estos LDHs funcionalizados, sulfona de bisfenol A resina epoxi y diamino difenil (DDS), y utilizando el método de mezclado de múltiples fases seguido por el proceso de curado apropiado, se han desarrollado series funcionalizado nanocompuestos LDH / epoxi.

• Relación Propiedades Estructurales;

La morfología estructural de nanocompuestos de LDH / epoxi se investigó por microscopía electrónica de transmisión (TEM) y de amplio ángulo de dispersión de rayos X (WAXS), revelando que LDH basado nanocompuestos epoxi multi-modificado mostraron mucho mejor estado de dispersión de los materiales compuestos epoxi que contienen ONU LDH modificado o solo LDH modificado

modificador. En contraste con los materiales compuestos epoxi basadas LDHs convencionales, los nanocompuestos de LDH epoxi basada funcionalizados muestran una mejora significativa tanto en resistencia a la llama, tales como pasar calificación V0 UL94 y una reducción significativa del pico de la tasa de liberación de calor, la liberación total de calor, el humo total, etc. y bien el mantenimiento de las propiedades de impacto, flexión, micro-mecánicos y anti-UV. Tal multifuncional nano-híbrido proporcionará una solución prometedora para desarrollar diversos materiales compuestos a base de epoxi funcionales para aplicaciones avanzadas.

Preface

This dissertation is submitted for the degree of Doctor of Philosophy in the Carlos III University of Madrid. The research described in this thesis was carried out at IMDEA Materials Institute (Madrid, Spain) during the period September 2012 to November 2015 under the supervision of Prof. Dr. DeYi Wang, senior researcher at IMDEA Materials Institute and adjunct professors at the Carlos III University of Madrid.

The results obtained during the course of this thesis have been published in peer-reviewed international journals in Materials Science and chemistry, including Material Chemistry A, etc. Moreover, this work has been well received at international conferences and workshops on Euromat 2013 as well as COST Action programs.

To the best of my knowledge, the work described in this dissertation is original, except where due reference has been made to the work of others, and nothing is included which is the outcome of work done in collaboration, unless otherwise stated. No part of this dissertation, or any similar to it, has been, or is currently being, submitted for any degree or other qualification at any other university.

Ehsan Naderi Kalali

Madrid

November 2015

Acknowledgment

I would also like to thank a number of people for their help and support during this PhD. Firstly, I wish to thank my supervisor, Prof. Dr DeYi Wang, for his expert guidance, assistance and patience in all aspects of this research. His impressments for doing and communicating research of quality have been inspirational. His scientific guidance and consideration was not limited to my PhD work but also touched other aspects of my life. I acknowledge Dr. Xin Wang and Dr. Nianjun Kang for tutoring my learning of synthesizing, processing and characterization techniques, respectively.

I would like to thank all the members (past and present) of IMDEA Materials Institute for creating a very pleasant working environment. The friendly supportive atmosphere inherent to the whole institute contributed to the final outcome of my studies during the working hours at the institute. To all of them, I am truly grateful.

I greatly acknowledge all of my friends for their helpful assistance during this time.

My deep and humble appreciation goes to my family, in particular my parents, Manijeh and Parviz and specially my brother Behnam for their unconditional love, encouragement and companionship. And finally, I owe my deepest gratitude to Marjan, that her companionship, understanding, solidarity, and patience were driving forces that kept me going in difficult moments. This thesis is dedicated to her with

deep love.

Table of contents

1   Introduction

1.1. Background: Nanotechnology in flame retardant polymeric materials

In the past few decades, nanotechnology has attracted considerable attention in the development of polymer-based nanocomposites. Polymer-based nanocomposites, with the nano-scale filler (< 100 nm) at relatively low fraction (< 10 wt%), have showed the great potential to match or exceed the mechanical, thermal, flame retardant performance of conventional composite [1]. However, enhancement efficiency depends strongly on the dispersion state of the nano-filler and the interfacial interaction between the filler and the matrix. In terms of maximal enhancement, homogeneous dispersion of the nano-fillers and strong interaction at the interface are favourable. At present, although nanocomposites employing various nano-scale fillers have been widely investigated, the intrinsic bundling of these nano-fillers via Van Der Waals force still is a major challenge that hampers the development of polymer/inorganic nanocomposites. Therefore, in order to improve the dispersion state of the nano-filler in polymer matrix, modification on the nano-filler is necessary.

In recent years, layered double hydroxides (LDHs), as a new fascinating nano-filler, have been widely investigated in polymer composites [2,3,4,5]. As is well known, the layered structure of LDHs can be used as a versatile intercalation host which can accommodate a wide variety of organic guest species. Table 1-1 summarizes organic anions that have been already used as flame retardants. The incorporation of organic anions can enlarge the spacing distance of LDHs that is beneficial to their uniform dispersion within polymer matrices, and thus leads to better fire retardant

performance than the un-modified ones.

Table 1-1: Summary of organic anion modified LDHs added to polymers and their flame retardant performance

Type of LDH	Organic anions	Polymer	Reduction in PHRR	Loading (%)	Reference
MgAl	Oleate	EVA	36%	10 wt%	[6]
ZnAl	Oleate	PP	25%	4 wt%	[7]
ZnAl	Undecenoate	PMMA	46%	10 wt%	[8]
MgAl	DPHPA	PMMA	35%	5 wt%	[9]
MgAl	DBS	PMMA	45%	10 wt%	[10]
MgAl	HDEHP	PS	33%	10 wt%	[10]

Note: DPHPA: N-(2-(5,5-dimethyl-1,3,2-dioxaphosphinyl-2-ylamino)-N-hexyl)formamide-2-propenyl acid; DBS: dodecyl benzene sulfonate; HDEHP: bis(2-ethylhexyl) phosphate.

Therefore, modification of LDHs is a key factor to obtain high performance polymer composites.

1.2 Motivation for the development of Multifunctional Layered Double Hydroxide (LDH) Based Epoxy Nanocomposites

Although LDH-based epoxy nanocomposites have attracted considerable interests in the past few decades, the uniform dispersion of the LDHs within epoxy matrices still is a major challenge that hampers the development of epoxy nanocomposites. Modification of LDHs is one of most common used methods to improve the dispersion state of LDHs within polymer matrices. Currently, most of cases of

modification of LDHs involve the single modifier. However, the dispersion of modified LDHs is still not satisfactory to obtain functionalized LDH-based polymer nanocomposites with enhanced fire resistance and mechanical properties simultaneously up to date. Therefore, novel functionalization of LDHs needs to be developed in order to obtain high performance polymer nanocomposites.

1.3 Objective of the study

Based on the discussion above, the main objective of this study is to exploit multi-modified system for LDHs and their multi-functional polymer nanocomposites. This study is focused on epoxy resins. Epoxy resins are widely applied in the fields of composites, electric and electronics, automotives, marine and civil engineering, due to many outstanding advantages, such as low shrinkage, high thermal and mechanical stabilities and excellent solvent and chemical resistance.

In order to endow epoxy resins with multi-functionality, multi-modifiers' system will be selected. Each component in the multi-modifiers' system possesses its own specialty:

- the best environmentally friendly flame retardants are derived from natural resources, such as cyclodextrin and phytic acid

- sodium dodecylbenzenesulfonate for facilitating LDH's dispersion in epoxy matrix

- taurine enhances the mechanical properties of the final product

- chalcone imparts the anti-UV property to epoxy matrix

- and metal oxide nanoparticles can improve the thermal resistance of the char.

The relationship between the structure and behaviors will be explored based on the experimental data, and provide the fundamental for the design of multi-functional epoxy nanocomposites in future.

1.4 Outline of the thesis

The dissertation is divided into seven core chapters regarding the preparation, properties and mechanism of multifunctional layered double hydroxide (LDH)-based fire retardant epoxy nanocomposites. Chapter 2 reviews the current progress of layered double hydroxide (LDH)-based fire retardant epoxy nanocomposites. The composition, preparation method and characterization of modifiers and functionalized LDHs discussed in chapter 3.

Chapter 4, 5 and 6 are representing the preparation method and characterization techniques and final results of the epoxy nanocomposites. Finally, the recommendation for the future work, list of publications and references explained in Chapter 7, 8 and 9.

2 State of the art

2.1. Epoxy resin

As an outstanding representative of thermosetting polymer, epoxy resin (EP) has been widely used in the fields of coating, adhesive, electronic/electrical insulation, laminates and composites [11,12,13]. EP possesses many fascinating advantages, such as low shrinkage, high thermal and mechanical stabilities and excellent solvent and chemical resistance [14,15]. In these application fields, safety requirements are currently becoming more and more serious in terms of the fire resistant performances. However, like most of polymeric materials, EP has a major drawback of high flammability, which has severely restricted the application fields. Therefore, to improve the fire resistance of EP has motivated many researchers' interests in the world wide range.

2.2. Thermal degradation of epoxy resin

The organic matrix of the cured epoxy resin decomposes releasing heat, smoke, toxic volatiles and soot when exposed to high temperatures (300–400 °C) [16]. Generally, four different reactions occurred in the condensed phase during the polymer combustion. Random-chain scissions or end-chain scissions are the main reactions that are able to generate radical species. Meanwhile, other functional groups or atoms that are not a part of the polymer backbone can be lock out which is known as chain stripping.

Cross-linking of the different radicals is the last predominant reaction which occurs

during the scissioning of the polymer chains to generate new thermally stable
polymers or char residue.
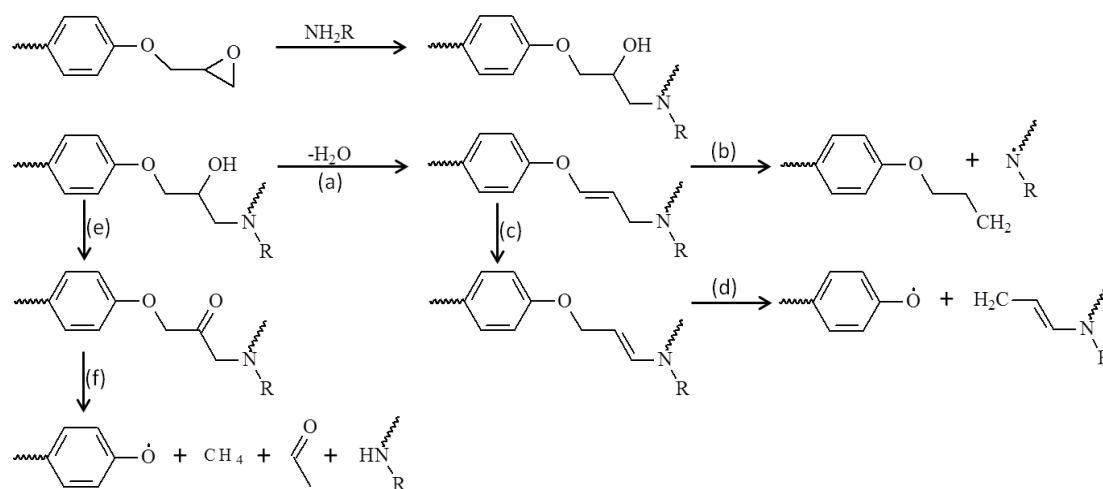
Figure 2-1: Thermal degradation paths of an amine cured epoxy resin.

The first step of thermal decomposition of the epoxy resins is the dehydration or
dehydrogenation of the secondary alcohol which is forming during the cross-linking
reaction resulted in generation of the allylic amides (Figure 2-1, a) [17]. Isomerisation
can occur for the unsaturated section (c) followed by bond scission of allylic-oxygen
groups (d) [18]. On the other hand, the weak C-N bond which is formed during the
curing will then undergo allylic-nitrogen bond scission (b) in order to generate
volatile particles or contribute to charring [19].

2.3. Flame retardants for epoxy resin

Currently, there are several kinds of predominant flame retardants for epoxy resins, as
shown in Figure 2-2. These flame retardants are mainly divided into four species:

- Halogenated flame retardants, including chlorinated and brominated compounds;

- Non-halogenated flame retardants, including phosphorus-, silicon-, nitrogen-, and

boron-containing compounds;

- Metal hydroxides, including aluminum hydroxide and magnesium hydroxide;

- Nano-scale flame retardants, including polyhedral oligomeric silsesquioxanes (POSS), carbon nanotube (CNT), graphene, layered double hydroxide (LDH), montmorillonite (MMT), etc.

Figure 2-2: Market shares of different flame retardants for EE applications (2007) [19].

2.3.1. Halogenated flame retardants

Halogenated flame retardants have been widely used in epoxy resins and now still represent a large portion of the flame retardants market for electronic/electrical applications. Halogenated flame retardants are famous for their high flame retardant efficiency due to their action in the gas phase by inhibiting the exothermic oxidation reaction in the flame through radical scavenging, and thus decreasing the energy feedback to the polymer matrix. Figure 2-3 illustrates how halogenated flame retardants act via radical scavenging [20].

$$X^{\cdot} + RH \longrightarrow HX + R^{\cdot}$$
$$H^{\cdot} + HX \longrightarrow H_2 + X^{\cdot}$$
$$HO^{\cdot} + RH \longrightarrow H_2O + X^{\cdot}$$
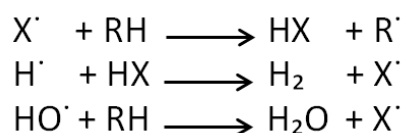
Figure 2-3: Gas phase reaction of halogenated flame retardants (X = Cl, Br).

Despite their benefits of reducing the flame spread or extinguishing the fire growth, halogenated flame retardants can also decompose to toxic gases during a fire scenario (such as hydrogen halogen) [21]. Particularly, halogenated flame retardants themselves are often toxic or even carcinogenic.
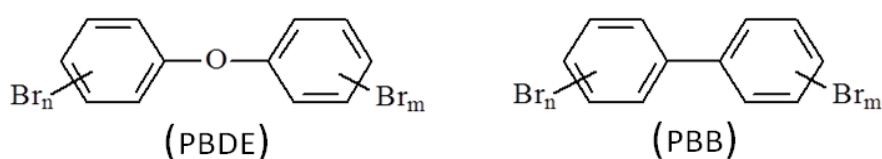
PentaBDE	n+m=5
OctaBDE	n+m=8
DecaBDE	n+m=1

Figure 2-4: Chemical structures of some halogenated flame retardants.

Their environmental impact and bio-accumulate properties have attracted more concerns. Due to the last mentioned doubts, PentaBDE and OctaBDE (polybrominated diphenylether, Figure 2-4) were banned production in North America and Europe by 2004 [22,23]. Polybrominated diphenylether (PBDE) and polybrominated biphenyl (PBB) (Figure 2-4) were also prohibited as flame retardants under EU´s RoHS and WEEE for the use in electronic/electrical application. Therefore, there is an inevitable trend to develop alternative flame retardants without health and environmental concerns.

2.3.2. Metal hydroxides

Metal hydroxide is one of the most commonly used halogen-free flame retardants for EPs. Metal hydroxides, such as magnesium hydroxide (MDH) and aluminium hydroxide (ATH), are favourable when applied as flame retardants. They are easy to obtain, very cheap and environmentally friendly.

Decomposition of the metal hydroxides led to generation of metal oxides and water, which is an endothermic reaction absorbing energy from the ignition source (see Equations 1 and 2). Meanwhile, the released water vapours can chill the surface of the polymer and dilute the flammable volatiles [24]. The residual metal oxides also form an insulative layer on the polymer surface to protect the underlying polymer from the further decomposition which is responsible for reducing the heat release rate and hence, reducing the amount of released toxic gases.

$$2\,Al(OH)_3 \rightarrow Al_2O_3\,(s) + 3H_2O\,(g) \quad \Delta H = 1.17\,^{kJ}\!/_g \quad (1)$$

$$Mg(OH)_2 \rightarrow MgO\,(s) + H_2O\,(g) \quad \Delta H = 1.36\,^{kJ}\!/_g \quad (2)$$
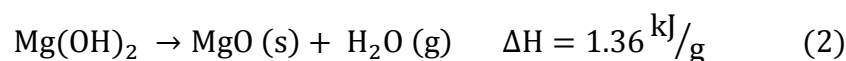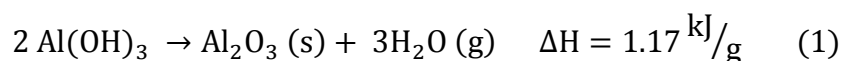
However, very high loadings are necessary to obtain satisfactory flame retardant properties (~30–60%). Such high loadings usually accompany with side-effects, such as processing difficulties and deterioration in other properties of the resultant epoxy composites.

2.3.3. Phosphorus-based flame retardants

In recent years, considerable attention has been focused on phosphorus-containing

flame retardant epoxy resins, since they are cost-efficient, non-toxic gases released and relatively low loading required. Furthermore, phosphorus compounds are available at different oxidation levels: elementary phosphorus (such as red phosphorus), inorganic or organic phosphates, phosphinates, phosphines, phosphonates or phosphites (Figure 2-5).
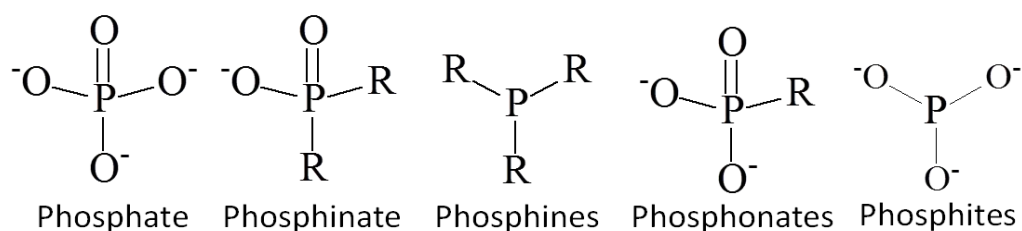
Figure 2-5: Chemical structure of different phosphorus-based compounds (R=alkyl).

Incorporation of the phosphorus-containing compounds into the polymers is generally beneficial to forming a carbonaceous barrier layer. They have the advantage of catalyzing the char formation and therefore possessing condensed-phase mechanism. Some phosphorus-containing flame retardants also contribute through a gas-phase mechanism. They can degrade during combustion of polymer and release radicals (PO• and PO_2•) which can effectively react with hydrogen radicals (H•) and hydroxyl radicals (OH•) in the flame. According to the previous report [25], phosphorus-based flame retardants are five times more efficient than brominated and ten times more efficient than chlorinated ones, respectively, at the same molar concentration. Gas-phase mechanism of the phosphorus-based flame retardants resembles to that of halogenated compounds (Figure 2-6). HPO_2• radical is the most frequently phosphorus-containing which can be involved, followed by PO•, PO_2• and HPO•.

Liu et al. [26] synthesized a new phosphorus-containing oxirane bis-glycidyl

phenylphosphate (BGPP) (Figure 2-7a), and a diamine, bis(4-aminophenyl) phenylphosphate (BAPP) (Figure 2-7b).

$$HPO_2 + H^\bullet \longrightarrow PO^\bullet + H_2O$$
$$PO^\bullet + H_2O \longrightarrow PO_2^\bullet + H_2$$
$$HPO_2 + OH\ PO^\bullet \longrightarrow PO_2^\bullet + H_2O$$
$$PO^\bullet + H^\bullet + M \longrightarrow HPO_2 + M$$
$$PO^\bullet + OH^\bullet \longrightarrow HPO_2 + M$$
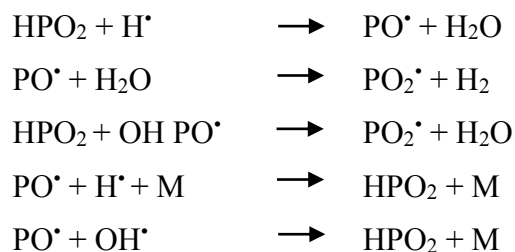
Figure 2-6: Interactions between radicals from the flame and from phosphorus-based flame retardants.

The technical literatures extensively report the use of 9,10-dihydro-9-oxa--10-phosphaphenanthrene 10-oxide (DOPO) (Figure 2-7a) as a flame retardant for epoxy resins. Owing to the rigid cyclic side-chain structure of DOPO, the resultant phosphorus-containing epoxy showed high glass-transition temperature and modulus and good thermal stability [30]. Besides the direct use of DOPO, a lot of DOPO-based derivatives have been used for flame retardant epoxy resins. For example, DOPO was reacted with quinone which leads to phosphorus-containing hydroquinone (Figure 2-7b), and this diol was used as a reactive flame retardant in combination with bisphenol A epoxy resin [27] or multifunctional novolac epoxy resin [28,29].
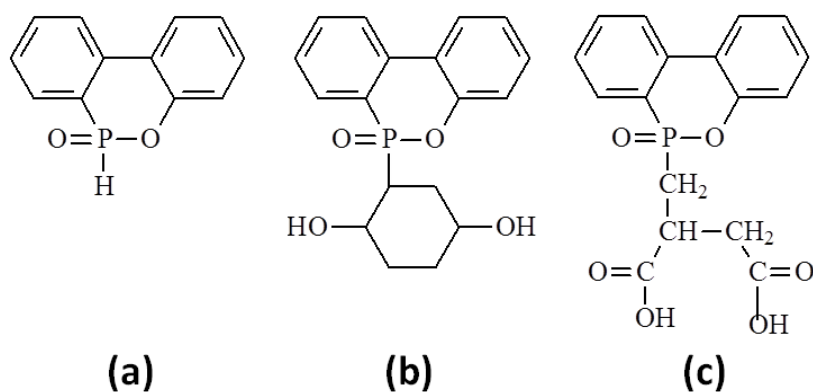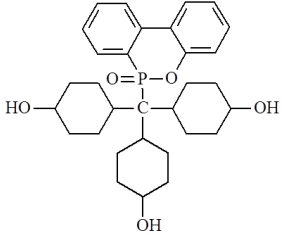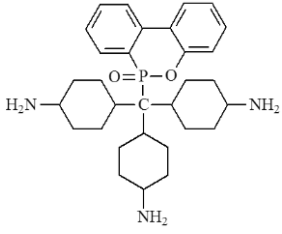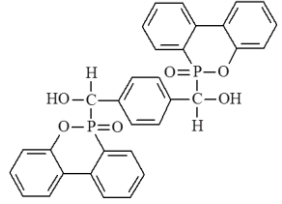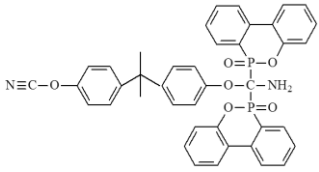
Figure 2-7: Chemical structures of DOPO and its derivatives.

Also, the commercially available condensate of itaconic acid and DOPO (Figure 2-8c) was reacted with the diglycidyl ether of bisphenol A (DGEBA) to obtain advanced epoxy resins [30]. Table 2-1 lists some DOPO-based flame retardants and their behaviors in epoxy resins. As can be seen, the DOPO-based flame retardants showed good flame retardant property, high char yield at relatively low phosphorus content (< 4 wt%).

Table 2-1: Chemical structures of some typical DOPO derivatives and behaviors of their flame retardant epoxy resins

Flame retardants	Type of epoxy	P content (wt%)	Comments	Reference
	DGEBA	1.87	UL-94 V0 rating, char yield of 27% in nitrogen	[31]
	DGEBA	1.8	UL-94 V0 rating, char yield of 25% in nitrogen	[32]
	Cresol novolac epoxy	3.8	LOI of 32.5%, char yield of 55.4% in nitrogen	[33]
	DGEBA	1.6	UL-94 V0 rating, char yield of 23% in nitrogen	[34]

Besides the flame retardant mechanism in the gas phase, the condensed phase flame retardant mechanism is the main mechanism for phosphors-based flame retardants. They were incorporated into epoxy resins via curing reaction. High char yields (32–52%) as well as high limiting oxygen index (LOI) values (34–49%) of these phosphorus-containing epoxy resins were obtained, demonstrating the usefulness of these phosphorus-containing compounds as flame retardants.
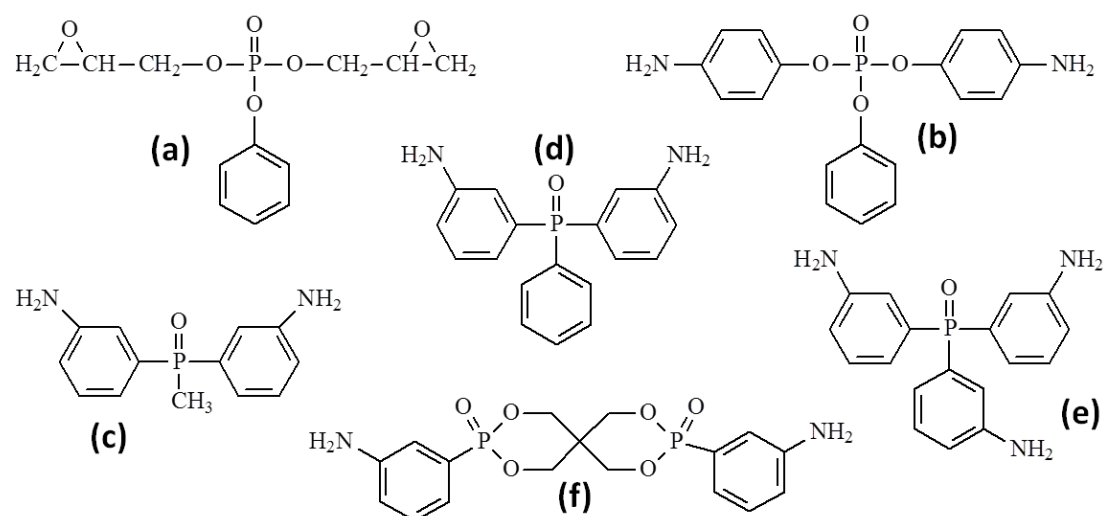
Figure 2-8: Chemical structures of several phosphorus-based flame retardants.

Additionally, bis(aminophenyl)methylphosphine oxide (Figure 2-8c) [35], bis(4-aminophenyl)phenylphosphine oxide (Figure 2-8d) [36], tris(3-aminophenyl)-phosphine oxide (Figure 2-8e) [37], and spirocyclic bisphosphonate (Figure 2-8f) [38] were also synthesized and showed good flame retardant effect in epoxy resins.

Braun and co-workers [39] investigated a comparative study of the pyrolysis of halogen-free flame-retarded epoxy resins containing phosphine oxide, phosphinate, phosphonate, and phosphate (phosphorus contents around 2.6 wt%). They found that

the thermally stable residue increased with increasing oxidation state of the phosphorus, whereas the release of phosphorus-containing volatiles reduced.

2.3.4. Nitrogen-based flame retardants

The nitrogen-based compounds have also widely utilized which is expected to impart flame retardancy to polymers. Nitrogen-rich group such as melamine can generate melam and melem via de-ammoniation reaction [40], and thereby inflammable ammonia gas degraded from melamine can dilute the flammable gas concentration. Furthermore, nitrogen also plays a significant role in enhancing char formation. Liu et al. [41] synthesized a hybrid monomer of 4-(N-maleimidophenyl)glycidylether (MPGE) with both oxirane ring and maleimide curable groups, as shown in Figure 2-9.

High LOI value of 38.0% was observed for the resins to imply their excellent flame retardant properties. The self-extinguishing behavior was also observed for the resins.

In addition to single use of nitrogen-based compounds, they are usually used in combination with phosphorus- and silicon-containing flame retardants to create synergism. Wu and co-workers prepared silicon-containing epoxy resins cured by nitrogen-based curing agents [42].Synergistic effect of nitrogen/silicon on enhancing LOI values were observed for epoxy resins.
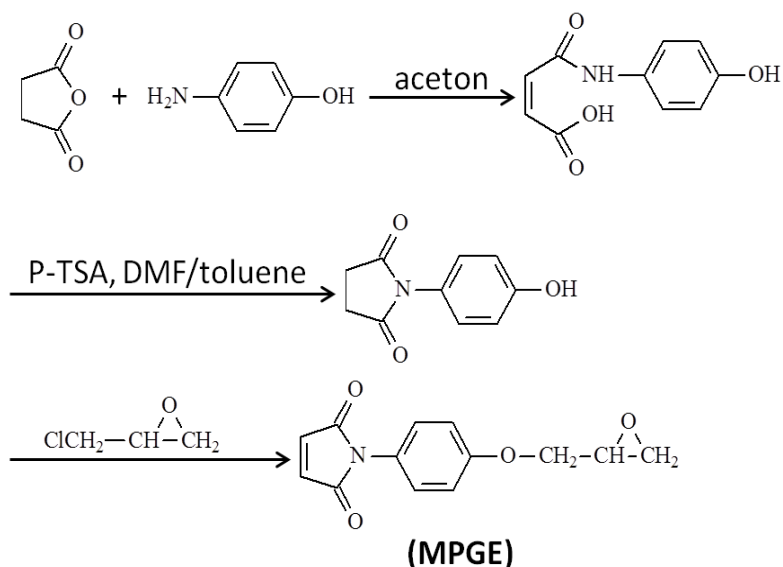
Figure 2-9: Synthetic route of 4-(N-maleimidophenyl)glycidylether (MPGE).

Synergistic effect of nitrogen/phosphorus on improving the flame retardancy of epoxy resins has also been demonstrated in other studies [43,44]. Gu et al. [43] synthesized two phosphorus–nitrogen-containing flame retardants, DP-DDE and DP-DDS (see Figure 2-10). At a relatively low addition amount of DP-DDE or DP-DDS (on the account of phosphorus content of 0.75 and 0.73 wt%, respectively), the epoxy resins can reach V-0 rating in UL-94 vertical burning tests, as well as high glass transition temperature (> 135 °C) and high char yields (>22% at 800 °C), implying high flame-retarding performance. You et al. [44] also prepared a halogen-free, phosphorus–nitrogen containing flame retardant (TNTP) (see Figure 2-10). With the loading of TNTP at only 5.0 wt %, the satisfied flame retardancy (UL-94, V-0) together with high char residue (27.3%) at 700 ºC can be obtained in epoxy resins.
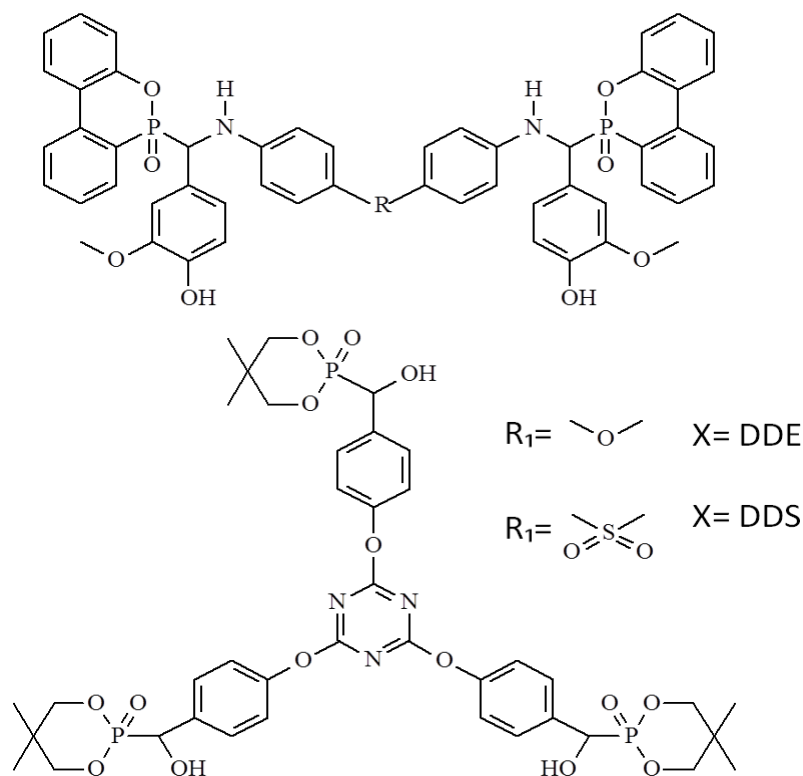
Figure 2-10: Chemical structures of DP-DDE, DP-DDS and TNTP.

2.3.5. Silicon-based flame retardants

Silicon, like phosphorus and nitrogen, is considered as an environmentally friendly flame retardant because it can decrease the harmful impact on the environments more than the existing materials. Previous investigation has shown that the addition of relatively small amounts of silicon-based compounds to polymeric materials has a flame retardant effect [45]. This is partly because these compounds dilute more combustible organic components and partly because the silicaceous residues can form a barrier to an advancing flame.

Hsiue et al. [46] synthesized a silicon-containing oxirane triglycidyl phenyl silane oxide (TGPSO) (Figure 2-11) and applied it into flame retardant epoxy resins. This silicon-containing resin possessed high char yield as well as high LOI of 35%,

demonstrating that incorporating silicon into epoxy resins is effective to improve their flame retardancy. Wang et al. [47] also incorporated TGPSO into flame retardant epoxy resins, and found that the silicone-containing group was in favor of the carbonization mechanism and the solid char yield at 800°C for TGPSO was 40 wt%. Meanwhile, TGPSO showed the high LOI of 35%, which was considered as an excellent flame retardant in the epoxy resin.
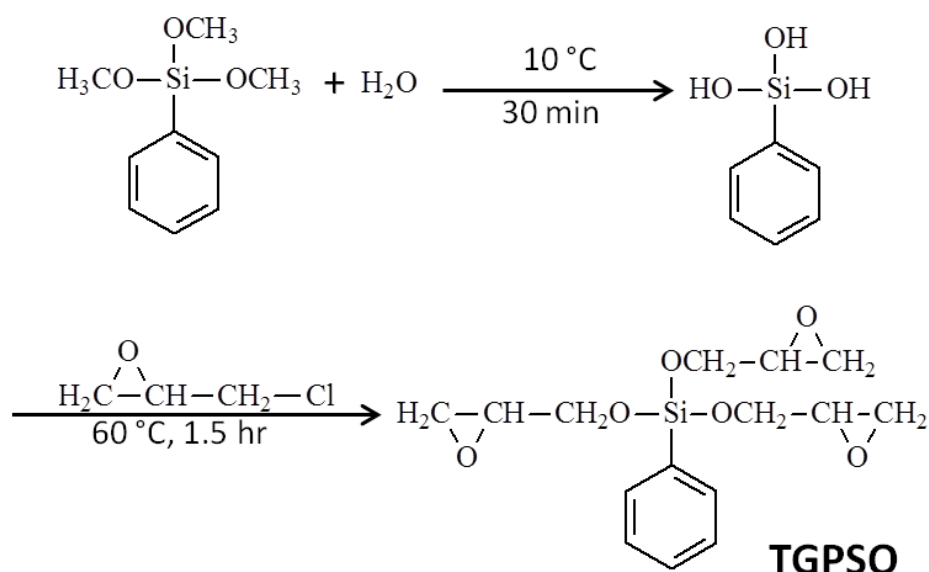
Figure 2-11: Synthesis scheme of silicon-containing compounds: TGPSO.

In another study, silicon-containing glycidyl monomers (TGPSO, BGDMSB and TGPS, Figure 2-12) were synthesized and cured by 4,4'-diaminodiphenylmethane [45]. The onset degradation temperatures reduced and the char yields increased as the silicon content increased. The high flame retardant property was confirmed by the high LOI value of these silicon-containing epoxy resins.
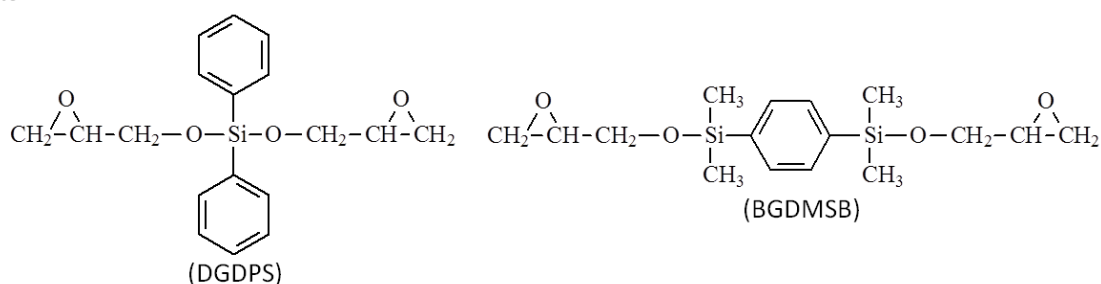
Figure 2-12: Chemical structures of silicon-containing compounds

2.3.6. Boron-based flame retardants

Boric acid have been well known as flame retardant additives from decades and zinc borates have also emerged as cheaper replacement for antimony oxides. The flame retardant mechanism involving the formation of the char is clearly related to the thermal action of boric acid with alcohol moieties [48], in a similar way to phosphoric acid. Martin and co-workers [48] prepared a boron-containing epoxy–novolac resin and investigated the flame retardancy of the resultant epoxy–novolac resin. The LOI values for the boron-containing epoxy–novolac resin were higher than the boron-free novolac resins. The enhanced flame retardancy was attributed to the presence of boron can produce a continuous inorganic layer of boric acid. In another study, a solid acid boron phosphate (BP) (Figure 2-13) was prepared and mixed with epoxy resins as flame retardants [49]. With the increase of the BP loading, the LOI value increased accordingly. However, the glass transition temperature of the resultant EP was slightly reduced observed from the differential scanning calorimetry results. Unlu et al. [50] investigated and compared the flame retardant properties of boron compounds with ATH in an epoxy system.
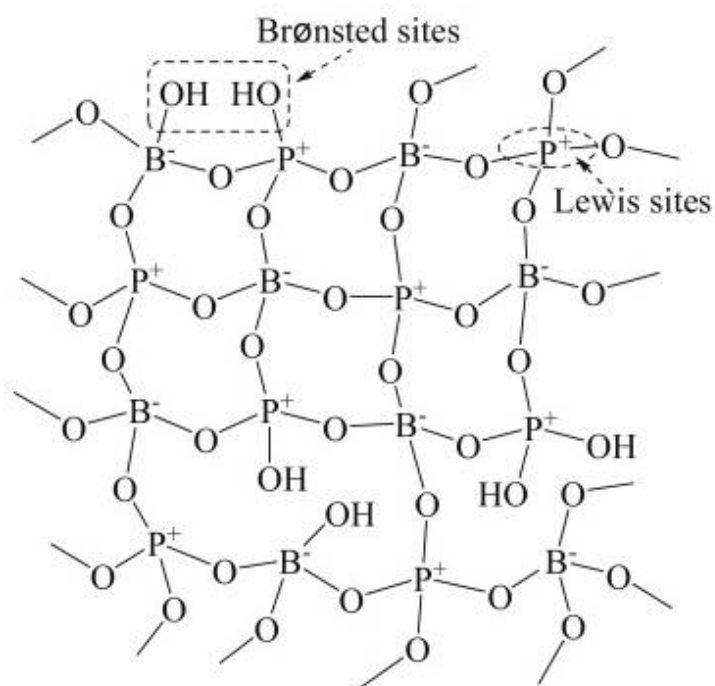
Figure 2-13: Chemical structure of boron phosphate

Six different boron-containing compounds, including colemanite (C), ulexite (U), boric acid (BA), boric oxide (BO), melamine borate (MB) and guanidinium nonaborate (GB), were selected as flame retardant additives. Based on the cone calorimeter test results, all boron-containing samples showed better fire retardant performances than ATH-containing sample; 40 wt% BO-containing samples exhibited the lowest peak heat release rate, total heat release and average heat release rate values. Dogan and co-workers further studied the synergistic effect of zinc borate (ZnB), boric acid (BA) and boric oxide (BO) with red phosphorus (RP) on the flame retardant properties of epoxy resins [51]. With the partial substitution of RP by boron compounds, lower heat release rate (HRR) and total heat evolved (THE) were observed. The boron compounds showed better flame retardant effect by increasing char yield in the condensed phase.

2.3.7. Intumescent flame retardant systems

Intumescence, from Latin 'intumescere', means the act or process of swelling or enlarging. The concept of intumescence is defined as formation of the protection layer which insulates the underlying material from heat and fire. Typically, such an intumescent system is composed of three major components: an acid source, a carbon source and a blowing agent [52]. Table 2-2 summarizes some typical examples of components used in intumescent systems.

The general mechanism has been proposed to describe the development of the intumescent phenomenon:

● the inorganic acid is released by decomposition of the acid source;

● the acid reacts with the carbon source via dehydration at temperatures slightly above the acid release temperature;

● the mixture of materials melt prior to or during esterification;

● released gases from the blowing agent and degradation products cause the carbonizing material to swell up;

● as the reaction nears completion, gelation and finally solidification occurs, the resulting solid is a multi-cellular foam.

A typical example is the case of EP-ammonium polyphosphate (APP)/ melamine (Mel)/pentaerythritol (PER) system [53].During burning, the epoxy coating started to intenerate and melt, APP decomposed to release polymetaphosphoric acid and phosphoric acid which led to the dehydration of the hydroxyl of PER to form the

char.

Table 2-2: Summary of some typical components used in intumescent systems.

(a) Acid source

Phosphoric acid

Sulphoric acid

Boric acid

Ammonium salts

Phosphates, polyphosphates

Borates, polyborates

Sulphates

Phosphates of amine or amide

Product of reaction of urea or guanidyl urea with phosphoric acid

Melamine phosphate

Alkyl phosphates

Haloalkyl phosphates

(b) Carbon source

Starch

Dextrin

Sorbitol, mannitol

Penthaerythritol monomer, dimer, trimer

Phenol-formaldehyde resins

Methylol melamine

Char forme polymers like poly(amide) 6,poly(amide) 6/clay nanocomposite, poly(urethane), poly(carbonate)

(c) Blowing agent

Urea

Urea-formaldehyde resin

Dicyandiamide

Melamine

Meanwhile, melamine decomposed to release ammonia, plumped up the melting coating, and formed the intumescent and compact charring layer to protect the matrix material well.

Furthermore, it was found that metal compound could enhance the flame retardancy of intumescent epoxy resins containing APP [54]. Yang et al. [55] prepared an intumescent flame-retardant epoxy resin system constructed by multiple flame-retardant compositions containing phosphorus and nitrogen heterocycle. The resultant epoxy resin systems exhibited excellent flame retardant properties: with the phosphorus content of 1% and 1.25%, the LOI values reached 37% and 38.5%, respectively, and achieved a UL94 V-0 rating.
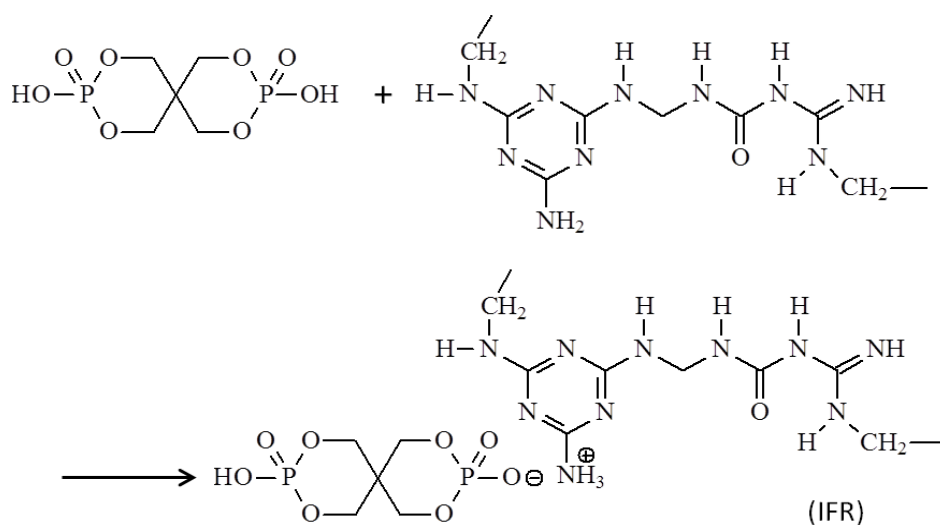
Figure 2-14: Synthetic route of IFR.

Recently, in order to reduce the loading of intumescent flame retardants, some new compounds combined acid source, carbon source and blowing agent into one molecule appear. Gao et al. [56] synthesized a pentaerythritol diphosphonate melamine–dicyandiamide–formaldehyde resin salt (Figure 2-14). By adding 25 wt%

of this flame retardant into epoxy resin, the LOI of 27.5% and UL-94 V-0 rating can be achieved.

2.3.8. Nanofiller as flame retardant

Nanocomposite technology has motivated considerable interests in the development of flame retardant polymeric materials because the addition of nanofillers not only provides fire retardant properties to the materials, but also, does not change the other properties or even enhance some of them, such as mechanical properties of the resultant polymer nanocomposites at a relatively low loading (< 10 wt%) [57].
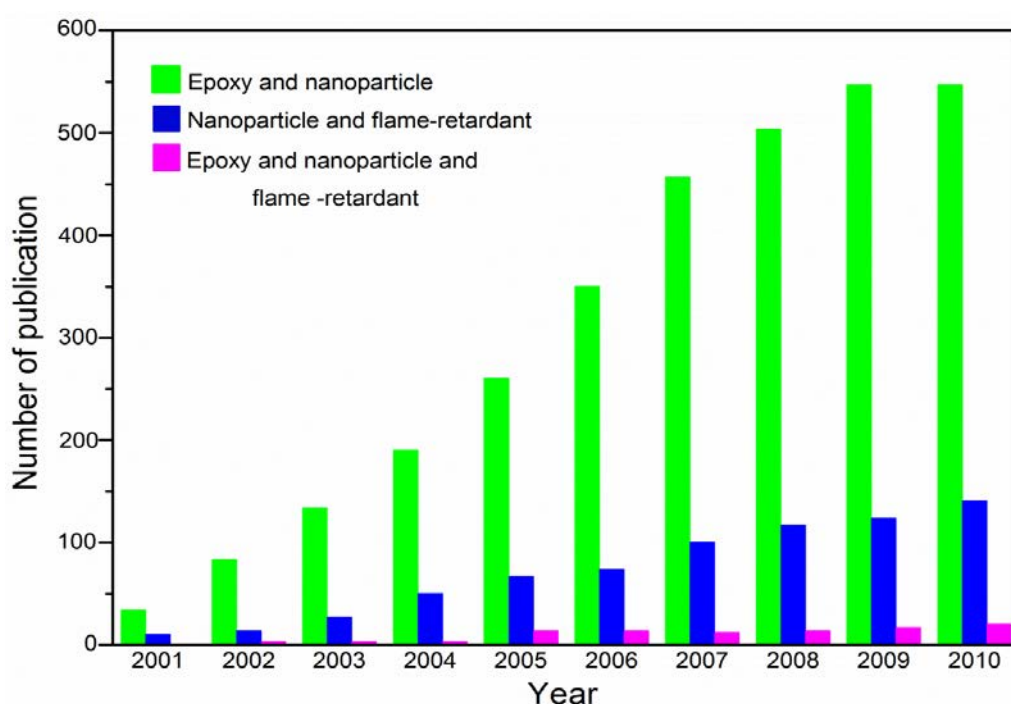
Figure 2-15: Number of publications per year for different keyword combinations (Web of Science, September 2015).

Up to now, nanofillers that have been found to be of flame retardant effect include carbon nanotube (CNT), graphene, clay, polyhedral oligomeric silsesquioxane (POSS), layered double hydroxide (LDH), cyclotriphosphazene, etc. Most of these

nanofillers have been applied into flame retardant epoxy nanocomposites. Many
literatures have provided wide description about the incorporation of the
nanoparticles in the epoxy resins to enhance their flame retardant properties (Figure
2-15).

Nano-clay

Nano-clay is well known as one of the most common flame retardant nanofillers in
various epoxy resins [58,59,60]. In general, clay-based composites classified into
three categories (Figure 2-16): (a) microcomposites: in which epoxy molecules does
not penetration into the lamellae of the clay; (b) intercalated composites: epoxy
molecules inserted into the clay structure, resulting in increase the spacing between
platelets in a regular fashion; (c) exfoliated composites: the single clay layers are
dispersed truly into the epoxy matrix.
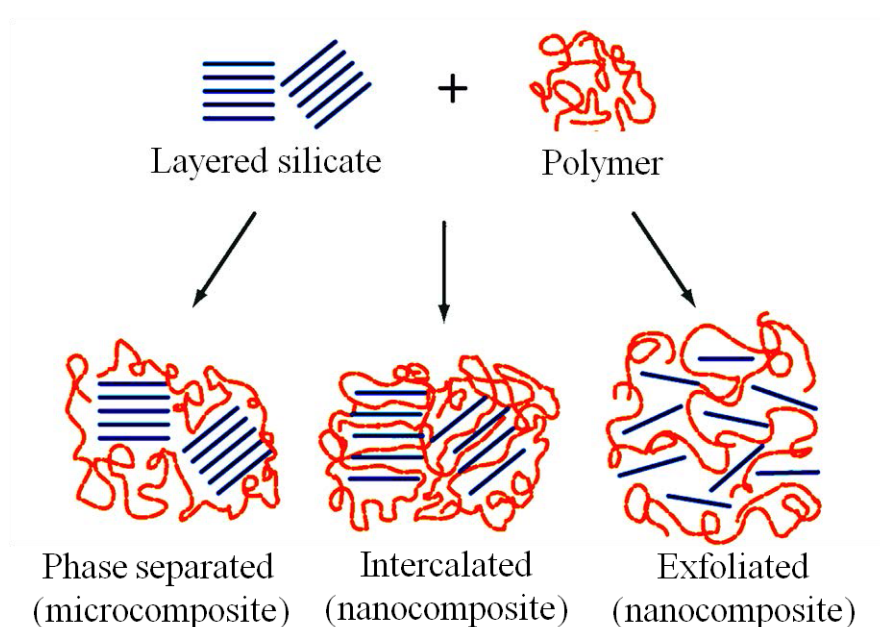
Figure 2-16: Scheme of different types of composite arising from the interaction between
layered silicates and epoxy chains: (a) phase separated microcomposite ; (b) intercalated
nanocomposite and (c) exfoliated nanocomposite [57]

Hartwig et al. [61] studied the combustion behavior of the clay-filled epoxy resins. Two different bentonites (5 wt%) based on a phosphonium or an ammonium cation as surfactants were incorporated into epoxy matrix. TEM measurements were employed to study about their dispersion state, and the results showed a non-uniform distribution of the bentonites in the matrix (Figure 2-17).

Horizontal burning test was utilized to evaluate the flame spread, in which the time required for burning 150 mm of the sample is recorded (Table 2-3).
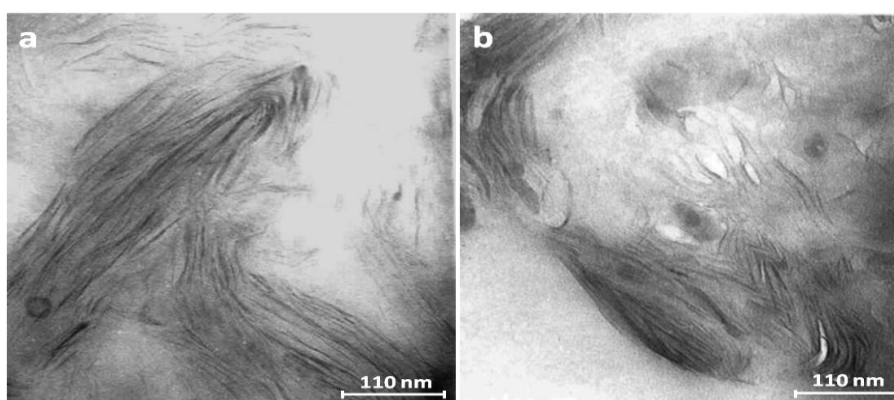
Figure 2-17: TEM image of a cross-section of the nanocomposite containing the (a) phosphonium bentonite and (b) ammonium bentonite.

Therefore, the enhanced flame retardant behavior attributed to the longer the time to ignition. In contrast, by the incorporation of bentonites into the matrix, the time required for burning the sample is intensively increased.

Table 2-3: Flammability characteristics of clay-filled epoxy resins.

Samples	LOI (%)	Horizontal burner test Time for burning 150 mm in horizontal position(s)
Virgin epoxy	18.3	260
Epoxy + ammounium (4.7 wt%)	19.7	434
Epoxy + phosphonium (4.7 wt%)	19.6	464

In addition, no dripping has been observed for the filled samples. Cone-calorimetry was conducted to further study about the fire retardancy of the samples (Figure 2-18). The maximum reductions of the peak of heat release rate (PHRR) were recorded for the nanocomposites and are reduced by 1/3 for an external heat flux of 70 kW/m². Camino et al. [62] reported more effective systems with different organo-modified montmorillonite (OMMT) in epoxy at 10 wt%. Microcomposite is probably synthesized instead of "real" nanocomposite at such a high loading. It was confirmed that the differences in the flame retardancy depended on the exchanged cation. As can be realized from the Table 2-4, the composite containing Nanofil 848 (octadecyl ammonium montmorillonite), showed the proper results, but not as good as Cloisite

Figure 2-18: Heat release rate for the different materials versus time applying an external heat flux of 70kW/m² (E+T= virgin epoxy, E+T+TMA= Epoxy + ammonium clay, E+T+TPP= Epoxy + phosphonium clay)[61]

30B (bis(2-hydroxyethyl) ammonium montmorillonite). In contrast with the Nanofil

848, Cloisite 25A (dimethyl hydrogenated-tallow(2-ethylhexyl) ammonium montmo rillonite) showed smaller reduction in PHRR.

Hartwig [61] reported that the incorporation of modified clays alone would not bring sufficient fire retardant properties to the materials. The reason might be attributed to that the barrier effect of nanoclays in epoxy was limited in this case. Therefore, nano-clay is usually used as synergist with other flame retardant additives in EP. DOPO [63] has been reported to create the synergistic effect with nanoclays.

Table 2-4: Cone-calorimeter data of epoxy nanocomposites at 50 kW/m² [62]

Sample	TTI (s)	pHRR (kW/m^2)	pHRR reduction (%)
Pure epoxy	34.5	2030	-
Epoxy/Nanofil 848 (10 wt%)	34.5	1250	48
Epoxy/Cloisite 30B (10 wt%)	34.5	650	68
Epoxy/Cloisite 25A (10 wt%)	44.0	1570	23

TTI: Time to ignition

pHRR: Peak heat release rate

In general, it can be concluded that the organoclays do not always show their full potential as flame retardants in epoxies, probably because of the difficulties for controlling their morphology in this matrix. However, their barrier effect could be useful in combination with other flame retardants.

Polyhedral oligomeric silsesquioxanes

POSS is a class of inorganic nanoparticles with a cage-like structure that has been used as flame retardants in various thermoplastic [64,65,66]. POSS is mainly

composed of a silicone-oxygen framework with general formulation of $(RSiO_{3/2})_n$ (n = 6, 8, 10…). The octahedron type of POSS is the most typical species (n = 8) (Figure 2-19). Hydrogen or any alkyl, alkylene, arylene, aryl or organo-functional derivatives of alkyl, aryl, alkylene or arylene group can be substituted instead of "R".
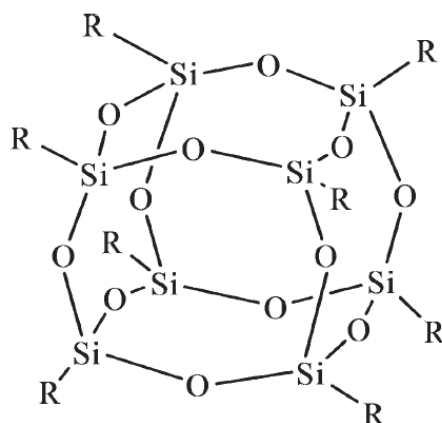
Figure 2-19: Structure of cage hexahedral silsesquioxane $(RSiO_{3/2})_8$.

OctaphenylPOSS

Glycidoxypropyl heptaphenylPOSS

Glycidoxypropyl heptaisobutylPOSS
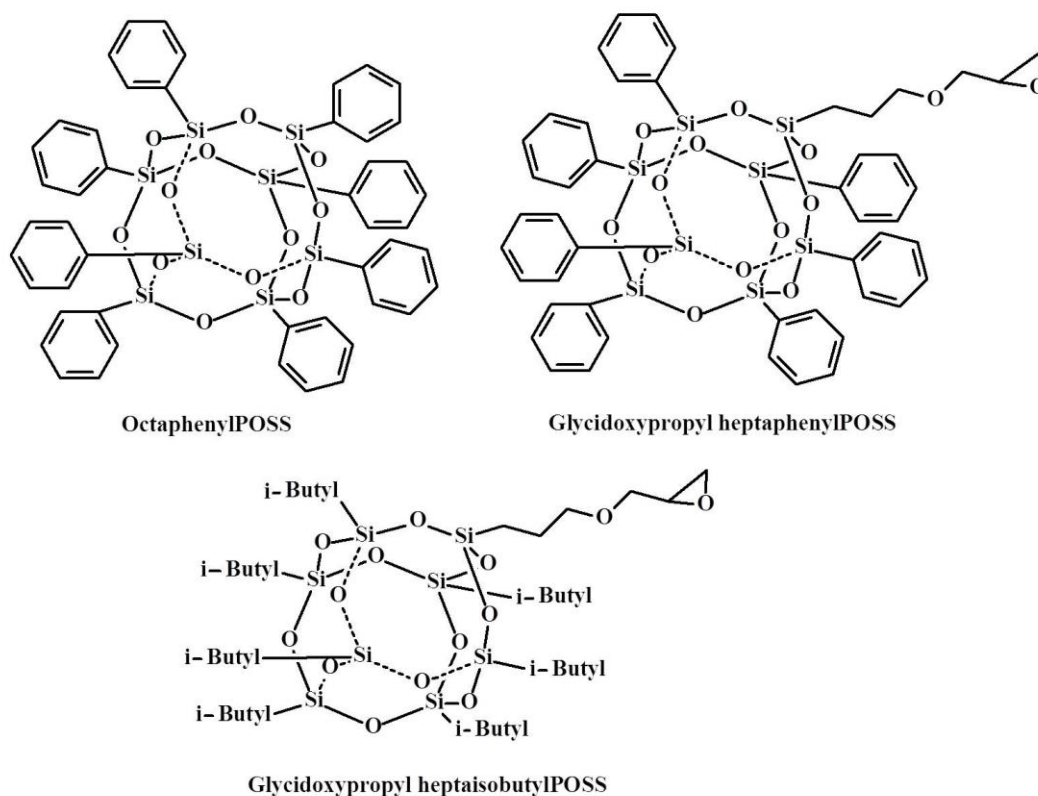
Figure 2-20: Chemical structures of octaphenylPOSS (left), glycidoxypropyl heptaphenylPOSS (middle) and glycidoxypropylheptaisobutylPOSS (right) (Ph=phenyl, i-But= isobutyl).

Functionalization of POSS can be realized by the highly tunable "R" group. Lu et al. [67] reported that LOI increased to 32.8% in the case of epoxy composite containing 5 wt % of cyclohexyltrisilanol POSS, as compared to the 22.6% of the virgin resin. Franchini et al. [68] conducted a study on the comparison between reactive and non-reactive POSS. Three different POSS were incorporated into epoxy matrix: octaphenyl-, glycidoxypropyl-heptaisobutyl- and glycidoxypropyl-heptaphenyl POSS (Figure 2-20). It was found that POSS bearing phenyl ligands were far more effective than POSS with isobutyl ligands.

Choi et al. [69] synthesized octa(aminophenyl)-silsesquioxane (OapPOSS) and used it as a curing agent for epoxy resin (Figure 2-21). The resultant epoxy nanocomposite showed greatly improved thermal stability and char yield as compared to the neat epoxy matrix.
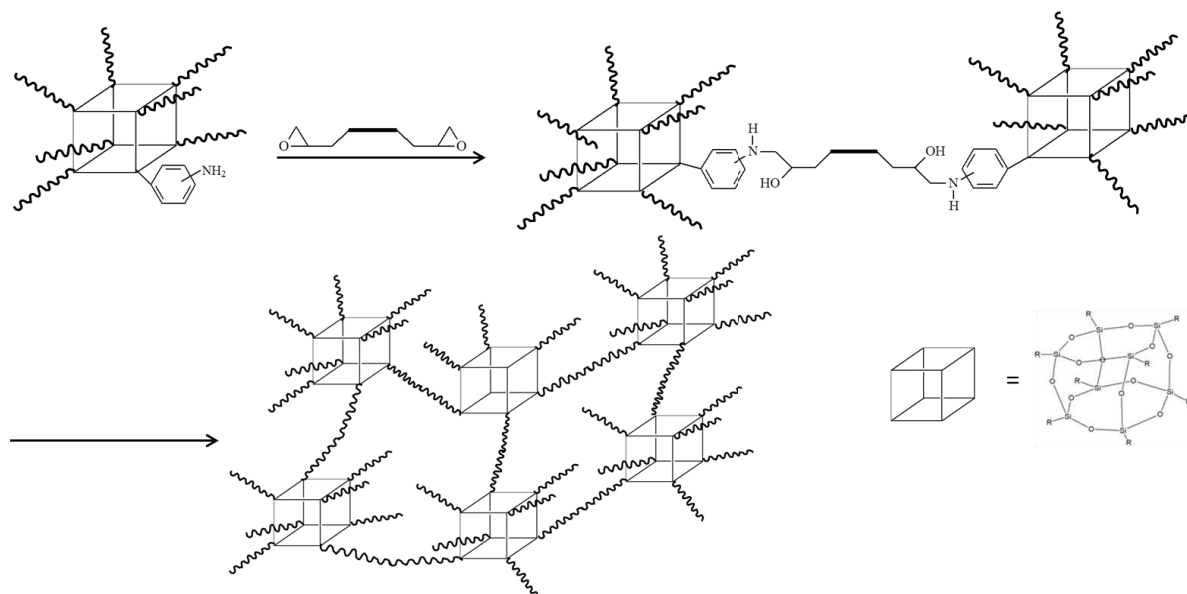
Figure 2-21: Tether formation from OapPOSS and DGEBA.

The isocyanate polyhedral oligomeric silsesquioxane/EP nanocomposite prepared by Chiu et al. showed an increase of char yield with the increase of the concentration of

POSS, indicating that the POSS segments provide the antithermal-oxidation effect for the epoxy nanocomposite [70]. Usually, single use of POSS cannot meet the flame retardant requirement of industrial standard, such as UL-94 V0 rating. Consequently, POSS has been used in combination with phosphorus or nitrogen-containing compounds to get a high flame retardant grade. Wang and co-workers have recently reported the combinations between octavinyl POSS and a phosphorus-containing resin to get higher enhancements on the fire retardant properties [71]. In this study, the phosphorus content was kept constant at 2 wt % in the epoxy system and the silicon content varied from 0 to 3 wt %. A maximum 44% reduction in PHRR was observed in micro-scale combustion calorimetry test in the case of epoxy composite containing 2 wt% phosphorus and 3 wt% silicon. Also, nitrogen-modified (Figure 2-22a) [72] and DOPO-modified POSS (Figure 2-22b) [73,74] were synthesized and exhibited flame retardant effect in epoxy nanocomposites.
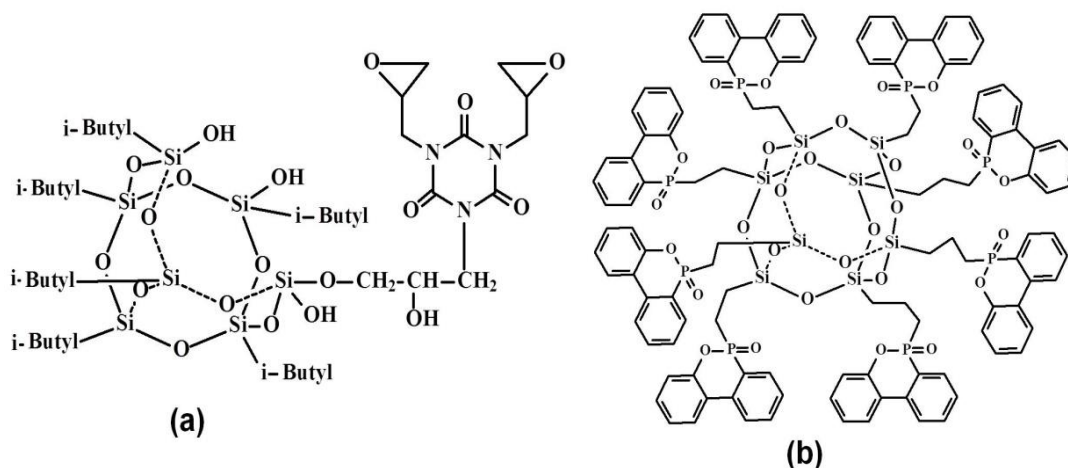
Figure 2-22: Chemical structures of nitrogen-modified POSS(a) and DOPO-modified POSS (b).

Carbon nanotube

Carbon nanotubes (CNTs) discovered in 1991 by Ijima [75] and, have been widely

used to fabricate the polymer nanocomposites due to their unique properties such as; special morphology, high thermal conductivity, high mechanical resistance and high electrical conductivity. There are two major types of carbon nanotubes: single-walled carbon nanotubes (SWNTs) and multiwalled carbon nanotubes (MWNTs) (Figure 2-23). The diameter of SWNTs ranges from 0.3 to 2 nm and generally, the length is more than 200 nm.
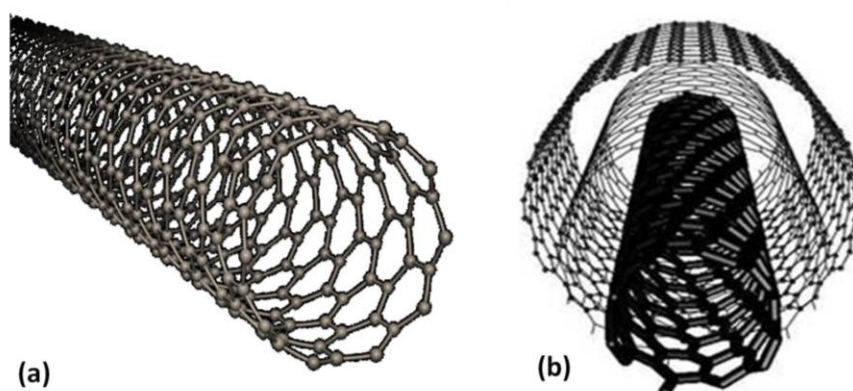
Figure 2-23: Carbon nanotubes: (a) Single-wall Carbon Nanotubes (SWNT) and (b) Multi-wall Carbon Nanotubes (MWNT).

Due to their structure, MWNTs exhibit higher diameters than SWNTs, typically between 10-50 nm and their aspect ratio can be as high as 10 000. The effect of CNTs on the flammability of epoxy matrix was studied by Rahatekar et al. [76] and the results of the peak mass loss rate (PMLR) during gasification are shown in Figure 2-24. Adding a small amount of MWNT (0.0025 wt %) has been shown a significant reduction (45 %) in the PMLR for epoxy nanocomposites, and the total time needed for complete mass loss is postponed. The authors attribute this to that nano-additives form a protective layer on the surface of the sample. By increasing the temperature, the amount of thermal energy which is reaching the underlying polymer is decreased. Due to the Van der Waals interaction between the different carbon nanotubes, it is

difficult to well disperse them into polymer matrix. Therefore, various methods have

been developed in order to improve the dispersion of nanotubes in the matrix.

Surfactant-assisted dispersion of CNTs is one example of these methods [77].
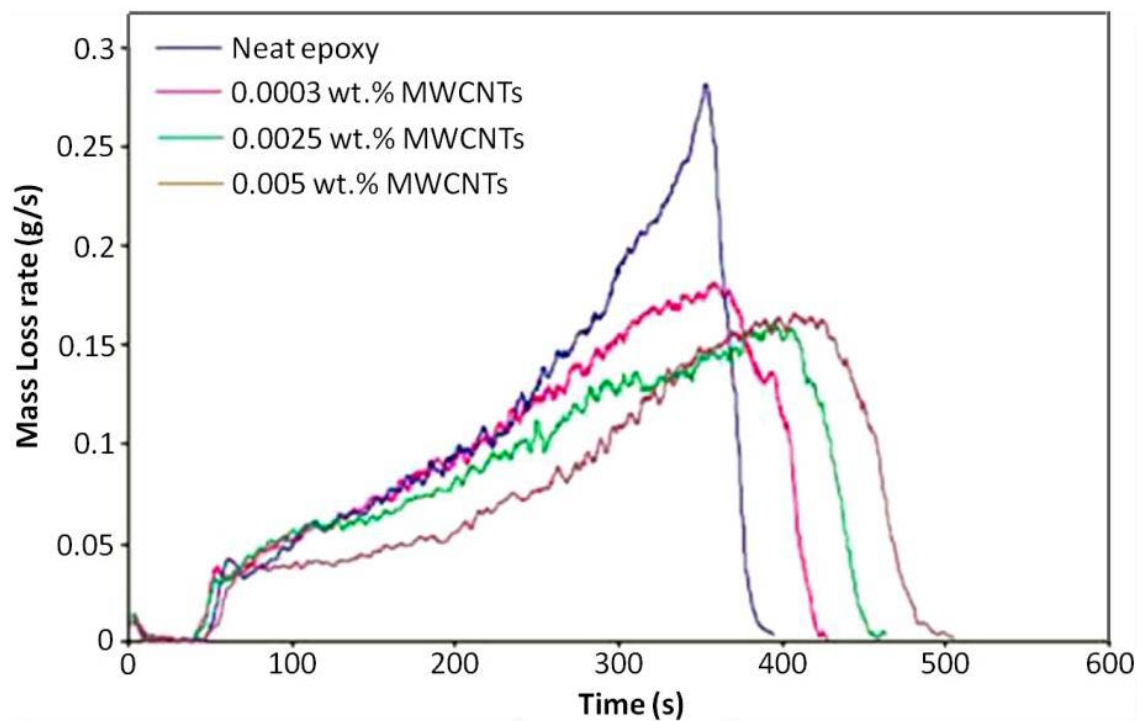
Figure 2-24: Mass loss rate versus time for different CNT-containing epoxies (Heat flux: 50 kW/m², N2 atmosphere) [76].

With the addition of only 1 wt% surfactant treated CNTs, the glass transition

temperature of the epoxy composites increased from 63 °C to 88 °C. In contrast, the

addition of un-treated CNTs only has moderate effects on the glass transition

temperature. Another simple way for dispersing CNTs in a polymer is covalent

functionalization of CNTs. Amine-functionalized CNTs is mainly known as one

suitable method to improve the dispersion state in the case of epoxy nanocomposites

[78].

Kuan et al. [79] reported the incorporation of the functionalized CNTs with

vinyltriethoxysilane (VTES) into an epoxy matrix via sol-gel method (Figure 2-25).

With the addition of 9 wt% functionalized CNT, the T_g was increased from 118 to 160 °C and char yield of composites at 750 °C was increased by 46.94%; simultaneously, the LOI of composites was increased from 22% to 27% and the UL-94 changed from V-1 to V-0.
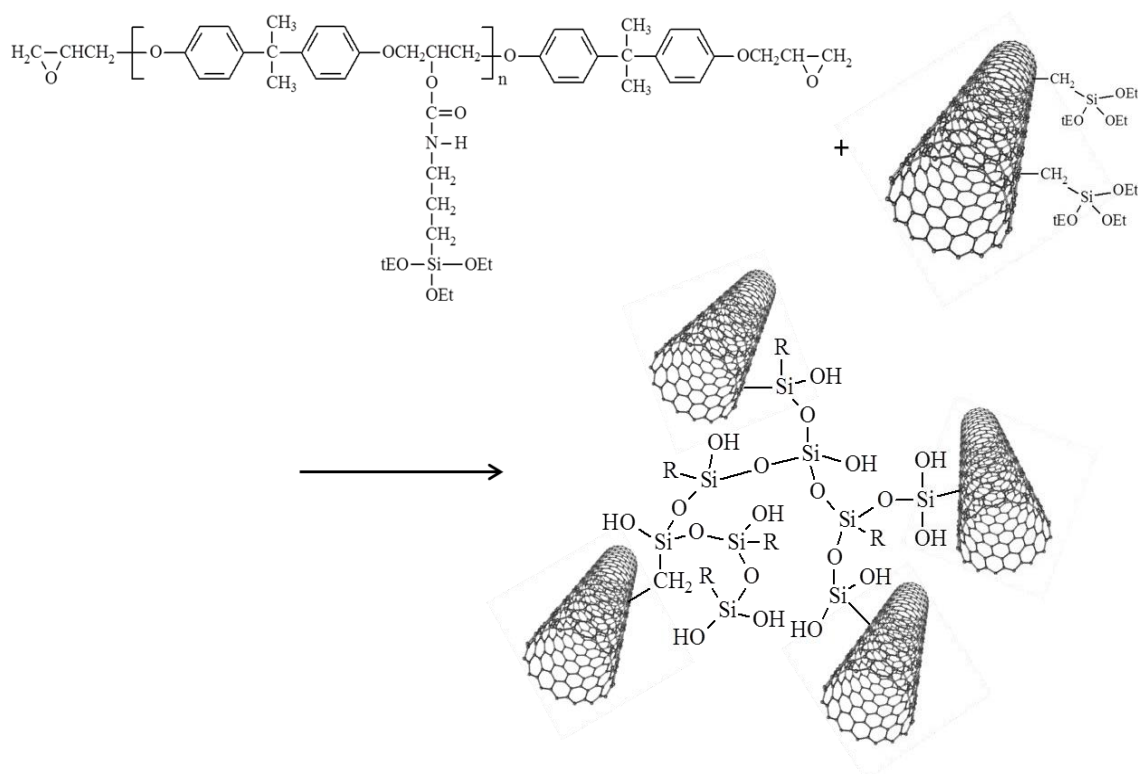
Figure 2-25: Schematic diagram for the preparation of Reaction scheme of epoxy/CNT nanocomposites [79].

Recently, Yu et al. [80] synthesized a molybdenum-phenolic resin (Mo-PR) and then grafted it onto the surface of MWCNTs to obtain functionalized MWCNTs (CNT-PR). The grafted Mo-PR improved the dispersion of MWCNTs in epoxy matrix and enhanced the interfacial interaction between CNTs and epoxy matrix. Also, the grafted Mo-PR showed high char yield during the process of combustion, as well as the improved flame retardancy of nanocomposites, especially for the heat release rate and total smoke production. In addition to functionalized CNTs with organic compounds, synergistic effect of CNTs with other inorganic fillers, such as

montmorillonite [81] and cyclotriphosphazene [82], on the flame retardant properties of epoxy resins has also been reported.

Graphene

Graphene, as a new member of carbon allotropes discovered in 2004 [83], has been arousing tremendous attention and research interest in the scientific community. With the unique structure of a 2-D monolayer of sp^2 hybridized carbon atoms, graphene has shown exceptional physical properties, such as ultrahigh specific surface area (calculated value, ~2630 m^2 g^{-1}) [84], excellent fracture strength (~125 GPa) and Young's modulus (~1000 GPa) [85], high electronic conductivity (~200 000 cm^2 V^{-1} s^{-1}) [86], and good thermal conductivity (~5000 W m^{-1} K^{-1}) [87]. These fascinating properties make graphene one promising nanofiller to be employed in nanocomposites for many multi-functional applications. In this section, we will focus on the flame retardant properties of graphene-based polymer nanocomposites.

Graphene with high purity is quite stable against combustion when exposed to a natural gas flame for a few seconds. The burned part turned red hot but didn't spread, and was quenched after the removal of the flame, clearly indicating the high intrinsic flame resistance of graphene (Figure 2-26a) [88]. However, the presence of potassium salt impurities in graphene oxide (GO) became highly flammable. A gentle touch with a hot spot could cause catastrophic and total combustion of such GO films (Figure 2-26b) [88]. Due to its good intrinsic flame retardant property, pristine graphene has been utilized directly to prepare flame retardant polymer composites via melt

compounding or solution blending methods. An interesting phenomenon was observed in graphene/epoxy composites: the PHRR displayed an increase trend compared with that of virgin epoxy resins, despite an increased LOI value and a reduced THR simultaneously [89].
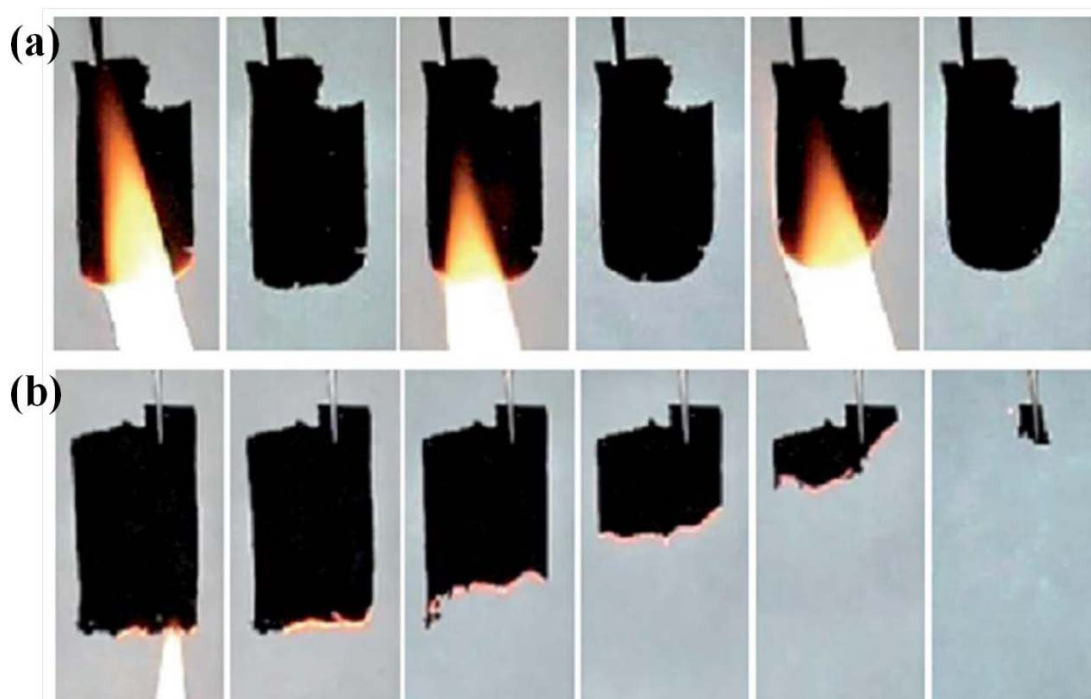
Figure 2-26: Snapshots of (a) flame treatments on reduced graphene oxide, (b) flame treatment on a reduced graphene oxide contaminated with KOH salts (1 wt%) [88].

The authors attributed this phenomenon to the balance between the effect of thermal conductivity and the barrier effect of graphene. As a precursor of graphene, GO contains abundant functional groups such as epoxy, hydroxyl, carboxyl and -C=C- groups at the edge area and basal planes [90], which provides many active sites for fabricating functionalized graphene. Recently, 9, 10-dihydro-9-oxa-10-phosphaphenanthrene-10-oxide (DOPO) [91] (Figure 2-27), 2-(diphenylphosphino) ethyltriethoxy silane (DPPES) [92], and polyphosphamide (PPA) [14] have been grafted to GO in order to overcome the challenge of GO in its burn out limits. As

expected, flame retardants functionalized graphene showed superior flame retardant properties over either organic flame retardants or pristine graphene as far as LOI, UL-94 rating and PHRR are concerned. For example, epoxy composites with 10 wt% of DPPES-graphene could pass UL-94 V-0 rating whereas its counterparts with the equivalent loading of either DPPES or graphene cannot [92].
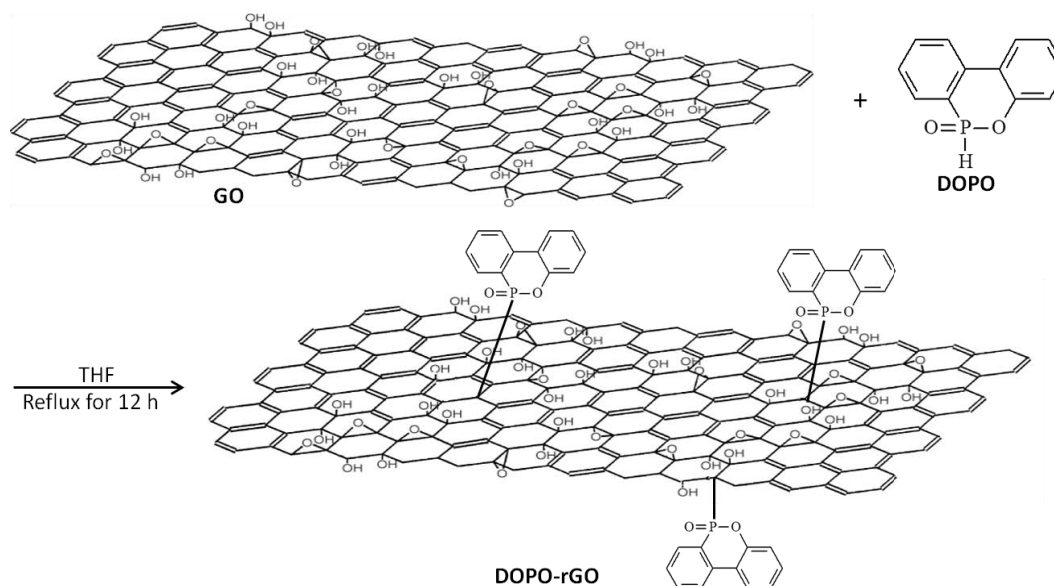
Figure 2-27: Schematic illustration of the synthetic route for the preparation of DOPO-rGO [91].

In addition to covalent functionalization, various inorganic/graphene hybrids, such as metal oxide/graphene, have been synthesized via non-covalent modification. Hu's group has done much innovative work on the application of LDH/graphene and metal oxide/graphene into flame retardant polymer nanocomposites [93,94,95,96,97]. Incorporation of metal oxide/graphene hybrids results in significant thermal stabilization of polymer: a 37 and 27 °C increment in the temperature of 5% mass loss is observed for SnO_2/graphene-epoxy and Co_3O_4/graphene-epoxy with the filler loading of 2 wt%, respectively, compared to that of pure EPs [93]. Only with 2 wt% of metal oxide/graphene hybrid, the PHRR value is decreased by at least 30% in

epoxy composites. Besides the heat-related fire hazards, the incorporation of LDH/graphene or metal oxide/graphene hybrid also leads to suppressed smoke production and reduced smoke toxicity compared to pristine graphene [97]. The inhibition of smoke is attributed to the reduced amount of the organic volatiles degraded from polymers, since the organic volatiles are the major source of smoke particles [98].

Layered double hydroxides

In recent years, layered double hydroxides (LDHs), as a new fascinating nano-filler, have been widely investigated in polymer composites. The chemical formula of LDHs can be represented by $[M^{2+}_{1-x}M^{3+}_x(OH)_2]^{x+}.[(A^{n-})_{x/n}\cdot yH_2O]^{x-}$, where M^{2+}, M^{3+}, and A^{n-} are divalent metal cations, trivalent metal cations, and interlayer anions, respectively (Figure 2-28) [99]. The composition of LDHs is highly tunable due to the versatility in the species of M^{2+}, M^{3+}, and A^{n-} together with the value of "x".
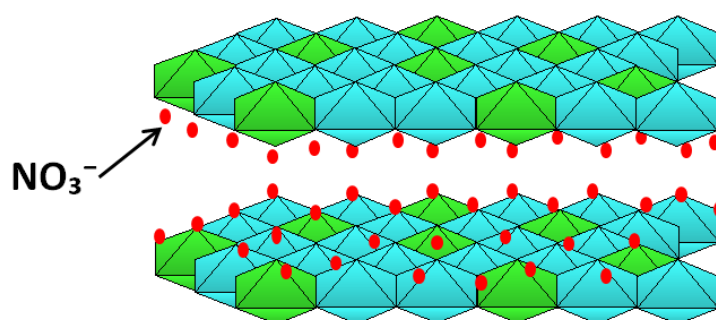
Figure 2-28. Schematic illustration of layered double hydroxides.

LDHs can be used as flame retardant additives because of its endothermic decomposition upon exposure to high temperatures: their decomposition can absorb

heat and release water and CO_2, which are able to dilute combustible gases, enhance the heat absorption and reduces the heat release during combustion. Moreover, a protective ceramic layer is generated on the top of the sample, providing a barrier effect [100]. Zammarano et al. [101] investigated the self-extinguishing behavior of epoxy/LDH nanocomposites at the horizontal UL-94 HB test. Great reduction in the pHRR during cone-calorimeter test has also been observed. In another study, Becker et al. [102] also studied mechanical and flame-retardant properties of epoxy/MgAl LDH composites, and they found that all samples containing 1%, 3% and 5% (w/w) of LDH showed self-extinguishing behavior in the vertical test while pristine epoxy cannot. Regarding the mechanical properties of the composites, the lowest concentration of LDH (1%) yielded the best performance, as higher concentration of LDH loadings might lead to agglomerates.

Like other nano-fillers, one of the challenge concerning LDHs is to destroy these aggregated structures which is highly detrimental to the composite properties and to improve the dispersion of LDHs in the matrix. As is well known, the layered structure of LDHs can be used as a versatile intercalation host which can accommodate a wide variety of organic guest species. This procedure can be employed for the modification of LDHs. Becker et al. [103] also prepared MgAl LDH intercalated with dodecyl sulfate and used it in flame retardant epoxy composites. All samples containing LDH showed self-extinguishing behavior in the vertical test and lower burning rate than pristine epoxy. Synergistic effect on improving flame retardancy was found between LDH and silica [104], as well as with graphene [97]. Compared to pure EP, the

addition of SiO$_2$@CoAl LDH brings about a 39.3% maximum decrease in PHRR

(Figure 2-29) [104]. Labyrinth effect of m-SiO$_2$ and formation of graphitized carbon

char catalyzed by CoAl LDH play pivotal roles in the flame retardant enhancement.
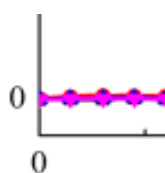
Figure 2-29: HRR curves of EP and its nanocomposites [104].

Based on the discussion above, modification of LDHs is crucial to obtain the uniform

dispersion and the optimum performance of the resultant composites. Currently, most

of cases of modification of LDHs involve the single modifier, such as salts of fatty

acids [105], sulfonates [106], and phosphates [107]. However, the dispersion of

modified LDHs is still not satisfactory to obtain functionalized LDH-based polymer

nanocomposites with enhanced fire resistance and mechanical properties

simultaneously up to now. Therefore, novel functionalization of LDHs will be

developed in order to obtain high performance polymer nanocomposites. Based on

this idea, in this work, multi-functional intercalation in layered double hydroxide

(LDH) has been developed via designed multi-modifiers with varied functions in order to transfer these functions to epoxy material by nanocarrier.

3   Design, preparation and characterization of functionalized LDH

3.1 Introduction

In order to facilitate the dispersion of LDHs in the epoxy resins, it is necessary to modify the pristine LDH to enlarge the interlayer space. A wide variety of anionic surfactants, such as fatty acid salts, [105] sulfonates, [106,108] and phosphates, [109] have been used as modifiers for LDHs. In our recent study, cyclodextrin (CD)-based (Scheme 3-1) derivatives have been used as modifier for LDH, showing a considerable decrease in flammability properties compared with conventional modified LDH.

One of the popular applications of epoxy composites is for manufacturing electrical appliances as encapsulating materials, and thus the photo-stability and the thermal stability of these encapsulating materials would be of great importance [110]. However, with extended exposure to UV radiation, the ultimate mechanical characteristics, especially stiffness and impact strength of polymers, are very sensitive to irradiation which can eventually lead to complete disintegration of the material [111,112]. Therefore, to improve the anti-UV properties for epoxy-based materials is very important. It is investigated that the chemical modification through introducing the fluorophore to the CD can alter its behavior from photochemical inert to active status [122]. In this works, modified β-CD with chalcone as the fluorophore have been synthesized (fCD) and used as a hybride compound in order to synthesize the functionalized LDH.

Transition metal oxides are usually used to improve the thermal resistance of char

residues. For this purpose, the surface of pristine LDH layers was firstly decorated with the iron oxide nano-particles, and then modified with Ph and hydroxypropyl-sulfobutyl-beta-cyclodextrin sodium (CDBS). The multi-modified LDH nanoparticles were characterized by transmission electron microscopy (TEM), wide angle X-ray scattering (WAXS), Zeta-Sizer, BET, BJH and thermogravimetric analysis (TGA).

3.2 CD based multimodiers modified LDH

In this work, hydroxypropyl-sulfobutyl-beta-cyclodextrin sodium (sCD) was synthesized as a first modifier for LDH, since sCD contains glucopyranose units possessing many rigid structures and large number of hydroxyl group that may lead to the formation of rich char residues (scheme 3-1). Cyclodextrin (cyclodextrin, CD) is a natural cyclo-oligosaccharides product bonded by glucosidic bond of 6-15 glucose molecules after `hydrolysed and bonded by the cyclodextrin gluconotransferase (CGT'ase), the common products are α-, β- and γ-CD, containing 6, 7, 8 molecules of glucose respectively, presenting a circular curtailed cone, with a hollow hydrophobic cavity.
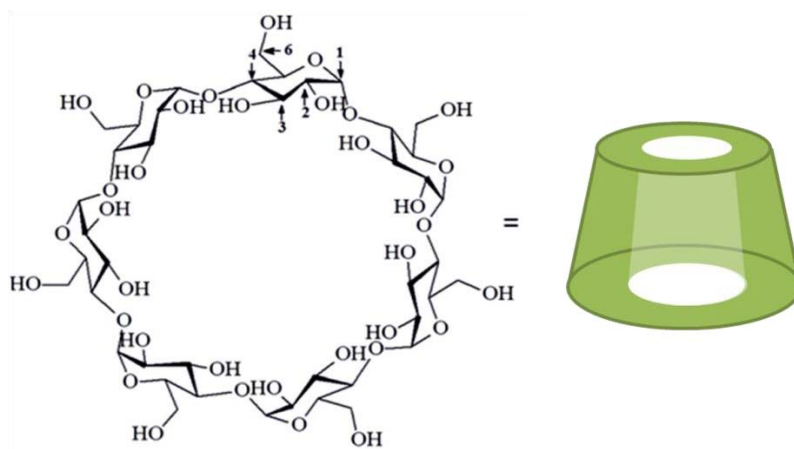
Scheme 3-1: The structure of b-cyclodextrin (CD).

With the special molecular structure of "hydrophobic inside and hydrophilic outside", CD can form a super-molecule with weak host and guest reaction between molecular with a variety of small organic molecules of suitable size. Therefore, it has high research and application values for the molecular recognition, mimic enzymes and chiral separation by chromatography, etc, and the applications on the agriculture, medicine, cosmetics and food industry are more promising. CD has a wide range of applications and research values in wide variety of application, but they are restricted for its solubility. The commonly-used β-CD possessing small water solubility (1.85%). CD derivative method is the substitution of the hydroxyl group of the unmodified CD with another substituent which changes the physiochemical properties of the water-solubility of the CD. The type and degree of substitution are significantly can influence the property and nature of the derivatives. A typical example is the addition of the hydroxypropyl group with C3 structure on the β-CD structure, hydroxypropyl-β-CD (HP-β-CD) has been widely used as drug excipients and used in the food industry at present due to its good water solubility, small degree of hemolysis and low toxicity. On the other hand, the change of average degree of substitution can also alter the performance and the use of derivatives (U.S. Pat. No. 5,134,127). In addition, the change of the degree of substitution can also change the liability property, for instance, the higher of the average degree of substitution of HP-β-CD, the less of complexing ability [113]. In this work butane sultone has been used as the modifier to prepare the hydroxypropyl-sulfobutyl-beta-cyclodextrin (scheme 3-2).

In a three-neck round flask equipped with iso-barically funnel, reflux-condenser, and

thermometer, β-cyclodextrin (0.02 mol), sodium hydroxide (0.11 mol) and de-ionized

water (45 ml) were introduced and stirred to dissolve completely. The solution was

heated to 75 °C, and then 1,4-butane sultone (0.08 mol) was added drop wise within 3

hours. The solution kept stirring for another 4 hours and then cooled down to the

room temperature. pH value was adjusted to neutral with hydrochloric acid, and the

by-products were removed by filtrate dialysis. After filtrate dialysis, the white-like

solid product (sCD) was obtained using rotary evaporation method.

ß-Cyclodextrin (CD)   **Butane Sultone (s)**   **sCD**
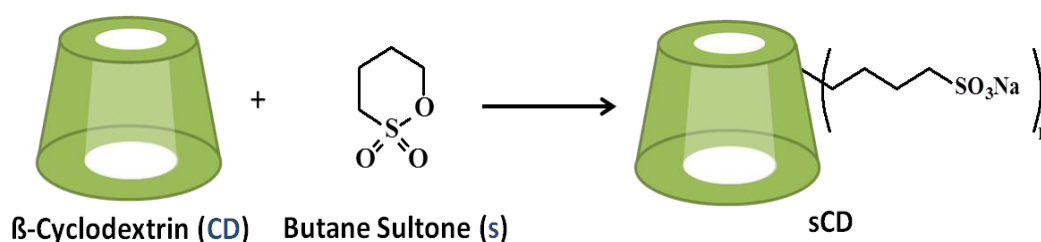
Scheme 3-2: The structure of hydroxypropyl-sulfobutyl-beta-cyclodextrin (sCD).

3-2-1 Analysis and characterization of hydroxypropyl- sulfobutyl- beta-cyclodextrin (sCD).

The sCD could be represented by the chemical formula of $C_{42}H_{70}O_{35}\cdot(C_4H_8O_3S)_x$,

where X is the substitution number of 1,4-butane sultone. On the basis of NMR (Fig.

3-1) and elemental analysis data (Table 3-1), the degree of substitution of 1,4-butane

was approximately 6, which means 6 sulfobutyl groups (s) have been covalently

attached to CD.

Table3-1: Elemental analysis of β-CDBS

Species	N	C	S	H
Content / wt%	1.37	35.49	9.15	7.27
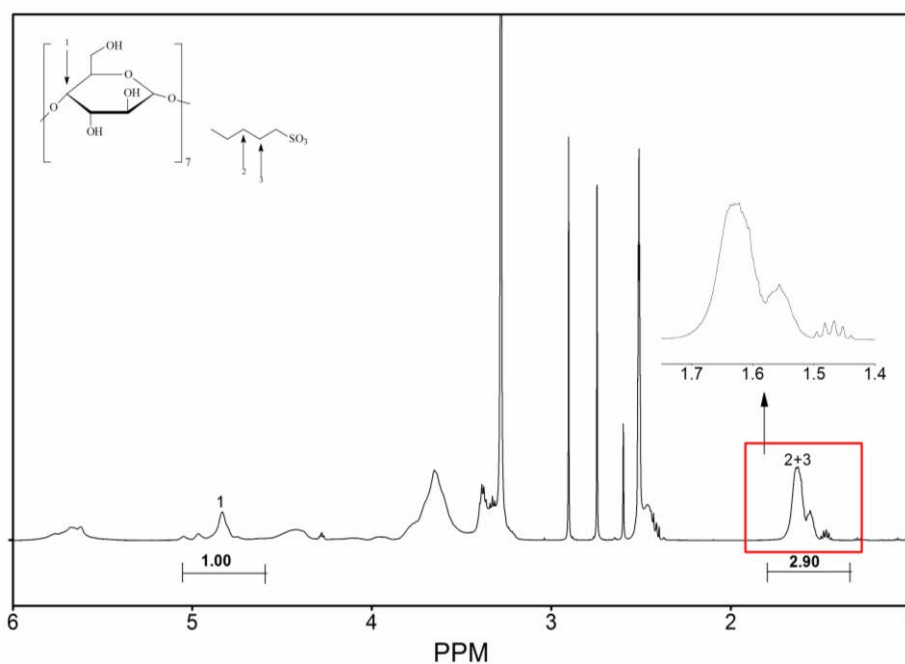
Figure 3-1: ^{1}H NMR spectra of sCD.

3-2-2 Preparation of un-modified and modified LDHs

In a 1000 ml three-neck round flask equipped with iso-barically funnel, reflux-condenser and pH meter, SDBS (0.05 mol), sCD (0.025 mol), taurine (0.025 mol) and de-ionized water (300 ml) were charged and stirred until completely dissolved. Subsequently, an aqueous solution containing $Mg(NO_3)_2 \cdot 6H_2O$ (0.2 mol) and $Al(NO_3)_3 \cdot 9H_2O$ (0.1 mol) in de-ionized water (300 ml) was slowly added to the flask. During the synthesis process, the pH value was kept at 10 ± 0.5 by adding a 1 M NaOH aqueous solution. The resulting slurry was continuously stirred for 30 min; afterward, it was allowed to age at 75 °C for 18 h. Finally, the resulting product was filtered and washed thoroughly with de-ionized water until the pH = 7.
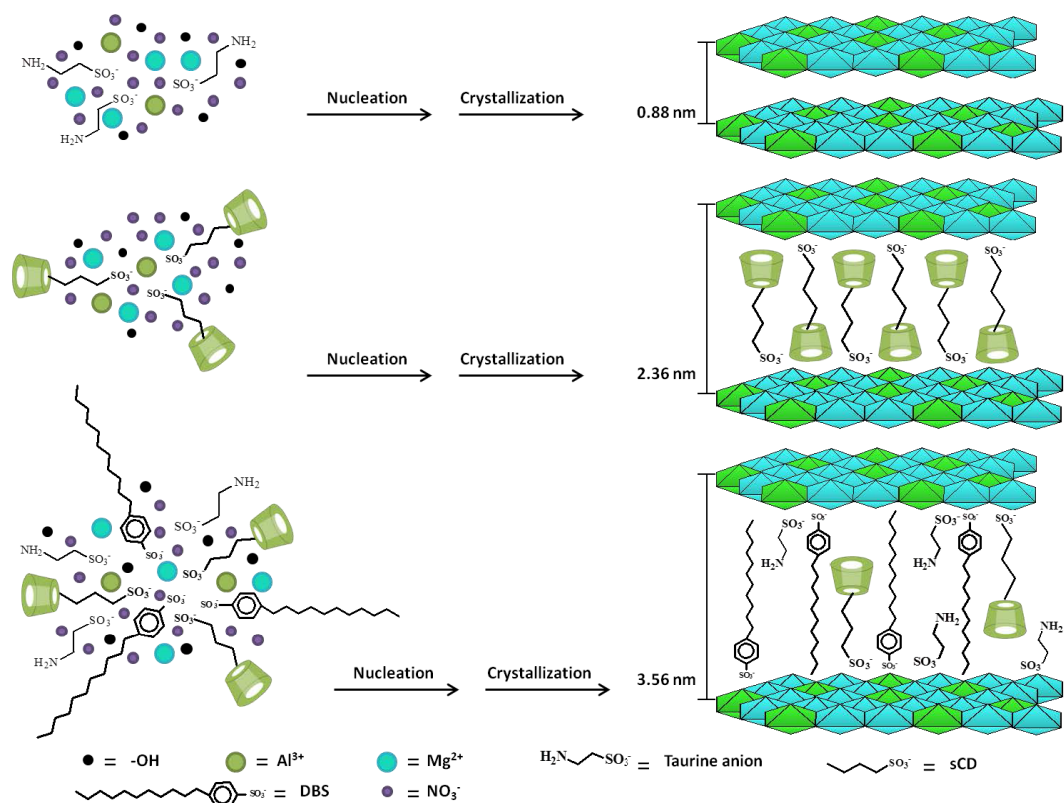
Scheme 3-3: Schematic illustration of anions structure intercalated in the functionalized LDH by one-step synthesis method.

3-2-3 Characterization of functionalized LDH

The filtrated cake was then dried in an oven at 80 °C until a constant weight was achieved, which was called sCD-DBS-T-LDH. In addition, unmodified LDH (NO$_3$-LDH), T-LDH and sCD- LDH were synthesized using the same method (scheme 3-3). The WAXS patterns of NO$_3$-LDH, and modified LDHs were shown in Fig. 3-2.

In the WAXS pattern of NO$_3$-LDH, the first basal reflection (003) appears at 2θ = 9.91° corresponding to an interlayer distance of 0.88 nm. For sCD-LDH, the (003) reflection shifts to 2θ = 3.75°, indicating interlayer distance of 2.36 nm. Combination of DBS with sCD and T into LDH shifts the (003) reflection to the lower angle,

corresponding to an interlayer distance of 3.56 nm, which is 4-fold increase in the interlayer distance compared with that of NO_3-LDH.
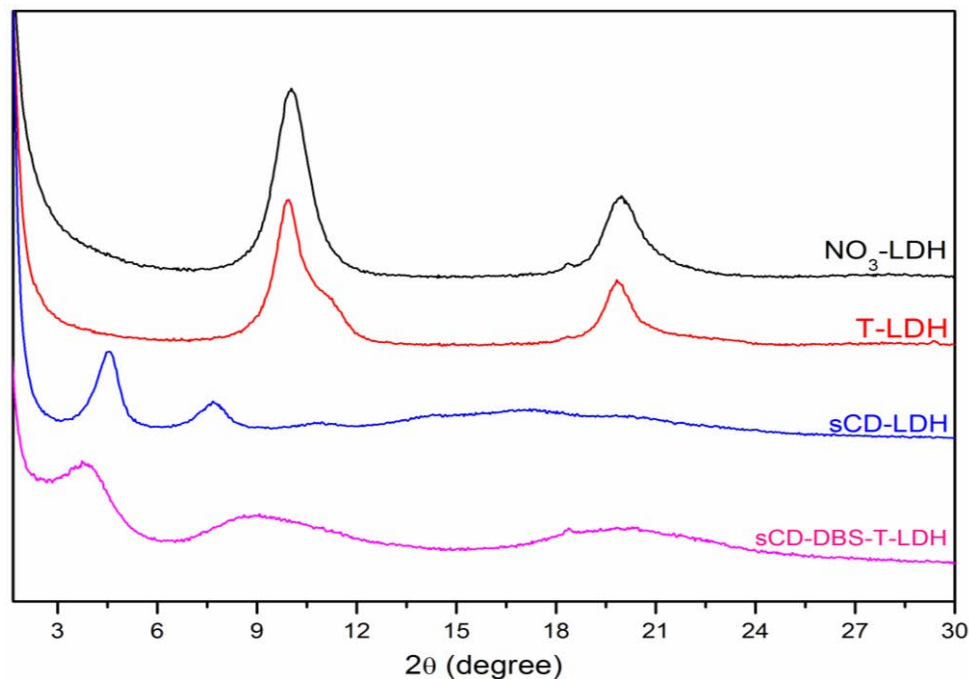
Figure 3-2: WAXS patterns of NO_3-LDH, T-LDH, sCD-LDH and sCD-DBS-T-LDH.

The enlargement of the interlayer distance could be attributed to the long molecular chain of the sCD and DBS. DBS is relatively larger (more than 0.8 nm) compared to the size of NO_3^- (around 0.1 nm) [19]. In contrast, incorporating taurine shows nearly no change in the interlayer distance due to its small molecular size.

Figure 3-3 shows the SEM micrographs of the morphological structure of the NO_3-LDH and modified LDHs. SEM micrographs (Nova NanoSem 230 FEG, Netherland) of the nano-particles were recorded to characterize the structures of LDHs before and after the modification. SEM was performed on the surface and cross-section of char residues after cone calorimetry using a Zeiss, EVO MA15

(Germany) scanning electron microscope. All the samples were sputter-coated in gold prior to the observation.

As can be seen, MgAl-NO$_3$-LDH (Fig. 3-3a) has a plate-like geometry of its primary particles with a microscopically smooth surface. The existence of sharp edges in most of the particles may be an indication of the incomplete process of crystal growth, resulting in no particular particle shape. The morphological feature of the organo-modified LDH (Fig. 3-3b and 3-3d) is similar to the NO$_3$-LDH, meaning that the intercalation of anions does not change the two-dimensional morphology of LDH.
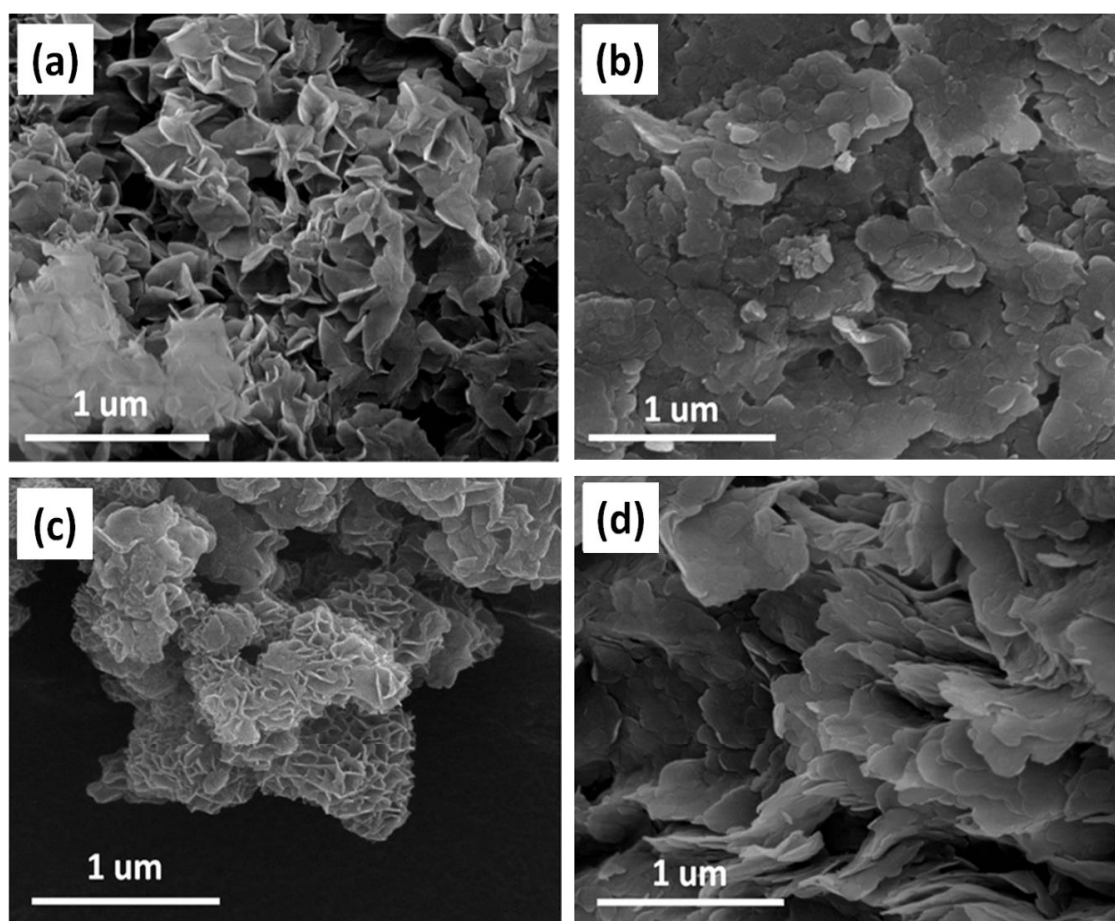
Figure 3-3: SEM images of (a) NO$_3$-LDH, (b) sCD-LDH, (c) T-LDH, and (d) sCD-DBS-T-LDH.

3-3 Chalcone inserted CD based multimodifiers modified LDH

3-3-1 Preparation of functionalized sCD (fCD)

In a three-neck round flask equipped with iso-barically funnel, reflux-condenser, and thermometer, sCD (0.02 mol) and de-ionized water (45 ml) were introduced and stirred until complete dissolution. The solution was heated to 40 °C, and then pre-heated chalcone solution (40 °C, 0.02 mol) was added dropwise within 3 hours. The solution exposed to the ultra-sonication for 5 minutes and then kept stirring for another 24 hours and then cooled down to the room temperature. The greenish yellow crystal-like solid product (fCD) was obtained using rotary evaporation method.

3-3-2 Characterization of functionalized sCD (fCD)

Figure 3-4 shows the X-ray powder diffraction patterns of sCD, chalcone and sCD-chalcone complex. The WAXS patterns of the samples were recorded by a XPERTPRO X-ray diffractometer. The Cu Ka (l ¼ 0.1542 nm) radiation source was operated at 45 kV and 40 mA with a scan speed of 2 min^{-1}.

As can be seen, sharp peaks at the diffraction angles of 10, 16, 20 and 22 degree are presented in the diffraction pattern of chalcone. The diffractogram of sCD exhibits some low intensity peaks at particular diffraction angles. In contrast, it is invisible to observe the characteristic peaks of chalcone in the diffraction pattern of sCD-chalcone complex.
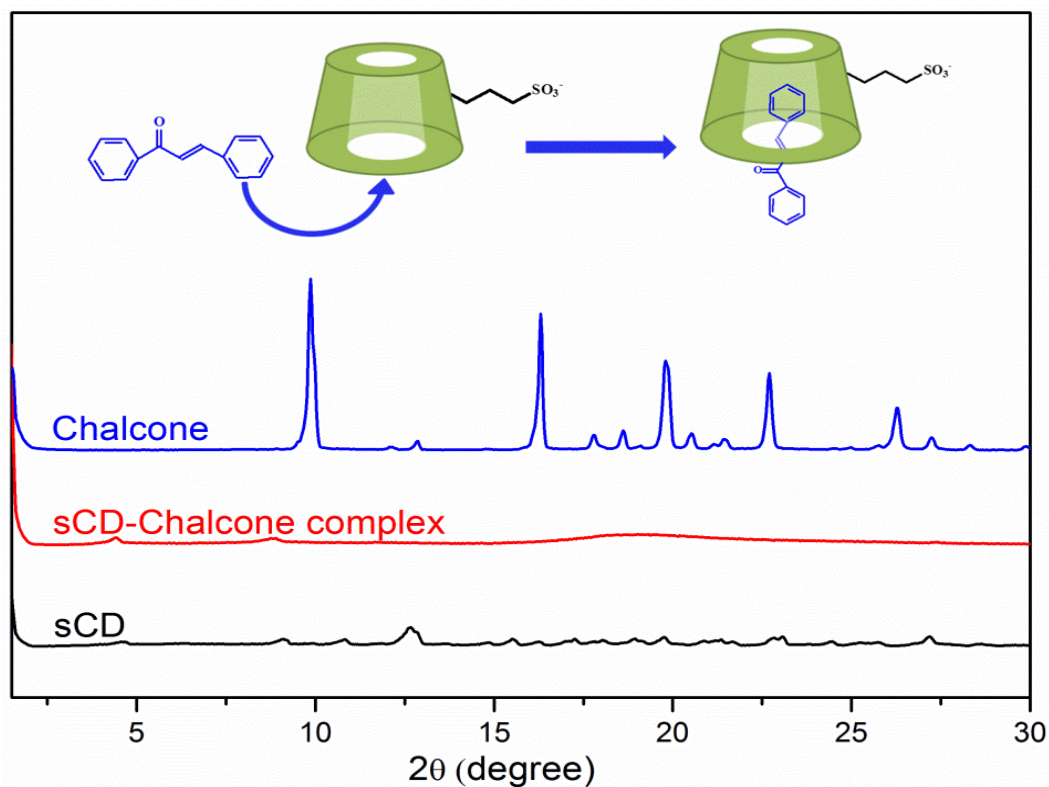
Figure 3-4: WAXS patterns of sCD, chalcone and sCD-chalcone complex

The substantial decrease in crystallinity of sCD-chalcone complex in comparison with chalcone and the appearance of amorphous corona indicates the incorporation of "guest" molecule (chalcone) into the inner hollow cavity of the "host" compound (sCD)(as shown in inset Fig. 3-4).

3-4 Synthesis of functionalized LDHs

In a 1000 ml three-neck round flask equipped with iso-barically funnel, reflux-condenser and pH meter, phytic acid sodium salt (0.03 mol), SDBS (0.04 mol), fCD (0.03 mol) and de-ionized water (300 ml) were charged and stirred until completely dissolved. The nitrate solution containing $Mg(NO_3)_2.6H2O$ (0.2 mol) and $Al(NO_3)_3.9H2O$ (0.1 mol) in 300 ml de-ionized water, was then slowly added to the above mixture with vigorous stirring at a constant pH = 10.0 ± 0.5, adjusted by

simultaneous drop-wise addition of 1 M NaOH solution. The obtained slurry was continuously stirred for 30 min; afterward, it was allowed to age at 75 °C for 18 h.
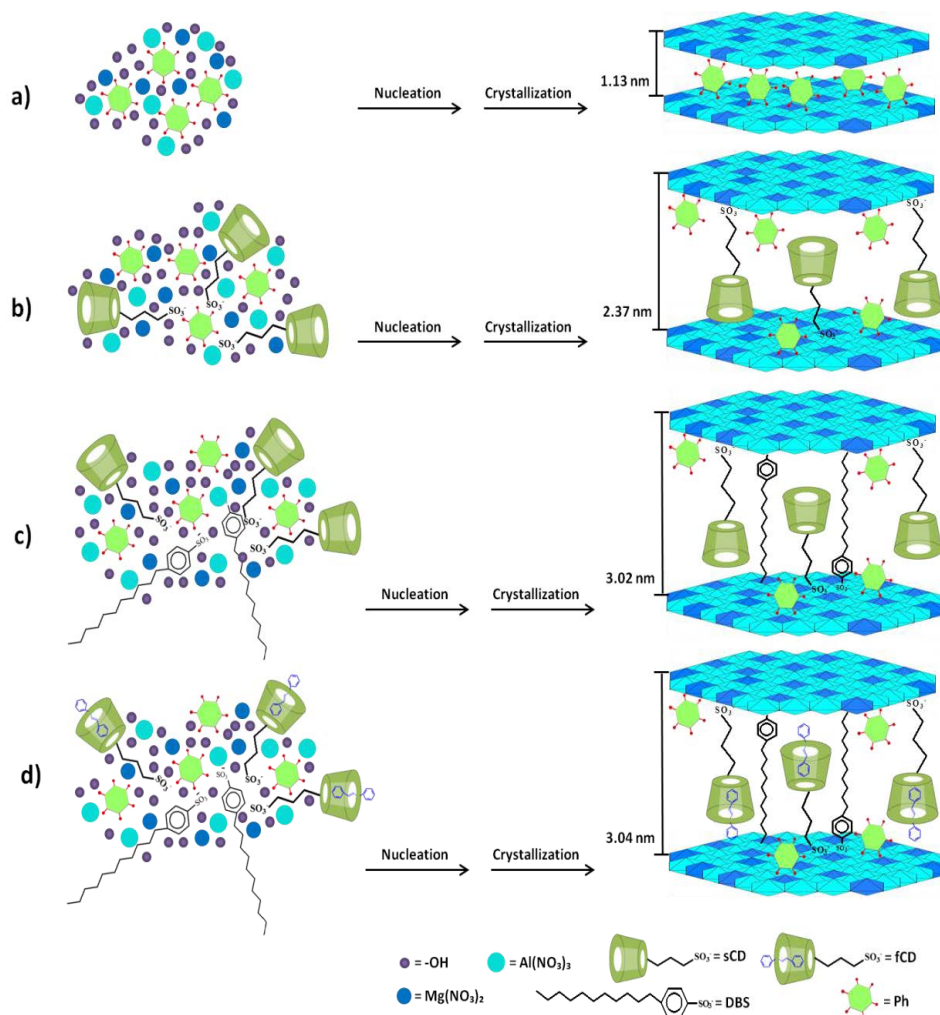
Scheme 3-4: Schematic diagram of anions structure and intercalated functionalized LDHs by one-step synthesis method. (a) Ph-LDH, (b) sCD-Ph-LDH, (c) sCD-Ph-DBS-LDH and (d) fCD-Ph-DBS-LDH.

Finally, the resulting product was filtered and washed thoroughly with de-ionized water until the pH = 7, and then dried at 80 °C until a constant weight which was called fCD-DBS-Ph-LDH. In addition, unmodified LDH (NO_3-LDH), phytic acid sodium salt modified LDH (Ph-LDH), sCD-Ph-LDH and sCD-DBS-Ph-LDH were synthesized using the similar method. The preparation procedures are shown in

scheme 3-4.

3-4-1 Characterization of functionalized LDH

The WAXS patterns of NO_3-LDH, and modified LDHs are shown in Fig. 3-5. In the

WAXS pattern of NO_3-LDH, the first basal reflection (003) peak appears at $2\theta = 9.89°$

corresponding to an interlayer distance of 0.89 nm. For Ph-LDH, the (003) reflection

shifts to $2\theta = 7.30°$ corresponding to the interlayer distance of 1.13 nm.

The co-addition of phytic acid and sCD-chalcone complex provided further increase

to the interlayer distance of LDH to 2.37 nm.
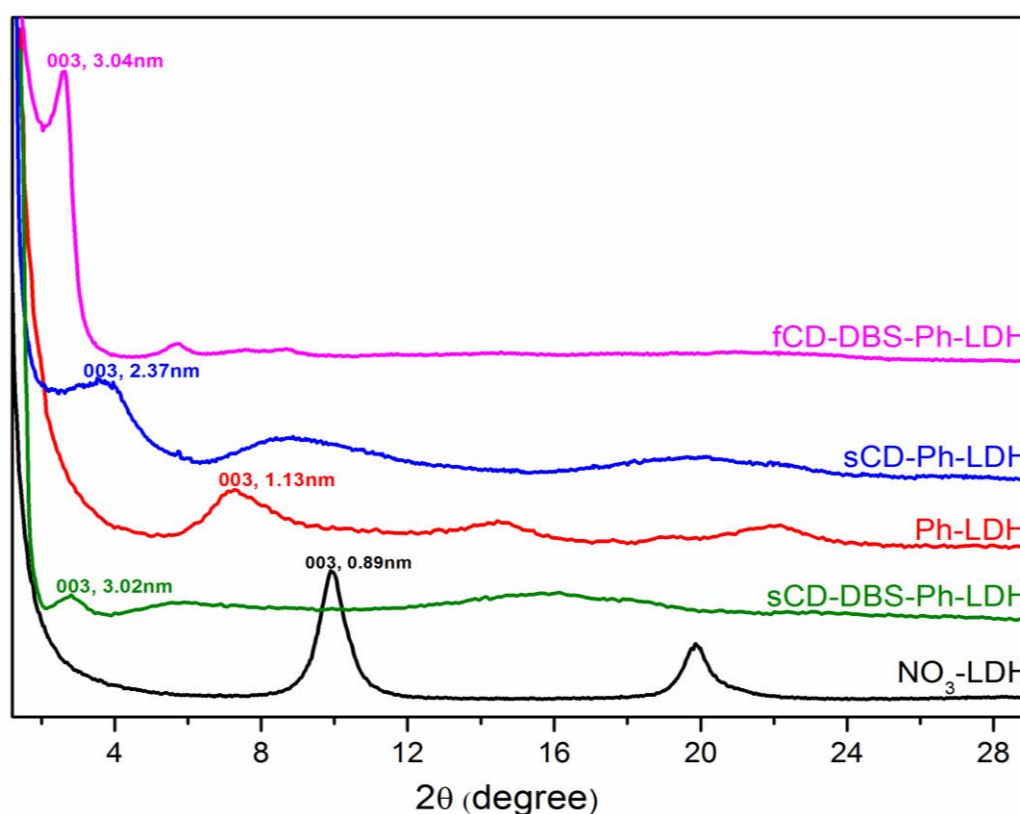
Figure 3-5: WAXS patterns of NO_3-LDH, Ph-LDH, sCD-Ph-LDH, sCD-DBS-Ph-LDH and fCD-DBS-Ph-LDH.

In the case of sCD-DBS-Ph-LDH and fCD-DBS-Ph-LDH the (003) reflection shifts

to a lower reflection angle corresponding to an interlayer distance of 3.02 nm and

3.04 nm, which is about 3.5-fold increase in the interlayer distance compared to that of NO_3-LDH. The enlargement of the interlayer distance is caused by the relatively long molecular chains of the sCD/fCD and DBS. DBS is possessing relatively larger molecular size (more than 2 nm) compared to the size of NO_3^- (around 0.1 nm) [9]. These results demonstrate that multi-modifier system is effective in enlarging the interlayer distance of LDHs.

3-5 Fe_3O_4 decorated CD based multimodiers modified LDH

The Fe_3O_4 nanoparticles were prepared as follows: 0.85 ml of 12.1 N HCl was mixed with 25 ml of distilled, deoxygenated water, and then 5.2 g of $FeCl_3$ and 2.0 g of $FeCl_2$ were dissolved in the above solution with stirring. The resultant solution was added drop-wise into 250 ml of 1.5 M NaOH solution under vigorous stirring. After the formation of the black precipitate, the supernatant was removed. De-ionized water was added to the precipitate and the solution filtered after centrifugation at 4000 rpm and this process repeated for three times. Then, 500 ml of 0.01 M HCl solution was added to the above precipitate with stirring to neutralize the negative charges on the nanoparticles. The slurry was filtered and washed with de-ionized water. The filtrate was then dried in an oven at 80 °C until a constant weight was achieved.

Calcinated LDH (c-LDH) was prepared by exposing unmodified LDH to 400 °C for 3 h in a muffle furnace. The resultant product was mixed with dried Fe_3O_4 powders (weight ratio of c-LDH/Fe_3O_4 = 10/1 by weight) using planetary mill (Fritsch Pulverisette, Germany) (speed = 300 rpm, 20 minutes milling in three cycles with the

intervals of 40 minutes). The above mixture was introduced into 200 ml of Toluene

and vigorously stirred for 30 minutes, exposed to high power ultra-sonication

(Bioblock, Vibracell 75115, France) with the amplitude of 70% for the cycles of 10

seconds running and 5 second intervals for the total time of 20 min and

simultaneously exposed to micro wave irradiation by using a domestic use oven at

800 W and micro wave frequency of 2450 MHz for the cycles of 5 seconds running

and 180 second intervals for the total time of 5 minutes.
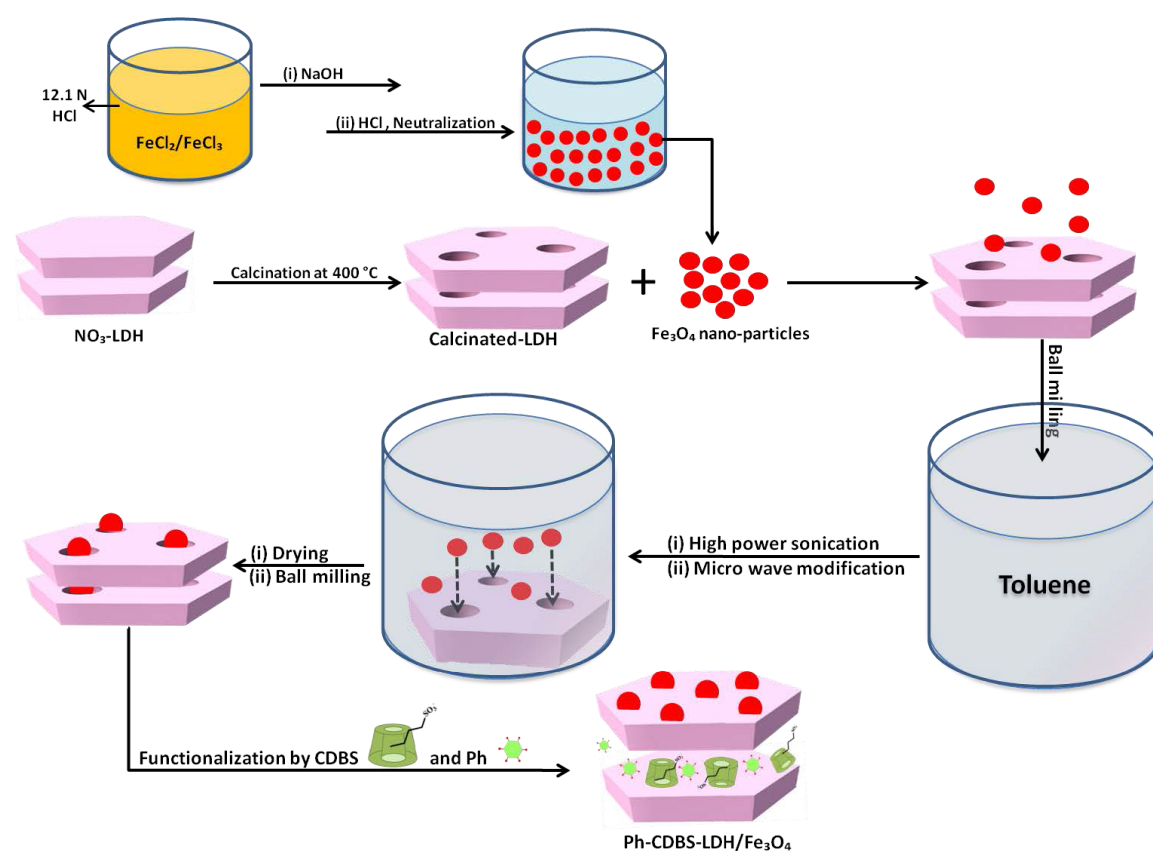
Scheme 3-5: Schematic illustration of Fe_3O_4 decorated orango-modified LDH hybrid.

The colloidal emulsion was filtered and the filter cake was dried at oven under 90 °C

for 8 h. The product was grinded and added to a 200 ml aqueous solution with a

combination of CDBS (0.05 mol) and Ph (0.05 mol) under vigorous stirring at 45 °C

for 12 h. The product was finally milled by a planetary mill with the maximum speed

of 300 rpm in three cycles, 20 minutes milling with 40 minutes interval. Overall scheme of the preparation procedures are shown in scheme 3-5.

3-5-1   Structural characterization

To determine the particle size of Fe_3O_4 nanoparticles, a small amount of Fe_3O_4 nanoparticles were suspended in the solution contained in a cylindrical cell. The suspension was sonicated for at least 20 min to assist with the dispersion of particles prior to the measurements. The particle size distribution of the measured particle size is shown in Figure 3-6. The results indicated that the size distribution of the Fe_3O_4 nanoparticles is from 5 to 9 nm.
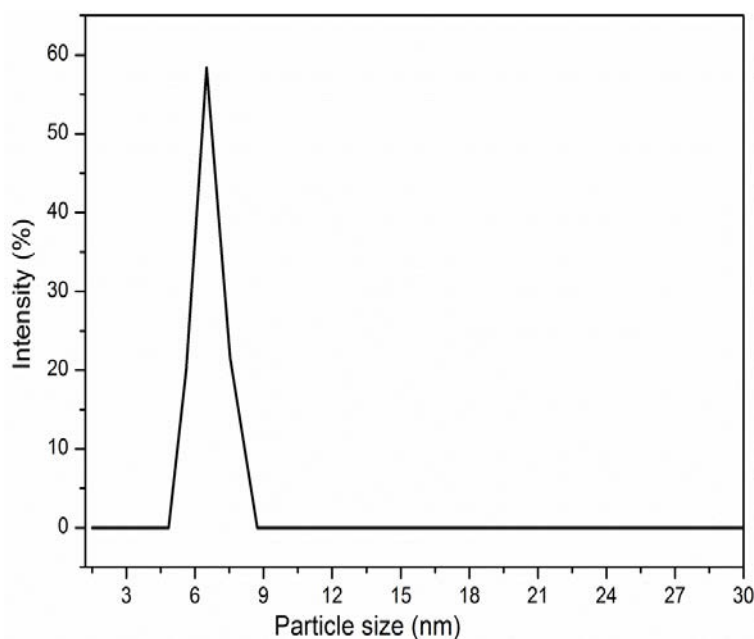
Figure 3-6: Particle size distribution of Fe_3O_4 nanoparticles.

The textural and pore size distribution properties of unmodified LDH and calcinated LDH samples were analyzed by nitrogen adsorption–desorption measurement. Both the unmodified LDH (Fig. 3-7a) and calcinated LDH samples (Fig. 3-7b) exhibit a

typical isotherm with a H1 and H3 type hysteresis loop, indicating the presence of

mesopores in the both samples. These results correspond well with the uniform

distribution of pore size as shown in Fig. 4-5c and 4-5d. The pore size distribution of

the unmodified LDH and calcinated LDH is listed in Table 3-2.

The pore diameter distribution of unmodified LDH covers a narrow range, with the

pore size average of about 15 nm which are corresponding to the voids and empty

spaces between the platelets. After the calcination at 400 °C, C-LDH sample showed

an increase in the trend for the specific surface area, pore size average and total pore

volume.

Table 3-2: Physicochemical properties of the unmodified LDH (NO_3-LDH) and calcinated
LDH

Sample	BET ($m^2.g^{-1}$)	Specific Volume ($cm^3.g^{-1}$)	BJH (nm)
NO_3-LDH	14.3	0.056	15.7
C-LDH	228.3	0.520	9.1

This may be resulted by the shrinking of the LDH crystallites during the calcinations

and hence, formation of a large number of the pores in the microcrystallites [25].

The WAXS patterns of NO_3-LDH and modified LDHs are shown in Fig. 3-8.

NO_3-LDH exhibits the characteristic peaks at the 2θ value of 9.95° and 19.90°, which

are corresponding to (003) and (006) reflections. According to the Bragg's equation,

the first basal reflection (003) at 2θ= 9.95° indicates an interlayer distance of 0.88

nm.

After thermal treatment, the calcinated LDH shows no visible characteristic peaks,

suggesting the destruction of the crystalline structure. For Fe_3O_4@LDH hybrid, the

characteristic peaks of LDH become very weak, while those of the Fe_3O_4

nanoparticles are appeared in the range of 30° to 45° (Figure 3-9c). In the previous

study [26], the reflection peaks at low angle regions disappear when the size of the

Fe_3O_4 nanoparticle is around 7 nm. In the case of $Fe_3O_4@Ph-CDBS-LDH$ hybrid, the

positions of (003) shift to $2\theta= 3.75°$, indicating interlayer distance of 2.36 nm.
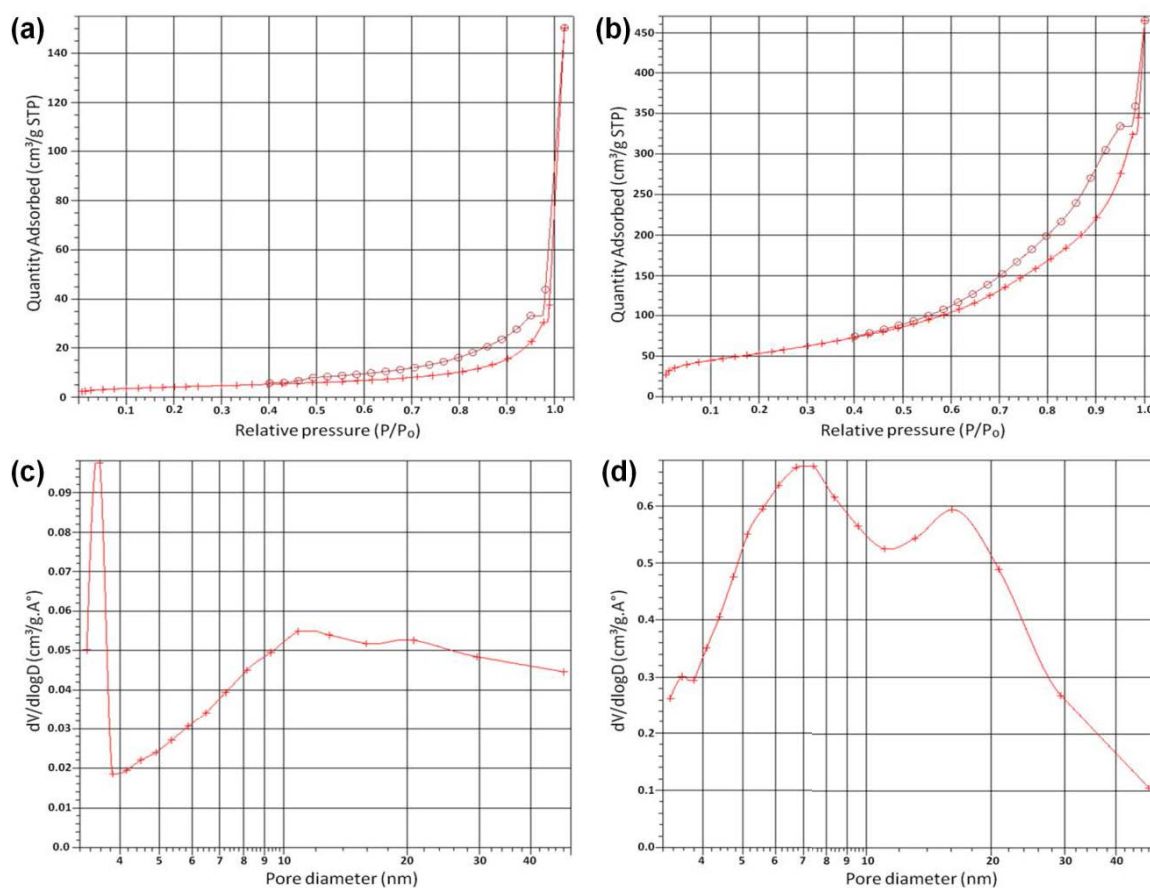
Figure 3-7: Nitrogen sorption isotherms of unmodified LDH (a) and calcinated LDH (b); Pore size distributions of unmodified LDH (c) and calcinated LDH (d).

The obtained results show that the interlayer distance of the $Fe_3O_4@Ph-CDBS-LDH$

hybrid is increased by around 2.6-fold compared with that of NO_3-LDH. The

enlargement of the interlayer distance could be attributed to the bigger molecular size

of the CDBS compared to NO_3^-.

The molecular size of CDBS is more than 0.8 nm which is relatively larger molecule

compared to the size of NO_3^- (around 0.1 nm) [27]. The morphological features of the

Fe₃O₄@Ph-CDBS-LDH hybrid were investigated by TEM, and the micrographs were

shown in Fig. 3-9d.

TEM (Tecnai T20, FEI Company) analysis gave high magnification and detailed

vision of the morphology and microstructures of the composites.
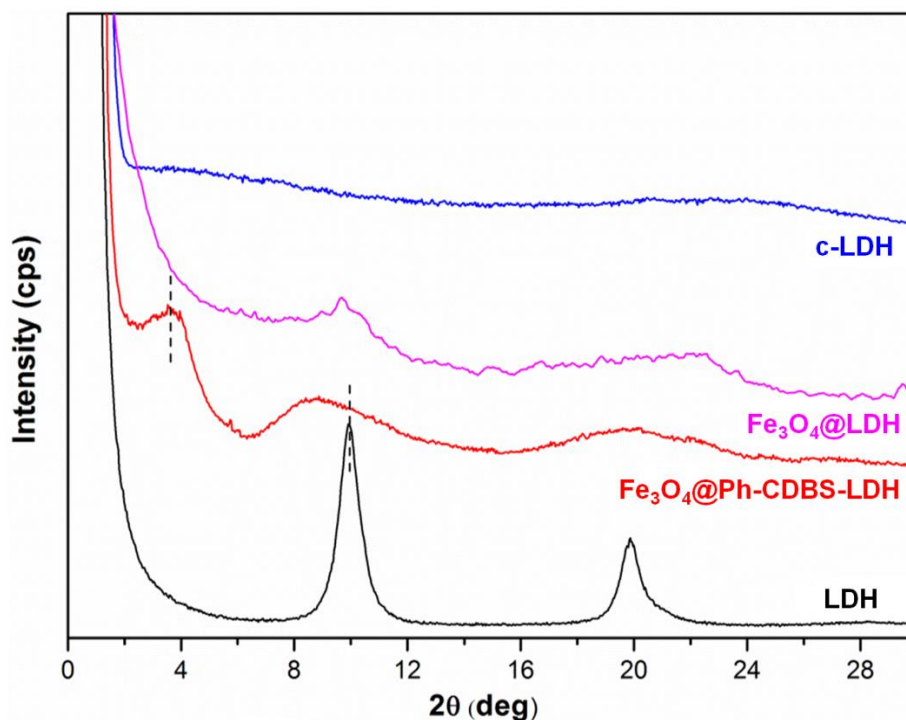
Figure 3-8: WAXs patterns of NO₃-LDH, Fe₃O₄-LDH, Ph-CDBS -LDH and
Fe3O4@Ph-CDBS-LDH nano-particles

Samples were prepared with a Leica ultramicrotome at room temperature.

Ultramicrotomy ultrathin sections had a thickness of 50 nm. 1% uranyl acetate was

added as a contrast agent.

TEM analysis was carried out at 200 kV in Bright Field imaging mode. It can be

observed that the Fe₃O₄@Ph-CDBS-LDH hybrid has a typical geometry of plate-like

with relatively rough surface due to the expansion of the basal spacing after the ion

exchange. The EDX analysis confirms the decoration of Fe₃O₄ nano-particles on the

LDH surfaces (Fig. 3-9 d). The dispersion state of the Fe_3O_4 nano-particles on the LDH layers was also studied by TEM. TEM images (Fig. 3-9 a and b) reveal that the Fe_3O_4 nano-particles are well decorated on the surface of the LDH plate. The black dots are Fe_3O_4 nano-particles and their size is below 10 nm.
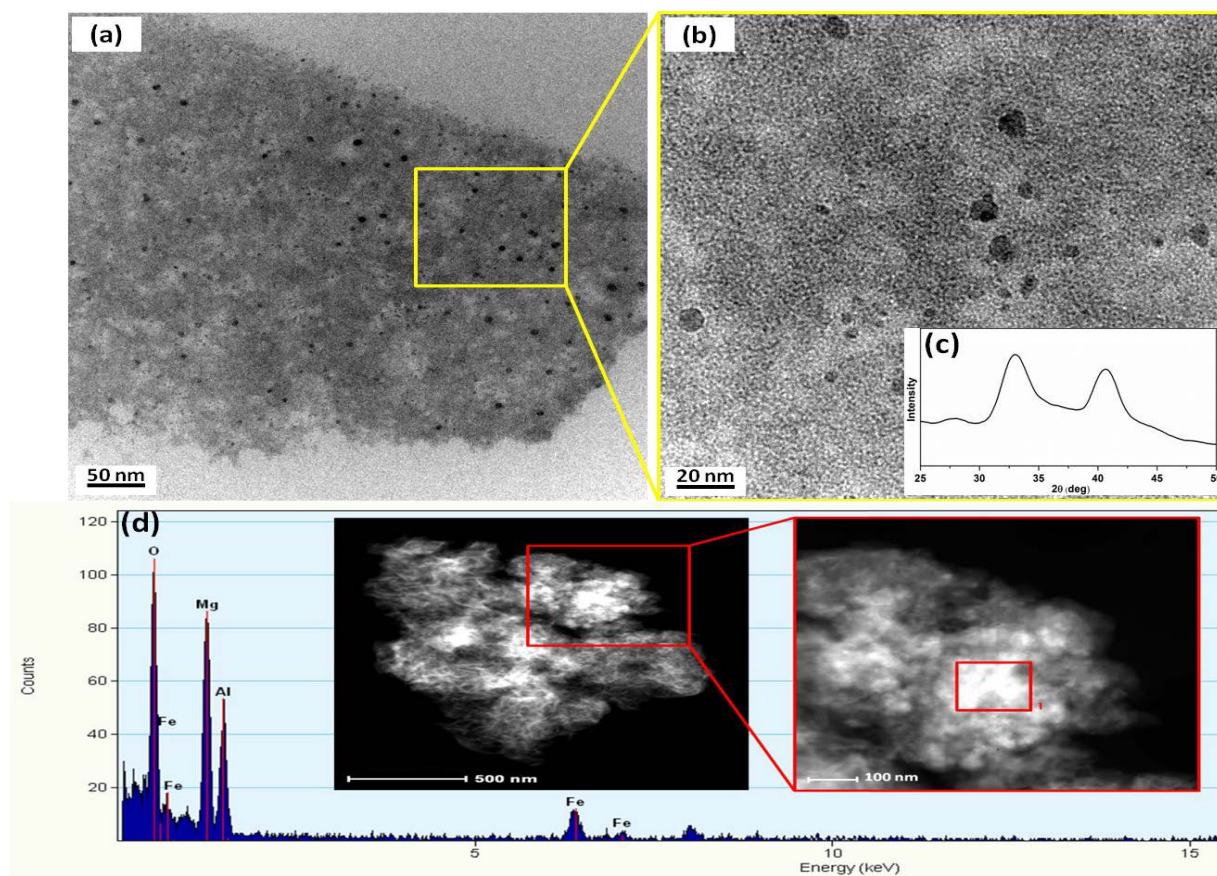
Figure 3-9: (a, b) TEM micrographs and in low and high magnification, (c) WAXs pattern of Fe_3O_4 nano-particles and (d) EDX analysis of Fe3O4@Ph-CDBS-LDH hybrid.

4 CD based multimodifiers modified LDH/Epoxy nanocomposits: preparation, characterization, fire behaviors and mechanical properties

4-1 Introduction

Epoxy resins play a very important role in the development of polymer matrix micro/nano-composite materials due to their overall superior mechanical properties [114, 115]. The addition of nano-scale inorganic fillers has recently attracted great interest due to its potential to improve the properties of pristine epoxy with relatively low filler content [116,117 and 118]. Some researches on LDH addressed their potential use as non-halogenated, non-toxic flame-retardant nanofiller for polymers [119,120]. Costa et al. [121] reported on the addition of a high content (>50 wt.%) of hydrotalcite (naturally occurring LDH) in order to obtain flame-resistant compositions. Such high concentrations often provide industrially acceptable flammability ratings, such as UL 94 V0, but the mechanical properties of the final composites are severely influenced. To obtain enhanced flame-retardancy in LDH nanocomposites, high degree of dispersion of nanofillers throughout the epoxy matrix is also necessary. In this context, new method of improving dispersion of metal hydroxide nano-layers on epoxy matrices regards the organic modification of the LDH and two-step mixing was proposed. On this context, the aim of this work is to incorporate very low loading of the modified LDHs into the epoxy resin to produce exfoliated or intercalated epoxy nanocomposites with improved flame-retardant and mechanical properties. The morphology, thermal stability, flame retardant and mechanical properties of these composites were investigated systemically.

4-2 Sample preparation

A fixed weight fraction of unmodified LDH (NO$_3$-LDH) or functionalized LDH (T-LDH, sCD-LDH and sCD-DBS-T-LDH) was used for the preparation of LDH/epoxy nanocomposites. In order to achieve a satisfactory dispersion state, two-step mixing method was applied. Firstly, LDH or modified LDH was incorporated into the epoxy matrix using a refined three-roll mill (EXAKT 80E, Germany) for 30 min; secondly, the mixture was dissolved in acetone and exposed to ultra-sonication for 20 min at 60 °C, and then acetone was removed by vacuuming at 110 °C to obtain a viscous mixture. The mixture was then heated to 180 °C in order to complete the chemical reaction between taurine and epoxy chains. Subsequently, the mixture was cooled down to 120 °C followed by adding DDS to the above mixture and stirring for 15 min until DDS totally dissolved. In order to remove the bubbles, the mixture was placed into the vacuum oven at 115 ºC for 5 minutes and then immediately poured into the pre-heated PTFE moulds. The curing procedure was set as 150 °C for 1 hour, 180 °C for 2 hours and 200 °C for 2 hours. Following this procedure, NO$_3$-LDH/EP, sCD-LDH/EP, T-LDH/EP and sCD-DBS-T-LDH/EP were prepared respectively.

4-3 Characterization

4-3-1 Structural characterization of LDH/EP nanocomposites

X-ray diffraction analysis

The structural morphology of layered nano-filler/epoxy nanocomposite was characterized by X-ray scattering patterns in order to determine the microstructures. Fig. 4-1 shows the WAXS patterns of pure epoxy matrix, NO_3-LDH/EP, T-LDH/EP, sCD-LDH/EP and sCD-DBS-T-LDH/EP composite. Pure EP has a broad and weak diffraction peak centered at a 2θ value of 17.3°, due to characteristics of an amorphous epoxy. NO_3-LDH/EP composite shows an intense diffraction peak at a 2θ value of 10.1° corresponding to an inter-gallery spacing of 0.88 nm, indicating the presence of the ordered structure of LDH in the epoxy matrix. T-LDH/EP exhibits a similar WAXS profile to NO_3-LDH/EP.
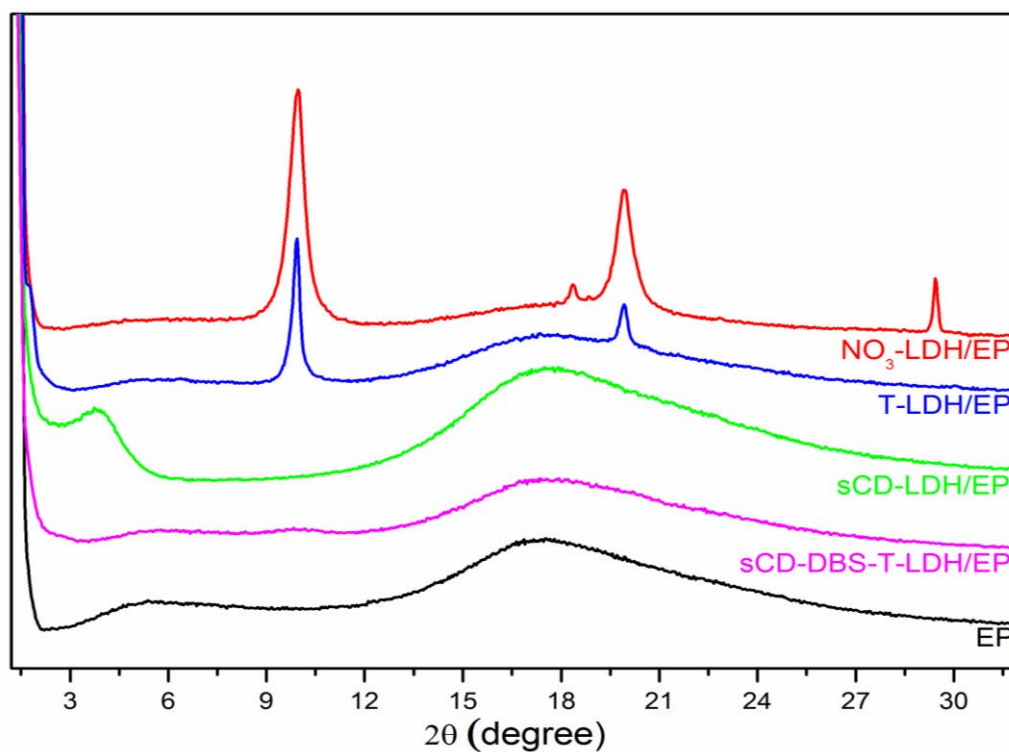
Figure 4-1: WAXS patterns of pure EP, NO_3-LDH/EP, T-LDH/EP, sCD-LDH/EP and sCD-DBS-T-LDH/EP composites

As discussed aforementioned, the inter-gallery spaces of NO_3-LDH and T-LDH are not large enough to allow the diffusion of the resin/curing agent mixture into the inter-layers. For sCD-LDH/EP composite, a weak diffraction peak at a 2θ value of 3.8º is observed corresponding to an inter-gallery spacing of 2.32 nm, suggesting the swelling of LDH platelets upon polymerization. In the case of sCD-DBS-T-LDH/EP composite, no visible reflection peaks are observed, indicating highly exfoliated and/or well intercalated LDH platelets within the epoxy resin [27]. However, this conjecture must also be confirmed by other techniques such as TEM observation.

Transmission Electron Microscopy (TEM)

TEM was employed to provide additional information in order to verify the results obtained from the WAXS analysis as well as to directly observe the dispersion state of LDH within the epoxy matrix and selected images shown in Fig. 4-2. Low and high magnification TEM images of NO_3-LDH/EP composite (Fig. 4-2a and 4-2d) show that the large aggregates of NO_3-LDHs with the average size of >500 nm are formed. In the low magnification TEM image of T-LDH/EP composite (Fig. 4-2b), similar phenomenon is observed; while at the high magnification TEM image (Fig. 4-2e), the ordered structure of LDH is clearly seen. This is the reason why in the WAXS patterns of NO_3-LDH/EP and T-LDH/EP, the (003) reflection peak could be still observed. The dispersion state of sCD-DBS-T-LDH/EP is quite different from that of NO_3-LDH/EP and T-LDH/EP. The low magnification TEM image of sCD-DBS-T-LDH/EP (Fig. 4-2c) reveals a relatively better dispersion of LDH in the

matrix. The high resolution image of sCD-DBS-T-LDH/EP (Fig. 4-2f) indicates a homogeneously disordered microstructure, which is in agreement with the WAXS observations.
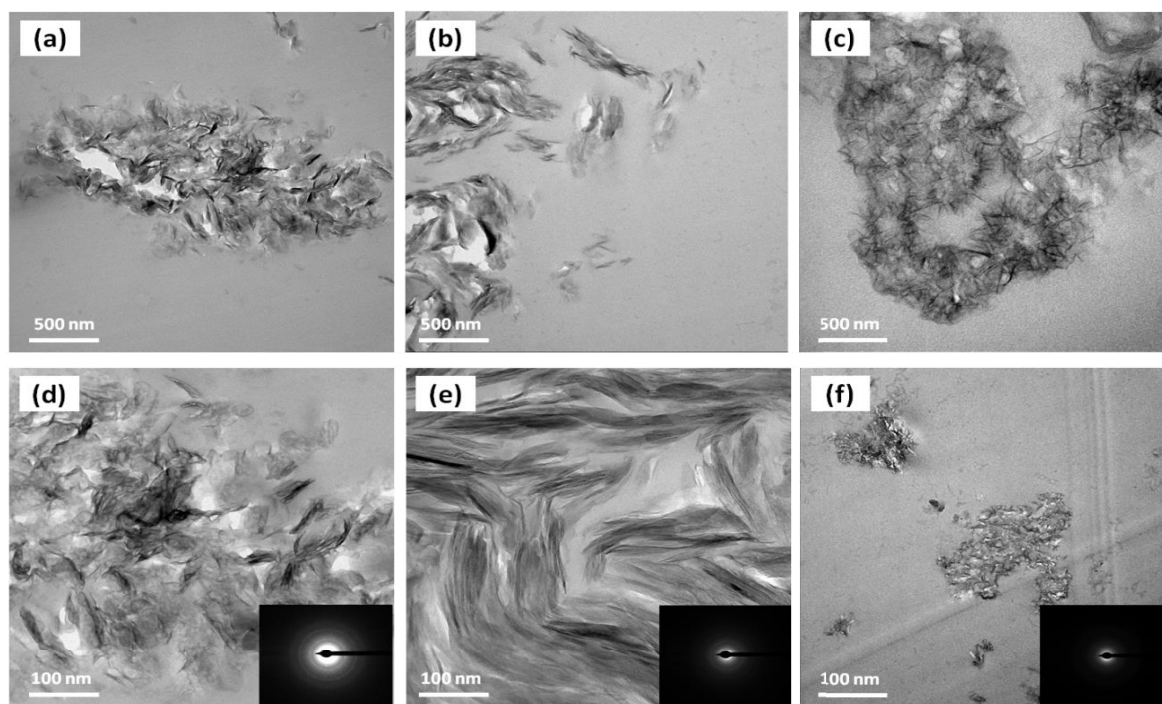
Figure 4-2: TEM images and diffraction patterns of NO_3-LDH/EP (a, d), T-LDH/EP (b, e) and sCD-DBS-T-LDH/EP (c, f). The bottom row is at high magnification.

As can be seen in Figure 4-2, for the TEM images of the NO_3-LDH/EP platelets and their selected area electron diffraction (SAED) patterns (Fig. 4-2 d), large number of dotes around the pointer could be observed, showing existence of large poly-crystalline structures. But as can be seen in the TEM diffraction image of sCD-DBS-T-LDH/EP (Fig. 4-2f), there is no dote around the pointer, which can represents quite small crystallites and excellent exfoliated nano- particles.

4-3-2 Thermal Stability of epoxy nanocomposites

Thermogravimetric analysis (TGA) of nanoparticles formulations and LDH/epoxy nanocomposites were performed on a TA universal analysis (TGA- Q50, USA) obtained in a N_2 atmosphere and the results are presented in Table 4-1. Thermogravimetric analysis (TGA) was carried out using a Q50 (TA Instruments) thermo-analyzer instrument at a linear heating rate of 10 °C min^{-1} under a nitrogen flow and the samples were pre-heated at 160 °C under the vacuum conditions prior to TGA measurement. The theoretical TG curve was computed by linear combination between the TG curves of neat EP and LDH. The formula is as follows:

$$W_{th}(T)_{LDH/EP} = x \times W_{exp}(T)_{EP} + y \times W_{exp}(T)_{LDH}, x + y = 1$$

, where $W_{exp}(T)_{EP}$: experimental TG curve of the pure EP; $W_{exp}(T)_{LDH}$: experimental TG curve of LDH; x and y are the weight percentages of the EP and LDH in the composites, respectively.

The results revealing that the thermal stability of functionalized LDH had lower initial degradation temperature ($T_5\%$) compared with that of unmodified LDH. This was caused by the introduction of organic structures in the modifiers. The thermal stability of pure EP and epoxy composites was investigated by thermogravimetric analysis, as shown in Fig. 4-3. The temperature at which the mass loss is 5% ($T_{5\%}$) and the temperature at which the maximum mass loss rate occurs (T_{max}) are listed in Table 4-1. Pure EP shows a main degradation stage ranging from 380 to 500 ºC which is attributed to the decomposition of macromolecules networks. All the epoxy composites exhibit a similar one-stage degradation process. However, $T_{5\%}$ of all the epoxy composites is lowered compared to that of pure EP, indicating the

multifunctional LDHs causes the earlier initial decomposition of composites. T_{max} of all the epoxy composites shows the similar tendency.

Figure 4-3: TGA curves of pure EP and epoxy composites under N_2 at heating rate of 10°C/min

Table 4-1: TGA results of LDH, organo-modified LDH and their epoxy composites

Sample	$T_{5\%}$ (°C)	T_{max} (°C)	Residue yield at 800°C (wt %)	
			Calculated	Experimental
NO$_3$-LDH	305	415	--	54.6
T-LDH	195	412	--	54.0
sCD -LDH	267	369	--	49.4
sCD-DBS-T-LDH	201	462	--	43.7
EP	397	425	--	14.1
NO3-LDH/EP	386	413	16.5	13.7
T-LDH/EP	376	405	16.4	14.9
sCD-LDH/EP	365	391	16.2	19.9
sCD-DBS-T-LDH/EP	358	400	15.8	19.1

The incorporation of the multifunctional LDHs leads to an increment in the char yield at 700 ºC. Pure EP has 14.9 % residue at 700 °C, whereas T-LDH/EP, sCD- LDH/EP

and sCD-DBS-T-LDH/EP composites have 17.9%, 20.8% and 20.4% residues, respectively, at 700 °C. Furthermore, the experimental char residue of NO_3-LDH/EP is lower than the calculated one, which could be ascribed to that nitrate might catalyze the decomposition of the EP matrix; while for sCD-LDH/EP and sCD-DBS-T-LDH/EP, the experimental char residue is higher than the calculated one, suggesting the existence of synergism among the modifiers.

4-3-3 Flammability

The LOI values were carried out using an Oxygen Index instrument (Fire Testing Technology, UK) according to ASTM D 2863-97. The sample dimensions were 130 mm× 6.5 mm× 3.2 mm; vertical burning test was carried out by a burning chamber (UL-94, Fire Testing Technology, UK) with the sample dimension of 127 mm× 12.7 mm× 3.3(±0.2) mm according to ASTM D 3801standard.

Pure epoxy exhibits a LOI value of 23.0% and is not classified in the UL-94 vertical burning test. When NO_3-LDH is added, the LOI value goes up to 25.2%, but this formulation still shows no rating in the UL-94 test. Incorporating T-LDH or sCD-LDH improves the LOI value slightly and both of them still cannot pass the UL-94 V0 rating. Adding sCD-DBS-T-LDH into epoxy results in a great improvement in fire resistance and the UL-94 V0 rating is achieved in vertical burning test (Table 4-2). The residual bars of epoxy composites at the end of UL-94 test are shown in Figure 4-4. It is clearly seen that NO_3-LDH/EP and T-LDH/EP burn throughout the bars, whereas sCD- LDH/EP and sCD-DBS-T-LDH/EP shows a self-extinguishment. From the above results, a synergistic effect between the

modifiers is demonstrated.

Table 4-2: LOI and UL94 test results

Sample	LOI (%)	UL-94	Observation
Pure EP	23.0	No rating	Fire with Sooty flame
NO_3- LDH/EP	25.2	No rating	Fire with Sooty flame
T-LDH/EP	24.0	No rating	Fire with Sooty flame
sCD-LDH/EP	23.5	V-2	Fire with Sooty flame
sCD-DBS-T-LDH/EP	26.8	V-0	Extinguished immediately

The cone calorimeter tests were carried out on a cone calorimeter (FTT, UK) by following ISO 5660-1. The squared specimens (100 mm × 100 mm × 4 mm) were wrapped with aluminium foil and placed in a frame without grid. The specimens were horizontally irradiated at a heat flux of 50 kW m^{-2}, corresponding to a medium fire scenario.
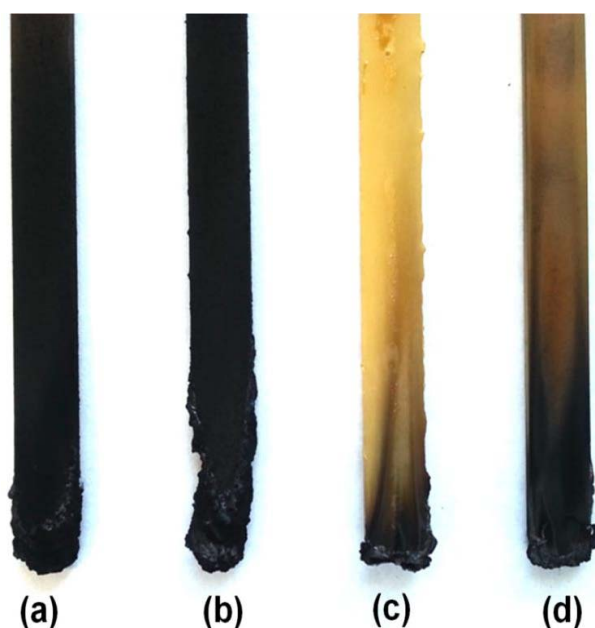
Figure 4-4: Photo of bars after UL-94 test of (a) NO_3-LDH/EP, (b) T-LDH/EP, (c) sCD-LDH/EP and (d) CD-DBS-T-LDH/EP.

Fig. 4-5 shows the heat release rate (HRR), total heat release (THR) and total smoke production (TSP) versus time curves of pure EP and its nanocomposites. Some

important parameters obtained from the cone calorimeter tests, such as the time-to-ignition (TTI), residual mass and the fire growth rate index (FIGRA), are also summarized in Table 4-3. From Fig. 4-5a, it can be seen that pure epoxy burns very rapidly after ignition and the peak heat release rate value is 931 kW/m^2. As expected, incorporating NO$_3$-LDH into epoxy resins enables the peak heat release rate decrease to 621 kW/m^2. In case of the functionalized LDHs, the peak HRR decreased significantly to 491 and 525 kW/m^2 for T-LDH/EP and sCD-LDH/EP, respectively. Furthermore, the peak HRR of sCD-DBS-T-LDH/EP exhibits a further decrease to 318 kW/m^2 corresponding to a 66% reduction. The best fire retardant properties of sCD-DBS-T-LDH/EP could be attributed to two aspects: firstly, the largest inter-layer distance of sCD-DBS-T-LDH leads to the good dispersion of nano-fillers in epoxy matrix; secondly, sCD species improve the char yield of epoxy composites during combustion. The THR curves (Fig. 4-5b) show similar trend as HRR, and the THR value of T-LDH/EP, sCD-LDH/EP and sCD-DBS-T-LDH/EP is significantly reduced by 8.6%, 35.8% and 34.6%, respectively, compared to that of pure EP. The significant reduction in THR means more epoxy chains participate in the carbonization process rather than go to the gas phase serving as "fuel". This is also evidenced by the increased residual mass (as listed in Table 4-3). With regard to the TSP, for pure EP remains the highest among all the samples. As can be seen from Fig. 4-5c, all the samples containing flame retardant additives show lower TSP compared to pure EP. The decrease in smoke formation in epoxy composites is probably due to the reduced amount of epoxy converted into organic volatiles, since the organic volatiles are the major source of smoke particles [29, 30].

From Table 4-3, it can be found that incorporation of sCD-LDH or sCD-DBS-T-LDH decreases the time-to-ignition (TTI) of the composites, owing to the thermally unstable organic modifiers. The FIGRA is calculated from the ratio of PHRR and time to PHRR for all samples, as listed in Table 4-3. The FIGRA value of pure EP is 7.16 kW/(m^{2}s), while that of NO$_3$-LDH/EP, T-LDH/EP, sCD-LDH/EP and sCD-DBS-T-LDH/EP is 4.97, 2.89, 3.18 and 2.27 kW/(m^{2}s), respectively. The dramatically reduced FIGRA means the low fire hazard of the material.

The detailed data is shown in Table 4-3, Compared with pure EP, NO$_3$-LDH/EP and T-LDH/EP nanocomposite burns slowly and the peak HRR decreased significantly from 931 kW/m^2 to 621 kW/m^2 and 491 kW/m^2, respectively, and the reduction in peak of HRR is 33% and 47% and in case of sCD-LDH/EP and sCD-DBS-T-LDH/EP nanocomposites, they burns slightly faster. As it can be seen, in the case of sCD-LDH/EP the peak HRR decreased from 931 kW/m^2 to 525 kW/m^2. sCD-LDH/EP and sCD-DBS-T-LDH/EP nanocomposites also showed considerable differences in the total heat release (THR) curves presented in Fig. 4-5b, most importantly showing that the sCD-DBS-T-LDH/EP nanocomposite reduced the total amount of volatile (fuel) available for combustion (318 kW/m^2), and the reduction in peak of HRR is 44% and 66%, respectively. At the end of burning, pure EP has released a total heat of 81 MJ/m^2, the NO$_3$-LDH/EP has released the same amount of heat (80 MJ/m^2), whereas only 53 MJ/m^2 has been released by the sCD-DBS-T-LDH/EP nanocomposite. This latter significant difference results from the addition of 6 wt% modified-LDH to the polymer, and indicates that a part of the

polymer was not completely burnt because while burning, an intumescing char was formed on the surface of the matrix which made a thermal insulation and stimulate the extinguishment of the flame and prevented combustible gases from feeding the flame, and also separated oxygen from burning materials [35]. This is in agreement with the reduced mass loss, as presented in Fig. 4-3.

From table 4-3, the sCD-DBS-T-LDH/EP nanocomposite shows a significantly higher char yields correspond to the lower THR. This indicates a condensed phase mechanism for the fire retardancy of sCD-DBS-T-LDH/EP. It is particularly interesting to note that this enhanced char performance was more obvious in the TG experiments, and also was clearly visible under the more severe conditions of the cone calorimeter at 50 kW/m^2. More char residues for sCD-DBS-T-LDH/EP nanocomposite might be related to the formation of the nanostructure which can reduce the transfer of heat and fuel in the burning process, at the same time, the metal in the nano-particles might catalyze the reaction leading to graphitization. More direct evidences could be found in the residues remaining after the cone calorimeter test.

Table 4-3: Combustion parameters obtained from cone calorimeter.

Sample	TTI (s)	pHRR (kW/m^2)	Time to pHRR (s)	FIGRA (kW/m^{2}s)	Residual mass (%)
Pure EP	58	931	130	7.2	14.3
NO$_3$- LDH/EP	65	621	125	4.9	21.**4**
T-LDH/EP	61	491	170	2.9	26.0
sCD-LDH/EP	37	525	165	3.2	24.0
sCD-DBS-T-LDH/EP	40	318	140	2.3	30.0

For Pure EP, there were very less chare residue after burning, for the NO$_3$-LDH/EP and T-LDH/EP samples intumescence but very fluffy and weak chare residues

illustrated, while for the sCD-LDH/EP and sCD-DBS-T-LDH/EP samples intumescence and stronger chare could be observed. The consolidated and thick char layer form a barrier which significantly reduced heat transfer and air incursion and thus enhances the flame retardant performance.

All the above data (HRR, PHRR, THR and Mass loss) indicated strongly that the heat transfer between the flame and the matrix in sCD-DBS-T-LDH/EP nanocomposite was decreased significantly due to the protection of the efficient char layer, so the flame retardancy was improved significantly.
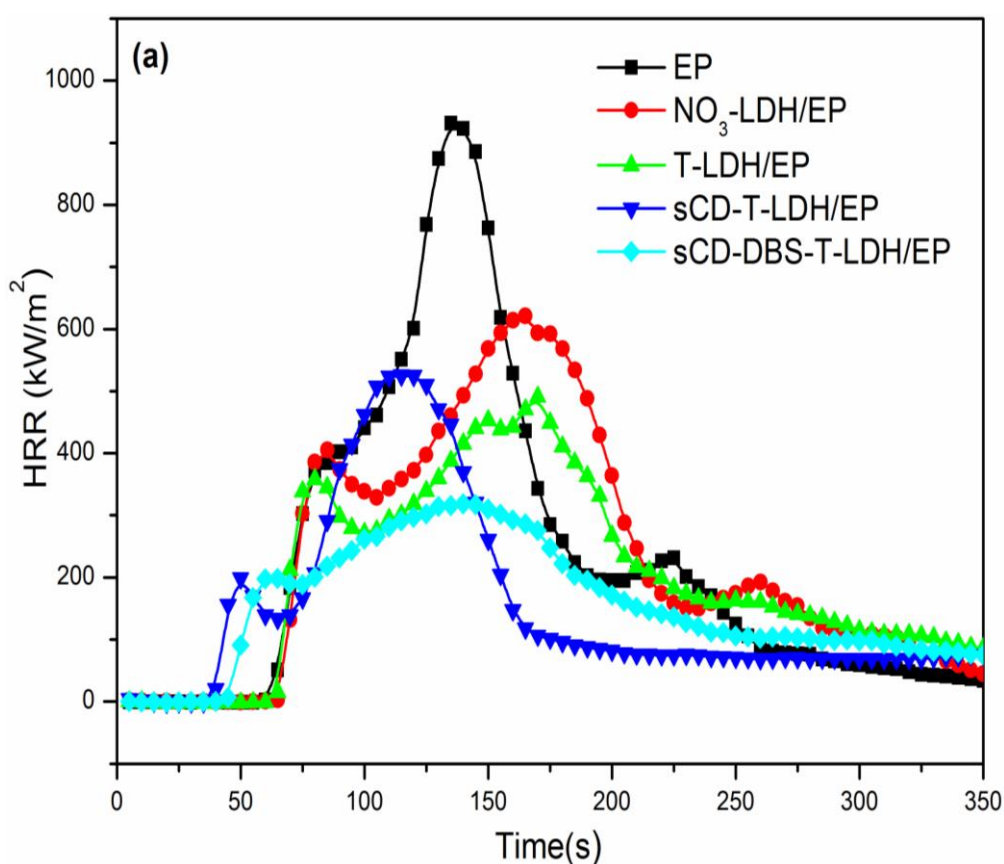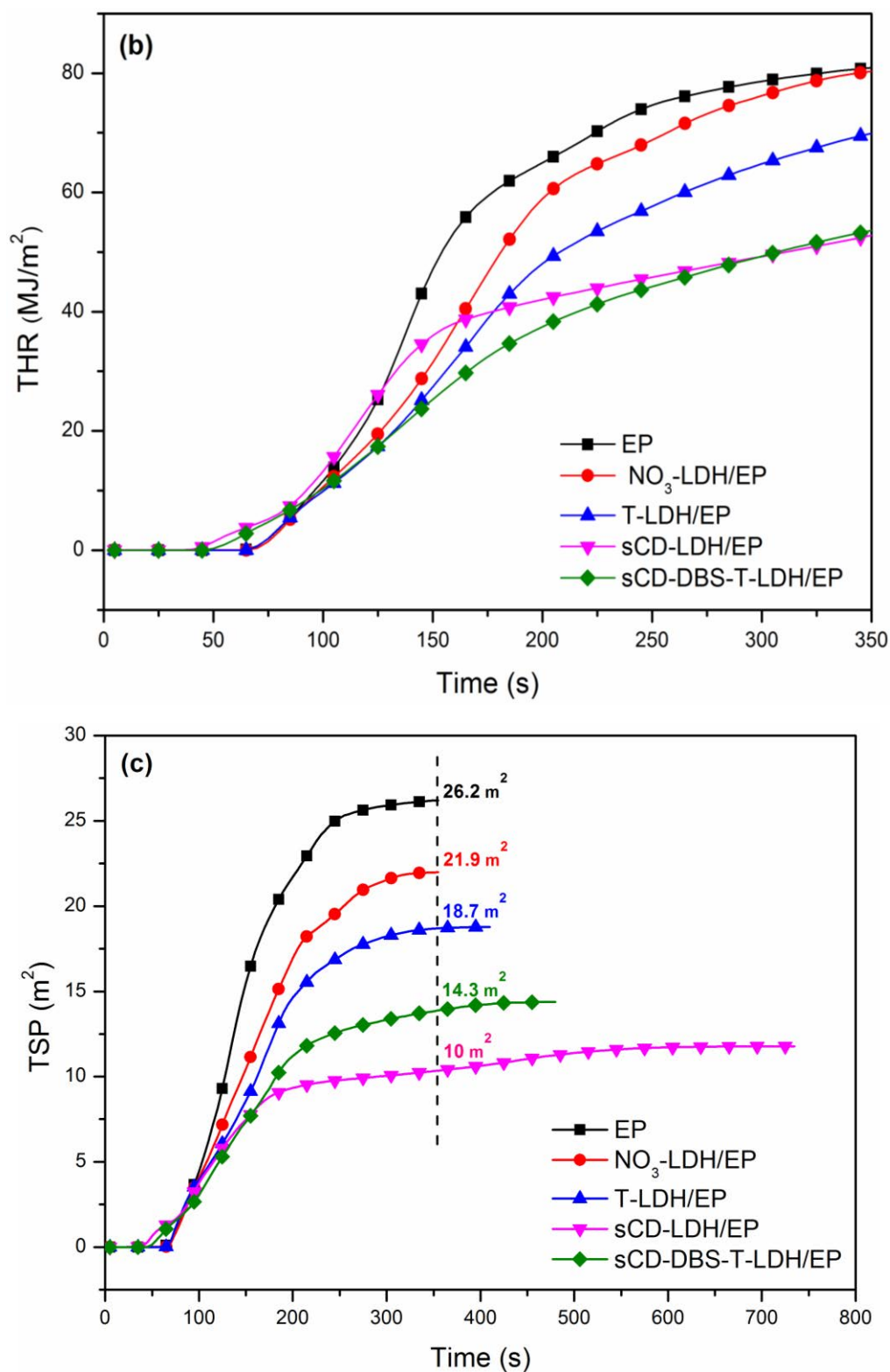
Figure 4-5: (a) Heat release rate, (b) total heat release and (c) total smoke production rate versus time curves of epoxy and its composites from cone calorimeter tests.

Based on the cone calorimeter results, the sCD-DBS-T-LDH/EP composite shows a

significantly lower mass loss and the higher char yield compared to other samples,

indicating a condensed phase mechanism for the fire resistance. The higher char yield means the less epoxy degrade into flammable gases, and also a thick char layer is formed on the surface of the matrix.

This thick char layer serves as a thermal insulating barrier that stimulates the extinguishment of the flame and prevented combustible gases from feeding the flame, and also separated oxygen from burning materials [35], as shown in Fig. 4-6a. This is in good agreement with the reduced heat release rate and total heat release in cone calorimeter test. To further prove this viewpoint, we performed SEM on the morphology of the char residues.
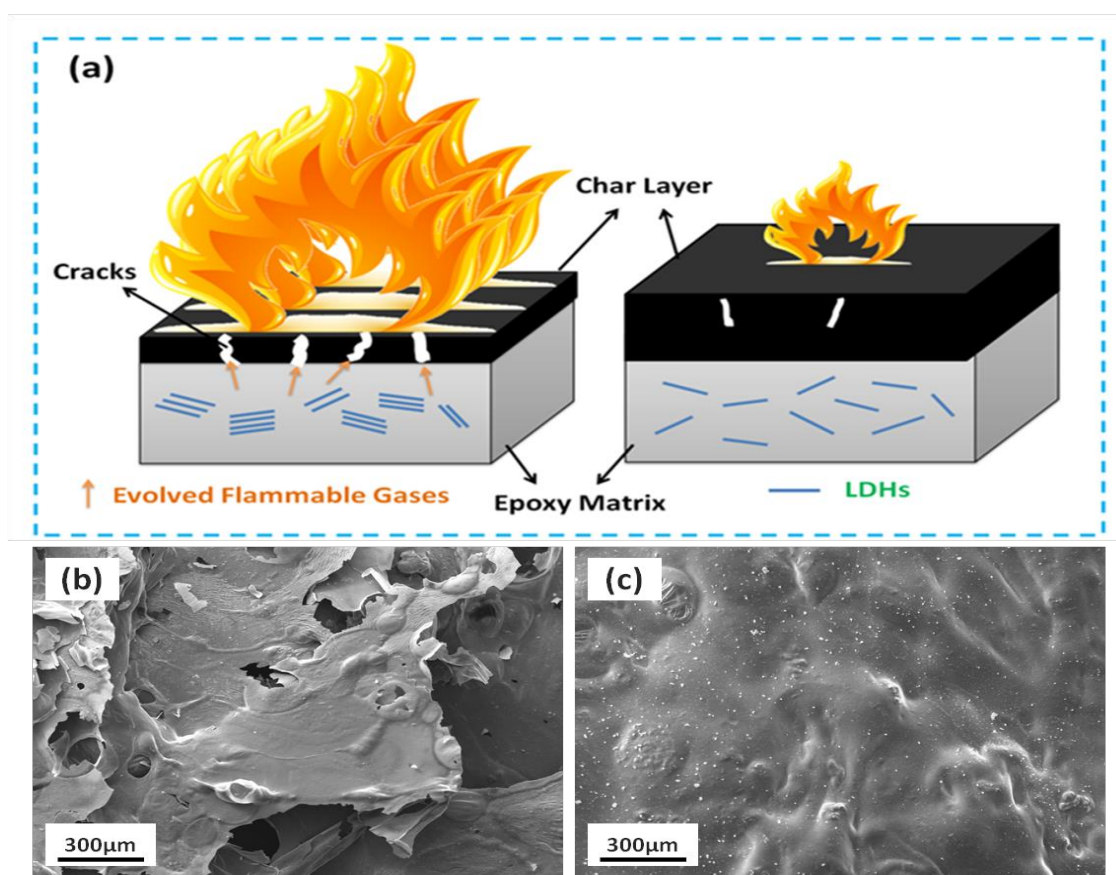
Figure 4-6: (a) Schematic illustration of the barrier effect of the LDH. SEM images of the residual chars of (b) NO3-LDH/EP and (c) sCD-DBS-T-LDH/EP after cone calorimeter test.

As can be seen from Fig. 4-6b and 4-6c, NO_3-LDH/EP shows a breaking char layer, while sCD-DBS-T-LDH/EP displays a consolidated and thick char layer which significantly reduced heat transfer and air incursion and thus enhances the flame retardant performance significantly.

4-3-4 Mechanical properties

Dynamic Mechanical Analysis (DMA)

The storage modulus and tan delta values of the pure EP and the epoxy composites are plotted against temperature in Fig. 4-7. Nanocomposite specimens with nominal dimensions of 60 mm × 10 mm × 2 mm were mechanically tested in the twopoint bending mode using a DMA Q800 Dynamic Mechanical Analyzer (TA Instruments), with an amplitude range of 30 mm and frequency of 1 Hz. The samples were heated from room temperature to 300 °C at a linear heating rate of 3°C min^{-1}. The storage modulus of T-LDH/EP is highest among all the samples, which is ascribed to that the addition of taurine enhances the interaction between modified LDH and epoxy resins. In contrast, NO_3-LDH/EP shows a lowered storage modulus compared to neat EP, indicating the poor interaction between the epoxy matrix and LDH layers.

The glass transition temperature (T_g) is determined by the peak of tan θ curves. It is notable that the T_g of the T-LDH/EP (190 °C) is obviously lower than that of the pure EP (200 °C) and sCD-DBS-T-LDH/EP (201°C).
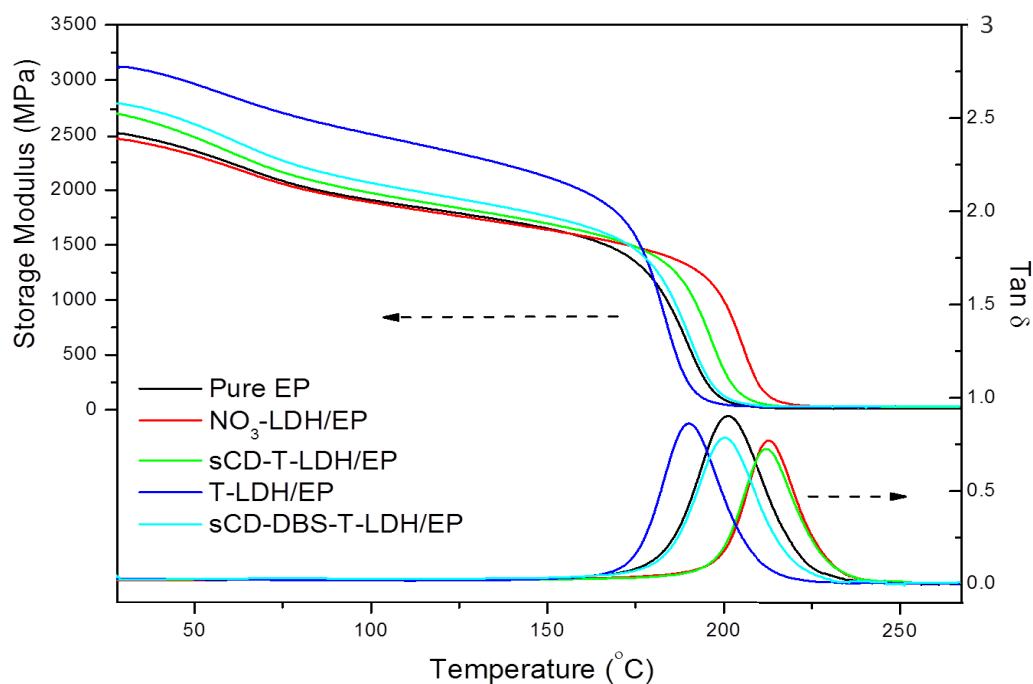
Figure 4-7: DMA storage modulus and tanδ versus temperature plots of epoxy and its composites.

Incorporation of mono-functional modifier such as taurine leads to a reduction in the cross-linking density, since epoxy groups are consumed to react with the taurine. The reduced cross-linking density is responsible for the decreased T_g.

Impact and tensile test

Impact, tensile and digital image correlation (DIC) results of pure EP and its LDH nanocomposites are presented in Fig. 4-8, 4-9 and Table 4-4. The tensile test samples were dumbbell-shaped with dimensions of 75 mm × 10 mm × 2 mm, complying with ISO 527-2 (1996) standard. An Instron 5966 (USA), universal tensile testing machine equipped with a digital image correlation (DIC) system was utilized to carry out the tensile tests at a 1 mm min^{-1} test speed.

The Charpy impact tests of the unnotched specimens were conducted, employing a Zorn Standal Instrumented Charpy Impact Tester (Germany) at an impact speed of

2.93 m s^{-1}. The geometry of the Charpy impact test samples was rectangular with dimensions of 50 mm ×6 mm× 4 mm, conforming to the DIN 53753 standard.

The results show that the addition of NO$_3$-LDH or T-LDH reduces the impact (Fig. 4-8) and tensile strength (Table 4-4) of the EP composite compared to the control EP. As aforementioned in TEM, large agglomerations are observed for the particles in the composites, which results in poor impact and tensile strength. In contrast with NO$_3$-LDH/EP and T-LDH/EP, sCD-DBS-T-LDH/EP shows much better impact and tensile strength.
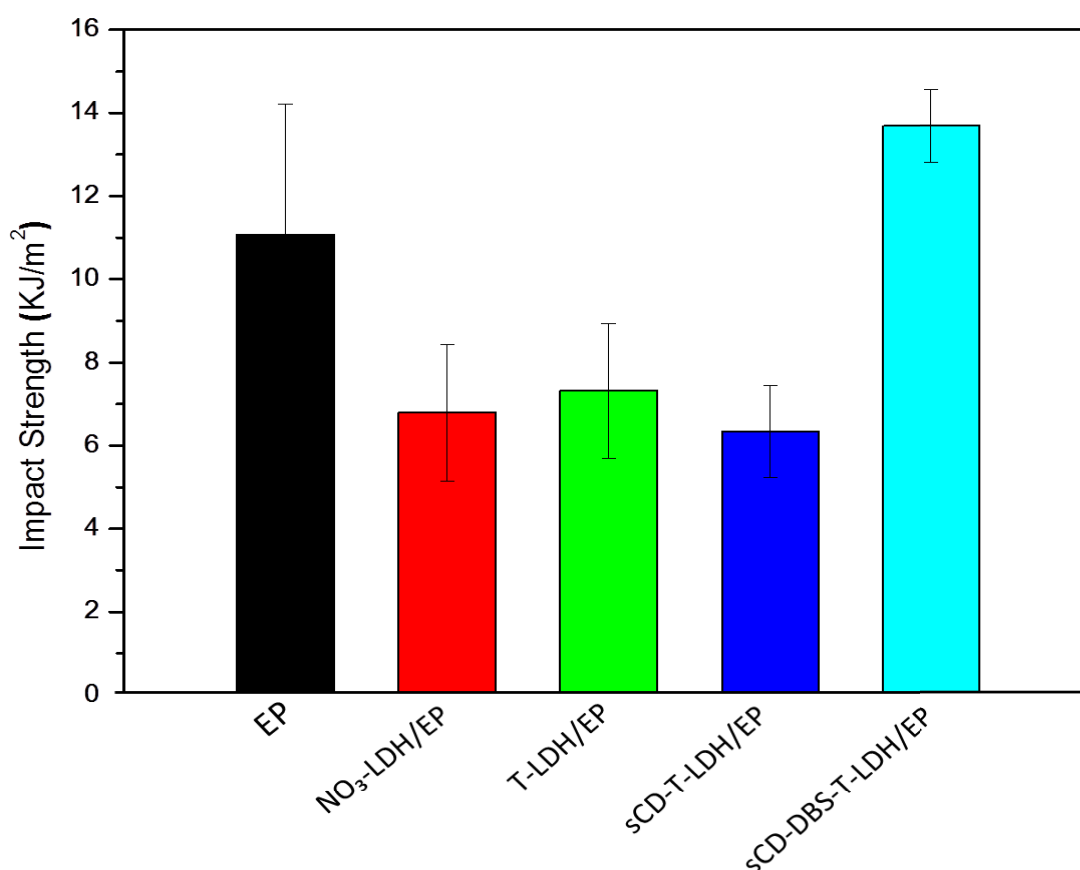
Figure 4-8: Impact behavior of pure EP and epoxy nanocomposites

This could be attributed to two factors: one is that a much higher inter-gallery distance of sCD-DBS-T-LDH facilitates the diffusion of the epoxy chains into the inter-layers of the LDHs and thereby obtain the good dispersion of modified LDHs;

the other is that the presence of taurine improves the interaction between epoxy matrix and LDH layers.

Following the standard EN ISO 527-2:1996, samples were prepared in order to perform the tensile testing. Table 4-4 shows the summery of the results of tensile testing of EP, NO_3-LDH/EP, T-LDH/EP, sCD-LDH/EP and sCD-BDBS-T-LDH/EP respectively. As can be seen, the highest yield stress belongs to the sCD-DBS-T-LDH/EP, while in the case of pure EP, NO3-LDH/EP, T-LDH/EP and sCD-LDH/EP, this amount of improvement in yield is not so significant. During tensile test, digital image correlation (DIC) technique has been conducted to capture the state of strain distribution on the samples. The state of strain distribution for sCD-DBS-T-LDH/EP and NO_3-LDH/EP has been selected and represented in Figure 5-9.

Table 4-4: Tensile tests data

Sample	Tensile stress at break (MPa)	Young modulus (GPa)	Elongation at break (%)
EP	56.4±8.6	3.2±0.1	4.2
NO_3-LDH/EP	36.7±2.7	3.6±0.2	4.0
T-LDH/EP	42.1±2.8	2.6±0.1	3.4
sCD-LDH/EP	40.0±3.0	3.7±0.1	2.6
sCD-DBS-T-LDH/EP	51.5±2.5	3.3±0.1	4.8

SCD-DBS-T-LDH/EP has higher homogeneity in strain distribution and poor distribution of strain can be observed in NO3-LDH/EP. Based on this evidence, more homogenous distribution of starin field in sCD-BDBS-T-LDH/EP resulted in higher mechanical performance of it. Therefore, this multi-modifier system, in which taurine serves as a bio-friendly cross-linker and sCD-DBS as an interlayer gallery promoter,

provided significant combined properties of epoxy composites.
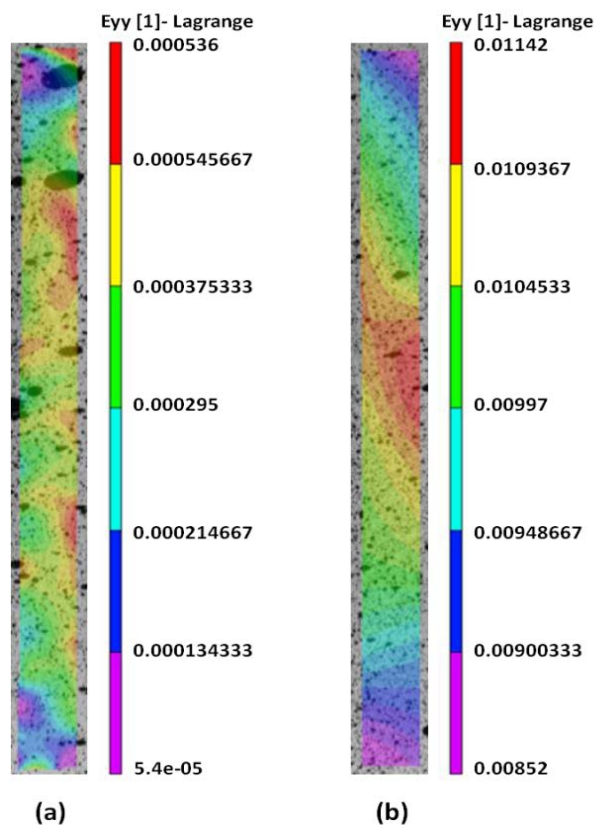
Figure 4-9: Digital image correlations of NO$_3$-LDH/EP (a) and sCD-DBS-T-LDH/EP (b)

4-4 Conclusions

In this work, a multi-modifier system for preparing functionalized LDHs and their epoxy composites have been developed by sophisticatedly utilizing hydroxypropyl-sulfobutyl-beta-cyclodextrin sodium (sCD) sodium dodecylbenzenesulfonate (DBS) and taurine (T) as functional modifiers. TEM and WAXS results revealed that sCD-DBS-T-LDH/EP showed a better dispersion state than other epoxy composites containing unmodified LDHs and/or other functionalized LDHs. A UL-94 V0 rating flame retardant material was achieved for the epoxy composite with 6 wt% of sCD-DBS-T-LDH. The cone calorimetry results

showed that the addition of sCD-DBS-T-LDH significantly reduced the

HRR, THR, FIGRA and improved the char residue after the fire test, compared with

those of other samples, indicating that sCD-DBS-T-LDH was a highly efficient nano

fire retardant for epoxy resin. This improved fire retardancy was attributed to the

efficient char protection layer formed during the burning which effectively inhibited

the heat and mass transfer and generated low organic degradation volatiles in the gas

phase. Also, sCD-DBS-T-LDH/EP exhibited improved impact and tensile properties

compared with its counterparts due to the good dispersion state of LDH and the

strong interaction between the epoxy matrix and LDHs. This multi-modifier system

developed in this paper offers a promising solution for developing multifunctional

high performance fire retardant polymer nanocomposites.

5   Chalcone inserted CD based multimodiers modified LDH/Epoxy nanocompoisites: preparation, characterization, fire behaviors and anti-UV properties

5-1 Introduction

In this context, aiming to develop high performance epoxy materials with both flame retardancy and anti-UV properties, functionalized LDHs were incorporated into the epoxy matrix. Then, cured epoxy/fLDH nanocomposites are prepared by classic epoxy curing procedure. The morphology of the resultant modified LDH based epoxy nanocomposites was investigated by XRD and transmission electron microscopy (TEM). The fire retardant behavior of LDH based epoxy nanocomposites were characterized by limited oxygen index (LOI), vertical burning test (UL-94), and cone calorimeter tests (CCT). Anti-UV properties are studied in term of the change of impact, flexural and micro-mechanical properties against the UV irradiation for 0, 100, 200, 300, 400h, respectively.

5-2 Sample preparation

A fixed weight fraction (7 wt%) of unmodified LDH (NO_3-LDH) or functionalized LDH (Ph-LDH, sCD-Ph-LDH, CD-DBS-Ph-LDH and fCD-DBS-Ph-LDH) was used for the preparation of LDH/epoxy nanocomposites. In order to achieve a satisfactory dispersion state, two-step mixing method was applied. At first, LDH or modified LDH was incorporated into the epoxy matrix using a refined three-roll mill (EXAKT 80E, Germany) for 30 min. In the next step, the mixture was diluted in acetone and exposed to ultra-sonication for 20 min at 60 °C, and then acetone was removed by increasing the temperature gradually until 110 °C and then kept for degassing under the vacuuming to obtain a bubbles-less and viscous mixture. Subsequently, the

mixture was heated up to 120 °C and DDS added to the above mixture and stirred for

15 min until DDS totally dissolved. In order to further degassing, the mixture was

placed into the vacuum oven at 120 ºC for 5 minutes and then immediately poured

into the pre-heated PTFE moulds. The curing procedure was set as 150 °C for 1 h,

180 °C for 2 h and 200 °C for 2 h. Following this procedure, NO_3-LDH/EP,

Ph-LDH/EP, sCD-Ph-LDH/EP, sCD-DBS-Ph-LDH/EP and fCD-DBS-Ph-LDH/EP

were prepared, respectively.

5-3 Characterization

5-3-1 Structural characterization of LDH/EP nanocomposites

X-ray diffraction

Usually, the structural morphology of layered nano-filler/polymer nanocomposite was

characterized by X-ray scattering patterns in order to determine the microstructures.

Figure 5-1 shows the WAXS patterns of pure epoxy matrix, NO_3-LDH/EP,

sCD-Ph-LDH/EP, sCD-DBS-Ph-LDH/EP and fCD-DBS-Ph-LDH/EP composites.

Pure EP had a broad and weak diffraction peak at a 2θ value of 17.3º, due to the

amorphous phase of epoxy. NO_3-LDH/EP composite reflected an intense basal

diffraction peak at a 2θ value of 9.96º corresponding to an inter-gallery spacing of

0.89 nm, indicating the presence of the ordered structure of unmodified LDH in the

polymer matrix. For sCD-Ph-LDH/EP composite, a weak diffraction peak at a 2θ =

3.9º was observed corresponding to an inter-gallery spacing of 2.26 nm, suggesting

the swelling of LDH platelets upon polymerization [9].
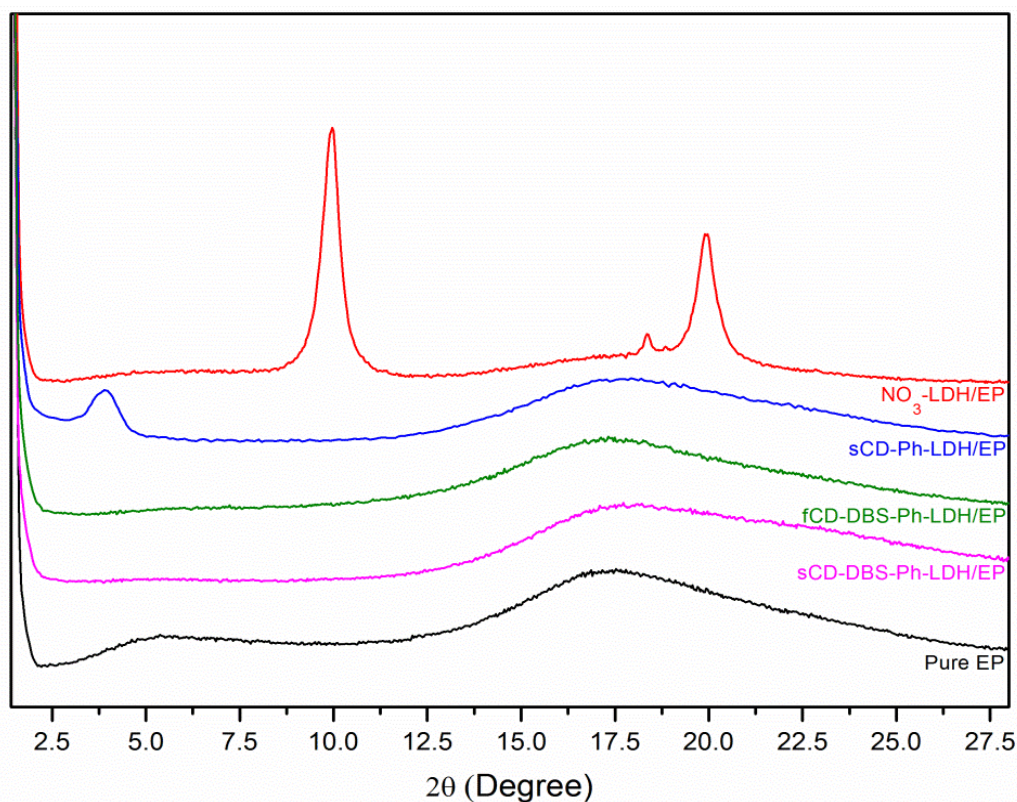
Figure 5-1: WAXS patterns of pure EP, NO₃-LDH/EP, sCD-Ph-LDH/EP, sCD-DBS-Ph-LDH/EP and fCD-DBS-Ph-LDH/EP composites.

In the case of sCD-DBS-Ph-LDH/EP and fCD-DBS-Ph-LDH/EP composites, no visible reflection peaks were observed below 10°, indicating highly exfoliated and/or well intercalated LDH platelets within the epoxy resin. Furthermore, this conjecture has been confirmed by TEM and TED.

Transmission electron microscopy (TEM)

The microstructures of the nanocomposites were characterized by means of transmission electron microscopy (TEM) employed to provide more information in order to investigate the results obtained from the WAXS analysis as well as to directly observe the dispersion state of LDH within the epoxy matrix, as shown in Figure 5-2.

Low and high magnification TEM images of NO_3-LDH/EP composite (Fig.5-2a, b and

c) showed that large agglomerations of NO_3-LDHs with the average size of >500 nm

were formed. This is the cause of observing the (003) reflection in the WAXS patterns

of NO_3-LDH/EP. The dispersion state of NO_3-LDH/EP was quite different from that of

fCD-DBS-Ph-LDH/EP. The low and medium magnification TEM image of

fCD-DBS-Ph-LDH/EP (Fig. 5-2d and 5-2e) revealed much better dispersion of LDH in

the epoxy matrix and the higher magnification image of fCD-DBS-Ph-LDH/EP (Fig.

5-2f) showed a homogeneously disordered nanostructure, which is in agreement with

the WAXS observations. Transmission electron diffraction (TED) patterns were also

utilized by TEM in order to investigate the crystalline parameters structures of the

specimens.
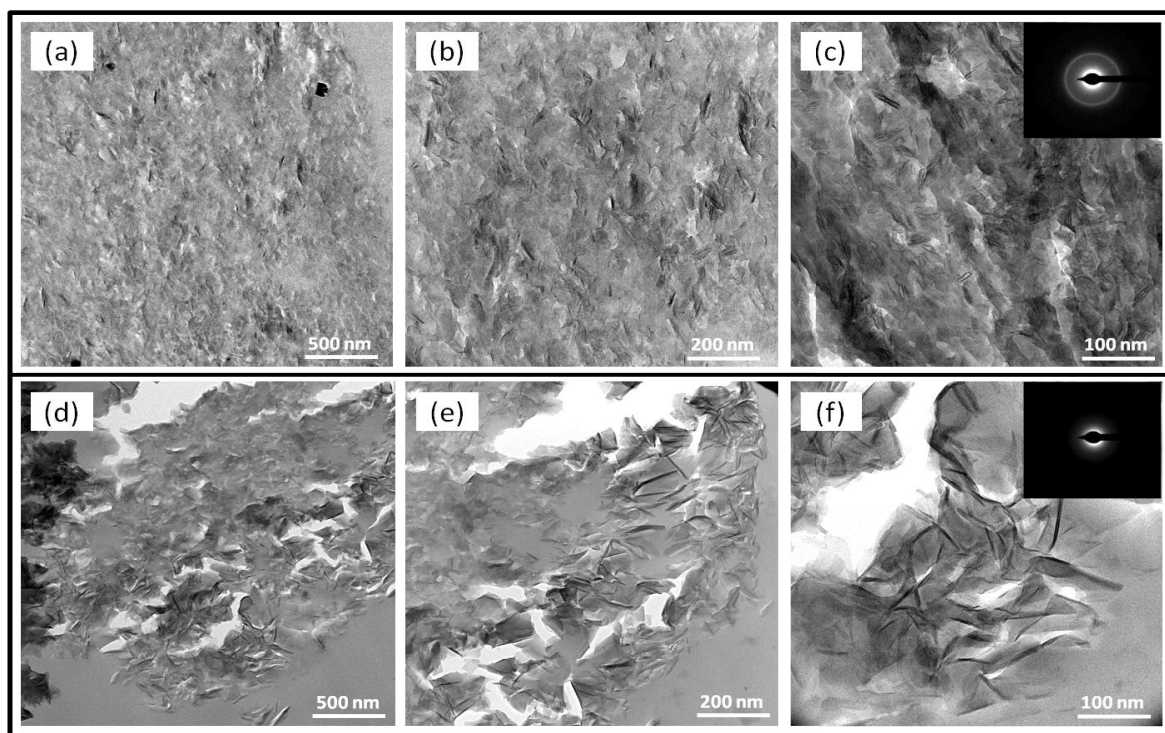
Figure 5-2: TEM images of NO_3-LDH/EP (a, b and c) and fCD-DBS-Ph-LDH/EP (d, e and f) nanocomposites.

In composite, selected area electron diffraction (SAED) patterns of the NO_3-LDH/EP indicated a clear corona around the pointer (Fig. 5-2c), implying the existence of large poly-crystalline structures. In contrast, in the SAED image of fCD-DBS-Ph-LDH/EP (Fig. 5-2f), there was no corona observed around the pointer, which indicated the existence of scant crystallites or excellent exfoliated nano-particles.

5-3-2 Thermal stability of epoxy nanocomposites

TGA thermograms of Un-modified LDH, modified LDHs, pure epoxy and epoxy nanocomposites with various contents are showed in Fig. 5-3, 5-4 and the detailed results were summarized in Table 5-1. Initial degradation temperature ($T_{5\%}$) of functionalized LDH indicated lower value compared with that of unmodified LDH, which was caused by the introduction of thermally instable organic modifiers into LDHs. In case of pure EP it is observed that the main degradation stage ranging from 380 to 500 $^{\circ}$C that was attributed to the decomposition of three dimensional macromolecular networks of the matrix. All the LDH-based epoxy nanocomposites exhibited one-stage degradation process similar to

pure EP.

However, the $T_{5\%}$ of all the LDH-based epoxy nanocomposites were descended compared to that of pure EP, as a result of the earlier initial decomposition leading by the addition of LDHs. Earlier initial decomposition requisite to form a char layer and hence, protect underneath polymer matrix against flame.
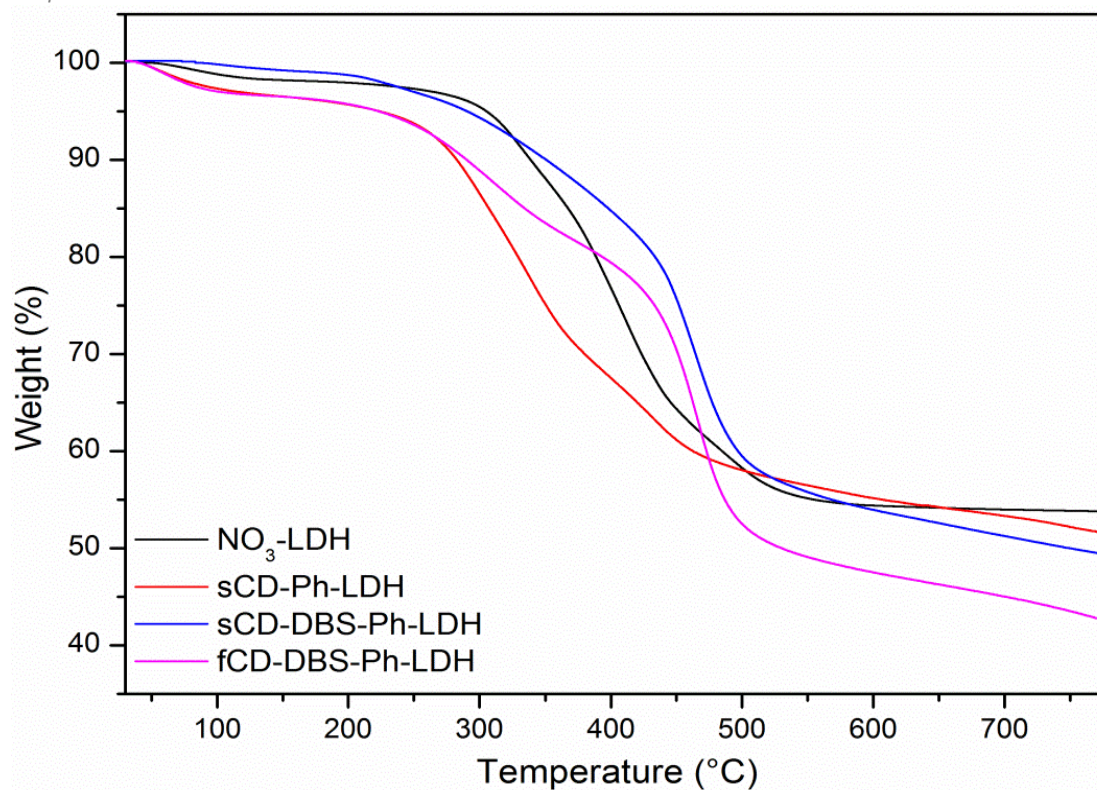
Figure 5-3: TGA of NO$_3$-LDH, sCD-Ph-LDH, sCD-DBS-Ph-LDH and fCD-DBS-Ph-LDH under N$_2$ at heating rate of 10°C/min.
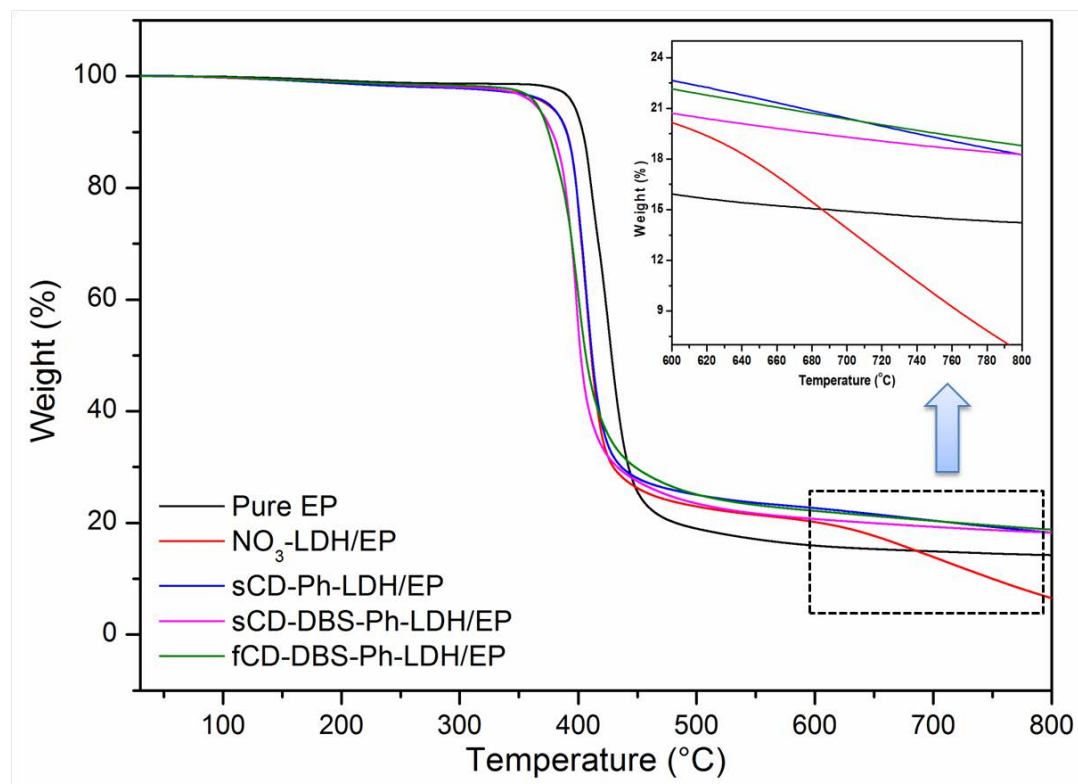
Figure 5-4: TGA curves of pure EP and epoxy composites under N$_2$ at heating rate of 10°C/min

93

It was observed that the residue yield at 750 $^\circ$C was increased due to the incorporation of the functionalized LDHs.

Table 5-1: TGA results of LDH, organo-modified LDHs and their epoxy nanocomposites

Sample	$T_{5\%}$ (°C)	T_{max} (°C)	Residue yield at 750°C (wt %)	
			Calculated	Experimental
NO$_3$-LDH	305	395	--	53.8
sCD-Ph -LDH	290	339	--	52.2
sCD-DBS-Ph-LDH	224	467	--	49.8
fCD-DBS-Ph-LDH	223	462	--	43.4
EP	384	413	--	14.5
NO$_3$-LDH/EP	372	407	17.2	10.1
sCD-Ph-LDH/EP	374	406	17.1	19.2
sCD-DBS-Ph-LDH/EP	361	398	16.9	18.7
fCD-DBS-Ph-LDH/EP	363	399	16.5	19.6

In case of pure EP, it produced 14.5% residue at 750 °C, whereas NO$_3$-LDH/EP, sCD-Ph-LDH/EP, sCD-DBS-Ph-LDH/EP and fCD-DBS-Ph-LDH/EP nanocomposites had 13.6%, 14.9%, 18.2% and 19.5% residues, respectively, at 750 °C.

5-3-3 Burning behavior

The experimental char yields of sCD-Ph-LDH/EP, sCD-DBS-P-LDH/EP and fCD-DBS-P-LDH/EP were higher than the calculated ones, suggesting that fCD and DBS are good charring agents in combination with phytic acid.

The flame retardant properties of the cured EP and epoxy nanocomposites were examined by measuring their oxygen index (LOI) and vertical burning test (UL-94) and the final results are summarized in Table 5-2. Pure epoxy showed a LOI value of

23.0% and no classification in the UL-94 vertical burning test. By adding NO_3-LDH, the LOI value increased to 25.2%, but still indicated no rating in the UL-94 test. Incorporating Ph-LDH and sCD-Ph-LDH improved the LOI value slightly, but both of them still cannot pass the UL-94 V0 rating.

Table 5-2. LOI and UL-94 data of pure EP and its nanocomposites

Sample	LOI (%)	UL-94	Observation
Pure EP	23.0	No rating	Fire with a sooty flame
NO_3- LDH/EP	26.2	No rating	Fire with a sooty flame
Ph-LDH/EP	23.7	No rating	Fire with a sooty flame
sCD-Ph-LDH/EP	26.5	No rating	Fire with a sooty flame
sCD-DBS-Ph-LDH/EP	26.0	V-0	Extinguished immediately
fCD-DBS-Ph-LDH/EP	26.5	V-0	Extinguished immediately

However, it was noted that adding sCD-DBS-Ph-LDH or fCD-DBS-Ph-LDH into epoxy provided a great improvement in LOI, 26 and 26.5 respectively and the UL-94 V0 rating was achieved in vertical burning test.

Measurements in Cone calorimeter have been widely used to detect the combustion characteristics of the polymeric materials. Fig. 5-5 showed the heat release rate (HRR), total heat release (THR) and smoke temperature versus time curves of pure EP and its nanocomposites. Other various important parameters obtained from the cone calorimeter tests, such as the time-to-ignition (TTI), peak heat release rate (pHRR), total smoke production (TSP), average HRR (Ave. HRR) and the char residue, are summarized in Table 5-3. Compared with pure EP, NO_3-LDH/EP, sCD-Ph-LDH/EP and sCD-DBS-Ph-LDH/EP composite, the peak of HRR decreased

from 835 kW/m^2 to 679 kW/m^2 (-19%), 766 kW/m^2 (-8%) and 349 kW/m^2 (-58%), respectively.

In the case of fCD-DBS-Ph-LDH/EP composites, from Fig. 5-5a, it can be observed that fCD-DBS-Ph-LDH/EP ignited rapidly due to the early initial degradation stage after ignition. The peak HRR of fCD-DBS-Ph-LDH/EP dramatically decreased to 232 kW/m^2, corresponding to a 72% reduction compared to that of pure epoxy. Similar trend was observed for the average HRR values of the pure EP and epoxy nanocomposites which are listed in the Table 5-3. Pure EP showed the Ave. HRR value of 330 kW/m^2, the NO$_3$-LDH/EP, sCD-Ph-LDH/EP and sCD-DBS-Ph-LDH/EP indicated 360 kW/m^2, 256 kW/m^2 and 234 kW/m^2 respectively, while fCD-SDBS-Ph-LDH/EP nanocomposite showed 162 kW/m^2 corresponding to a 50% reduction in the Ave. HRR. The good dispersion state of the LDH layers into the epoxy matrix was due to enlarged inter-layer distance of fCD-SDBS-Ph-LDH and improved char yield of epoxy nanocomposites during combustion due to existence of fCD and Ph species are the major aspects of the improved fire retardancy of fCD-DBS-Ph-LDH.

Figure 5-5b showed the total heat release rate of the Pure EP and epoxy nanocomposites. At 350 second after the ignition, pure EP released a total heat of 96.7 MJ/m^2, the NO$_3$-LDH/EP, sCD-Ph-LDH/EP and sCD-DBS-Ph-LDH/EP released 87.8 MJ/m^2, 76.6 MJ/m^2 and 66.4 MJ/m^2 respectively, whereas fCD-SDBS-Ph-LDH/EP nanocomposite only released total heat of 47.2 MJ/m^2.
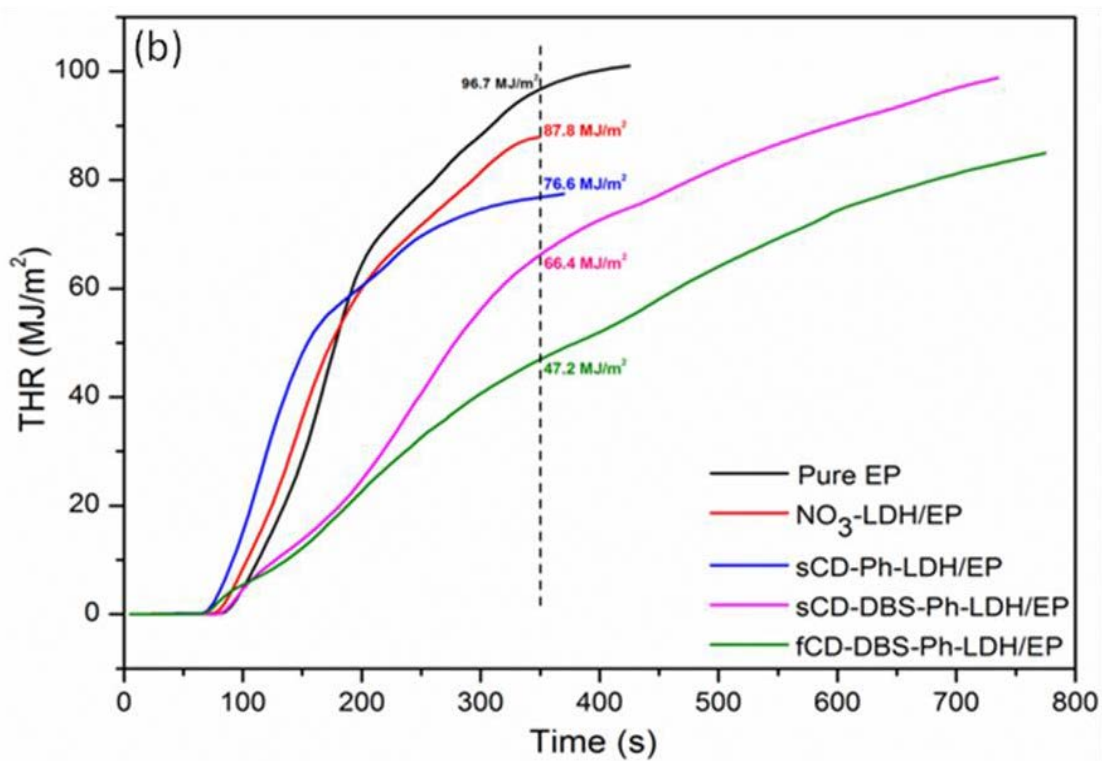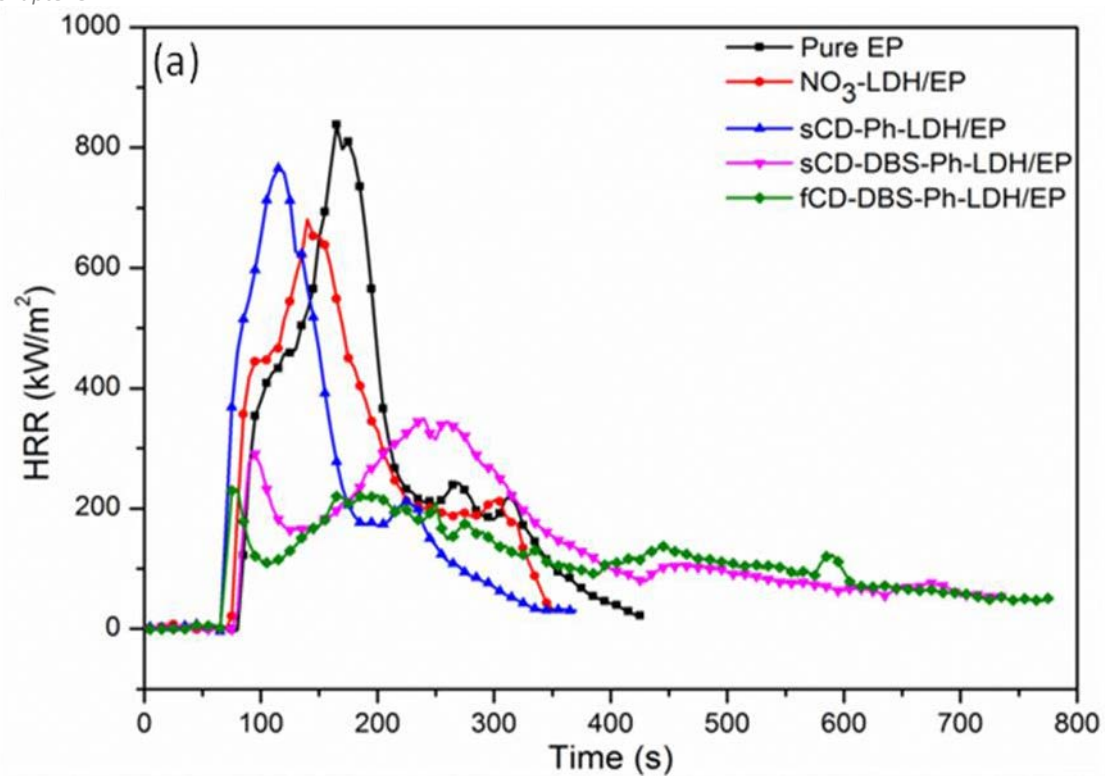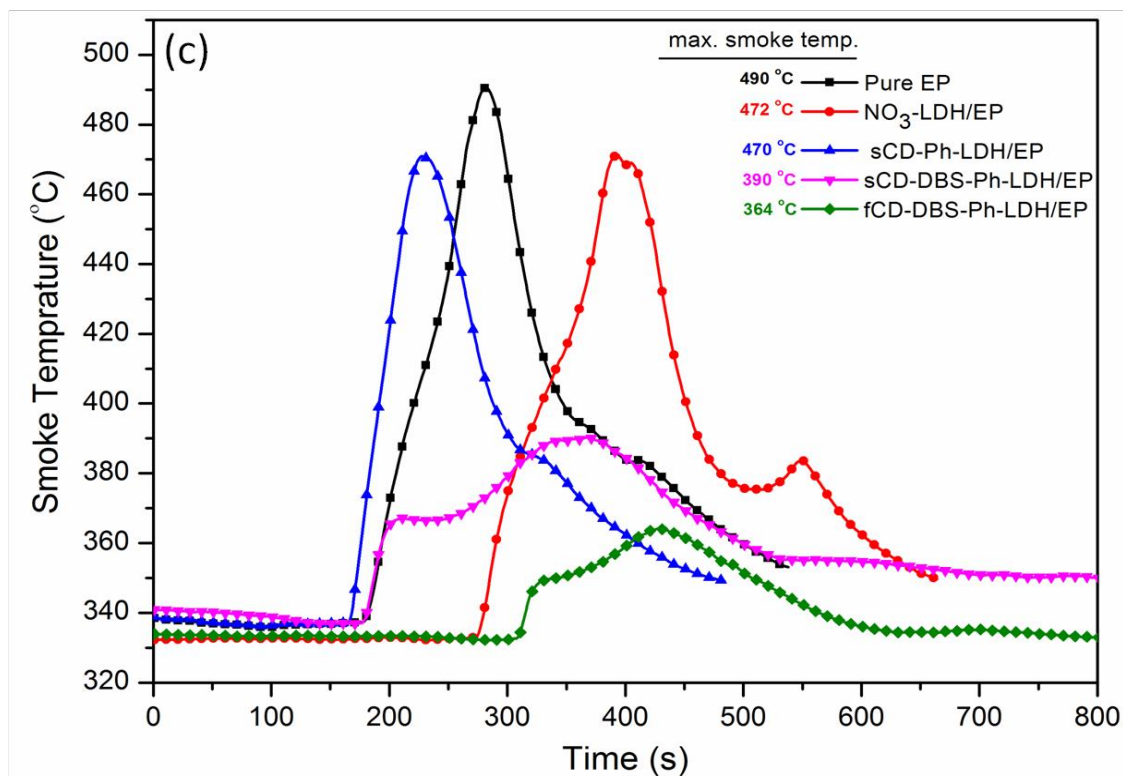
Figure 5-5: (a) Heat release rate, (b) total heat release and (c) smoke temperature rate versus time curves of epoxy and its nanocomposites from cone calorimeter tests.

Participation of the organic species in the carbonization process and their presence in the condensed phase instead of going into the gas phase as "fuel" is the main reason of significant reduction of THR in the epoxy resin. This was also can be proved by the increased char residues (as listed in Table 5-3). With regard to the smoke temperature (as shown in Fig. 5-5c), pure EP also displayed the highest smoke temperature among all the samples.

The addition of fCD-SDBS-Ph-LDH/EP resulted in relatively decreased smoke temperature compared to pure EP. The decreased smoke temperature in epoxy nanocomposite was probably due to the reduced heat release of epoxy converted into organic volatiles, as the organic volatiles were the major source of heat [9].

According to the TSP values (as listed in Table 5-3), pure EP shows the highest value

among all the samples. In the case of the fCD-SDBS-Ph-LDH/EP nanocomposites,

lower TSP (63.5% reduction) was observed compared to pure EP.

Table 5-3: Combustion parameters obtained from cone calorimeter

Sample	TTI (s)	pHRR (kW/m^2)	TSP (m^2)	Ave. HRR in 300 s	Char residue (%)
Pure EP	76	837	61.9	330	14
NO$_3$- LDH/EP	75	679	52.0	360	20
sCD-Ph-LDH/EP	66	762	37.2	256	16
sCD-DBS-Ph-LDH/EP	78	390	36.2	234	25
fCD-DBS-Ph-LDH/EP	69	232	22.5	162	27

The decrease in smoke formation in epoxy nanocomposites was probably due to the

reduced amount of epoxy converted into organic volatiles, since the organic volatiles

are the major source of smoke particles [30]. Based on the cone calorimeter results,

the fCD-DBS-Ph-LDH/EP indicating a condensed phase mechanism, hence showed

significantly lower mass loss and higher char yield compared to other samples. The

higher char yield resulted in quenching the flame which means less epoxy converted

into flammable gases. Formation of a thick char layer was on the surface of the

matrix served as a thermal insulating barrier to separate oxygen from burning

materials and also, prevent combustible gases from feeding the flame zone, as

showed in Fig. 5-6b. This was the reason for the reduced heat release rate and total

heat release of fCD-DBS-Ph-LDH/EP composite in the cone calorimeter test.

More investigation achieved by study the morphology of the char residues of the

samples after cone calorimeter test by SEM.
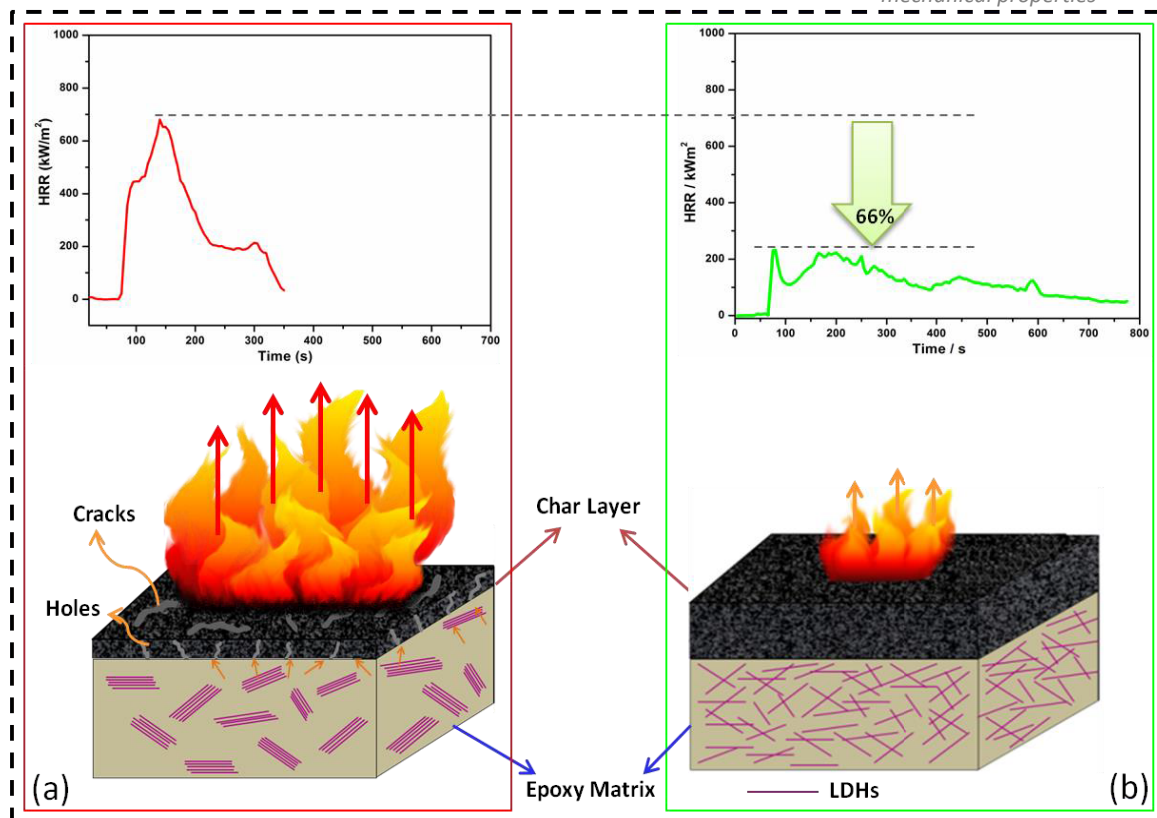
Figure 5-6: Schematic illustration of the barrier effect of the (a) NO_3-LDH/EP and (b) fCD-DBS-Ph-LDH/EP.

As shown in Fig. 5-7a, b and c, the char residues of NO_3-LDH/EP, sCD-Ph-LDH/EP and sCD-DBS-Ph-LDH/EP showed a cracked, fluffy and full of open wholes toward
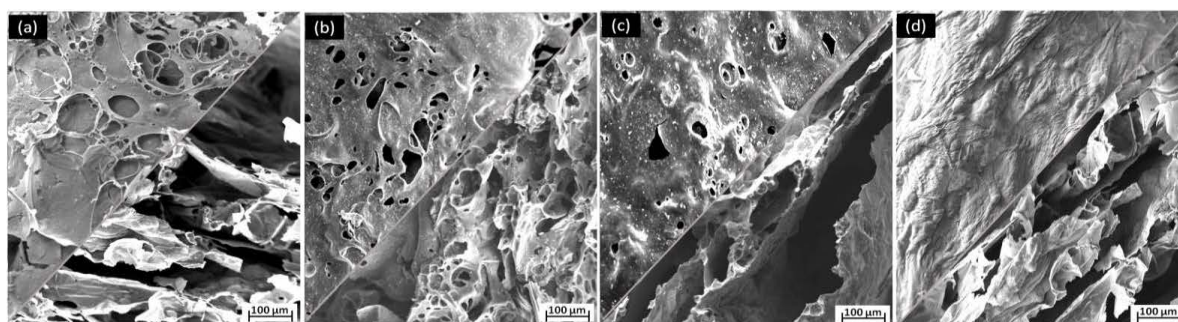
Figure 5-7: SEM images of the surface and cross-section of the residual chars of (a) NO_3-LDH/EP, (b) sCD-Ph-LDH/EP, sCD-DBS-Ph-LDH/EP and fCD-DBS-Ph-LDH/EP after the cone calorimeter test.

the surface of the char layer, while fCD-DBS-Ph-LDH/EP displayed a consolidated wafer structure in the cross-section and thick and continues char layer which resulted in significant reduction of heat and mass transfer and thus significantly enhanced the

flame retardancy.

5-3-4 UV stability properties

Impact properties

Impact results of non-exposed and ultraviolet (UV) exposed pure EP and its nanocomposites are presented in figure 5-8. UV radiation was performed in a Solarbox 3000e, equipped with a Xenon lamp with 550 W/m^2 irradiance at 60 °C for 0, 100, 200, 300, 400h, respectively.

For the non-exposed samples, it was indicated that the addition of NO$_3$-LDH resulted in decreasing the impact strength of the nanocomposite compared to those of pure EP. Poor interfacial interaction between fillers and epoxy matrix was attributed to the large agglomerations of NO$_3$-LDH which is observed in the TEM images of NO$_3$-LDH/EP. In contrast, fCD-DBS-Ph-LDH/EP showed better impact strength as compare to the NO$_3$-LDH/EP and sCD-DBS-Ph-LDH/EP. Higher inter-gallery distance of fCD-DBS-Ph-LDH facilitated the diffusion of the epoxy chains into the inter-layers of the LDHs, hence uniform dispersion state obtained and it was resulted in improving the impact strength of fCD-DBS-Ph-LDH/EP.

It is indicated that 400h UV radiation had very significant deteriorative effect on the impact strength of the pure EP (-40%), NO$_3$-LDH/EP (-25%) and sCD-DBS-Ph-LDH/EP (-37%).
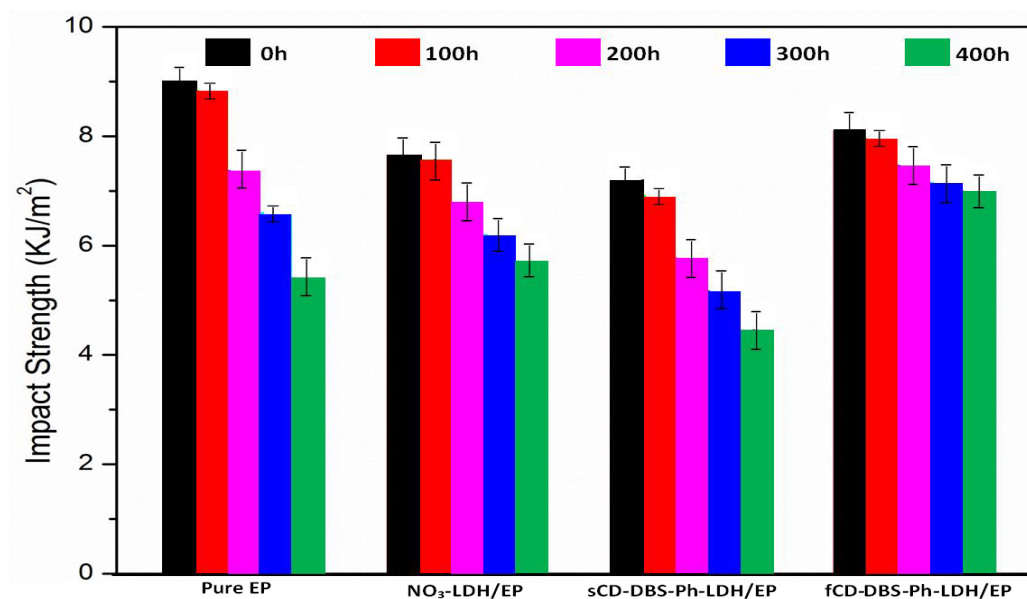
Figure 5-8: Impact behavior of pure EP and epoxy composites before and after UV exposure.

In contrast, fCD-DBS-Ph-LDH/EP showed much lower reduction (-13%) in the impact strength by increasing the time of exposure to 400h which might be attributed to the UV protection effect of chalcone species.

Micro-indentation test after UV exposure

Micro-indentation was used to determine the series of material properties across the interface from the UV exposed surface to the bulk material [24]. Micro Indentation tests were conducted by a Zwick Roell type BZ2.5/TS1S indenter with loading of 5N. Figure 5-9 illustrating typical indentation loading and unloading curves for Pure Epoxy and epoxy nanocomposites upon exposing time, indicating similar behaviors between the neat epoxy and nanocomposite. Figure 5-9 presents the displacement profiles plotted as a function the distance from the specimen surface. The change in displacement was a reflection of the diffusion process of free radicals and oxygen

causing the degradation from the exposed surface into the depth of materials.
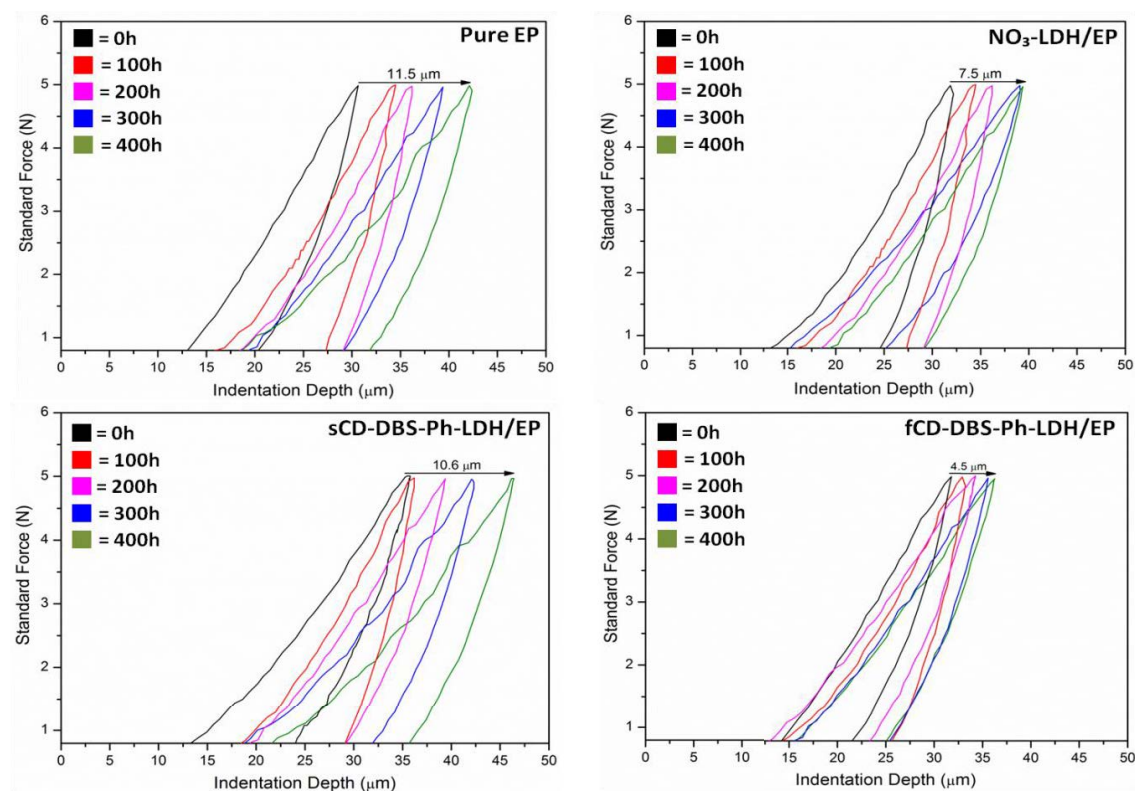
Figure 5-9: Micro indentation of pure EP and epoxy nanocomposites before and after UV radiation.

With an increased exposure time, the effect was felt deeper in the material, which suggested a thicker degraded layer for a longer exposure time. When comparing the displacement profiles for the neat epoxy and the nanocomposite, their degradation behaviors and mechanical responses were very different.

The displacement profile increased gradually from the surface and deeper into the material for neat epoxy, NO_3-LDH/EP and sCD-DBS-Ph-LDH/EP whereas, the profile dropped very rapidly and reached a steady state at much shallower depth for the fCD-DBS-Ph-LDH/EP nanocomposite which functionalized by chalcone. This may explain how the diffusion process of free radicals and oxygen and the associated degradation were delayed by the nanocomposite functionalized by chalcone.

The synergistic effect of the chalcone and exfoliated layers of LDH with a high aspect ratio served as barrier walls to restrict the movements and interactions between the species causing photo-degradation within the confined free volumes between the polymer molecules [26]. It can be concluded that the degraded thickness gradually increased with exposure time for pure EP, NO_3-LDH/EP and sCD-DBS-Ph-LDH/EP without UV barrier, and it was consistently smaller for the functionalized nanocomposite with UV barrier. The comparison confirmed the ameliorating effect of chalcone against the deterioration caused by photo-degradation. Figure 5-10 shows optical micrographs of the specimens before and after being subjected to the UV exposure
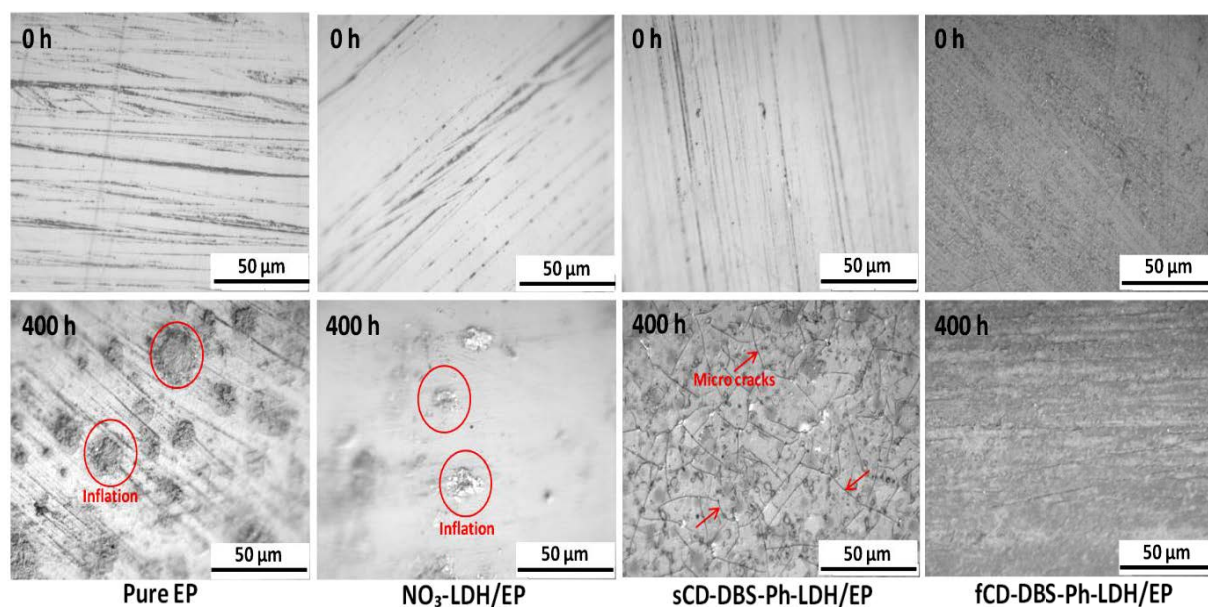
Figure 5-10: Optical microscope images of the pure EP and epoxy nanocomposites before and after the UV exposure.

As it can be observed from the images of pure EP, NO_3-LDH/EP and sCD-DBS-Ph-LDH/EP, revealed the formation of inflammation and micro-cracks in the surface of the epoxy matrix. This phenomenon was induced by the polymer

matrix becoming excessively brittle due to increased crosslinking resulting from photo-oxidation reactions caused by UV radiation. In contrast, 400h of UV exposure did not result in any significant changes in morphology of fCD-DBS-Ph-LDH/EP sample.

Three Point Flexural test

Stiffness versus time results of pure EP and its LDH composites are presented in Fig. 5-11. Three point flexural tests were conducted at cross head speed of 0.5 mm min^{-1} by an Instron 5966 universal bending testing machine. The samples used were rectangular shape with dimensions of 50 mm × 6 mm × 5 mm according to ASTM D-790 standard.

Pure epoxy exhibited a steep decrease in the stiffness with increasing the exposure time.

In contrast to pure epoxy, NO$_3$-LDH/EP showed more reduced trend in the stiffness as the UV exposure time increases, indicating the poor UV resistance. In the case of the sCD-DBS-Ph-LDH/EP composite, the stiffness also decreased with the increase of the UV exposure time. As for the fCD-DBS-Ph-LDH/EP nanocomposite, the stiffness was reduced slowly after UV irradiation which was indicated the diffusion of the UV radiation significantly decreased due to the UV absorption effect of chalcone species while the LDH layers served as physical barrier for shielding the underlying matrix from UV irradiation.
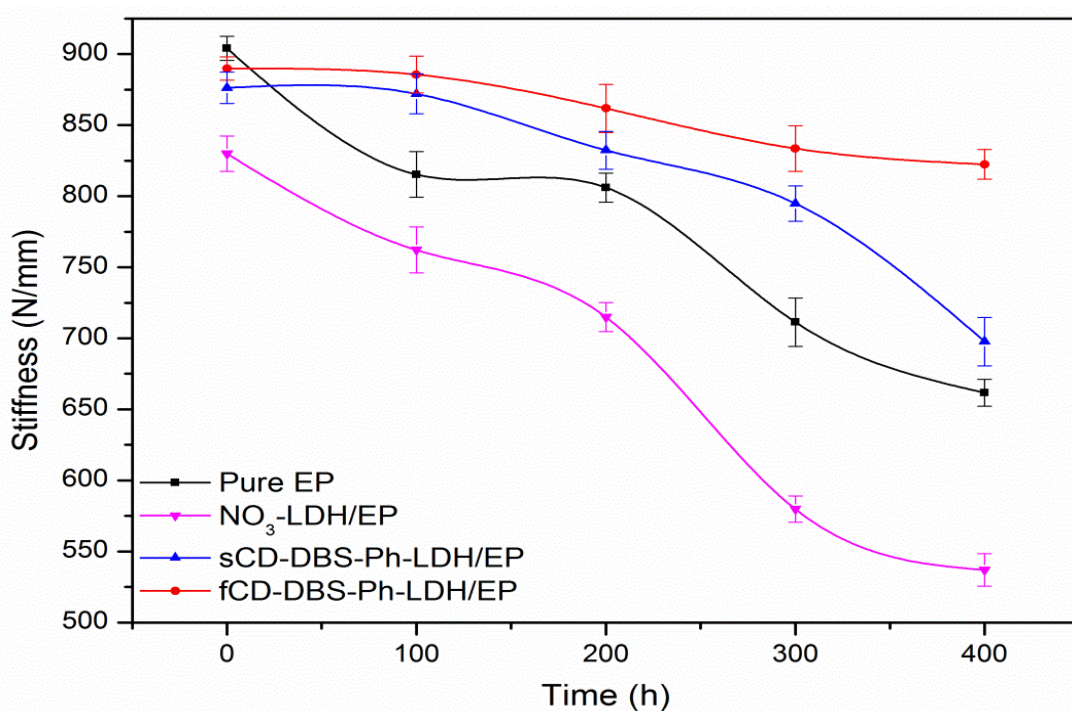
Figure 5-11: Stiffness versus UV radiation time plots for pure EP and its nanocomposites.

Chemical changes due to UV radiation

FTIR spectroscopy equipped with ATR was used to determine the effects of UV radiation on the chemical structure of epoxy and its composites. The chemical structure of the prepared samples was identified by FTIR (ATR-IR) which were recorded on a Thermo Scientific Nicolet IS50 FT-IR spectrometer.
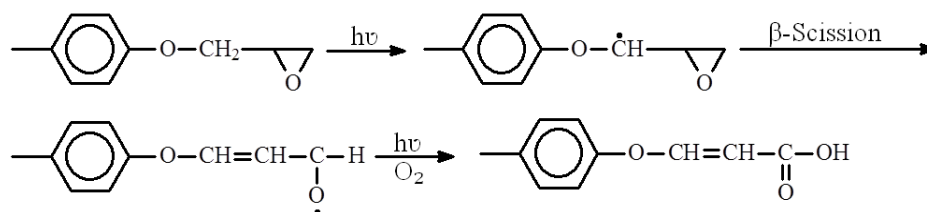
Scheme 5-1: Chain scission of epoxy matrix during the UV exposure.

Figure 5-12 displays ATR-FTIR spectra of pure EP and fCD-DBS-Ph-LDH/EP nanocomposites at different UV irradiation time.

The chemical structure of pure EP is unambiguously identified by characteristic FTIR bands: aromatic ring (1590, 1505 cm^{-1}) and C-O-C bond (1100 cm^{-1}), and methyl and methylene groups (2960, 2860 cm^{-1}).
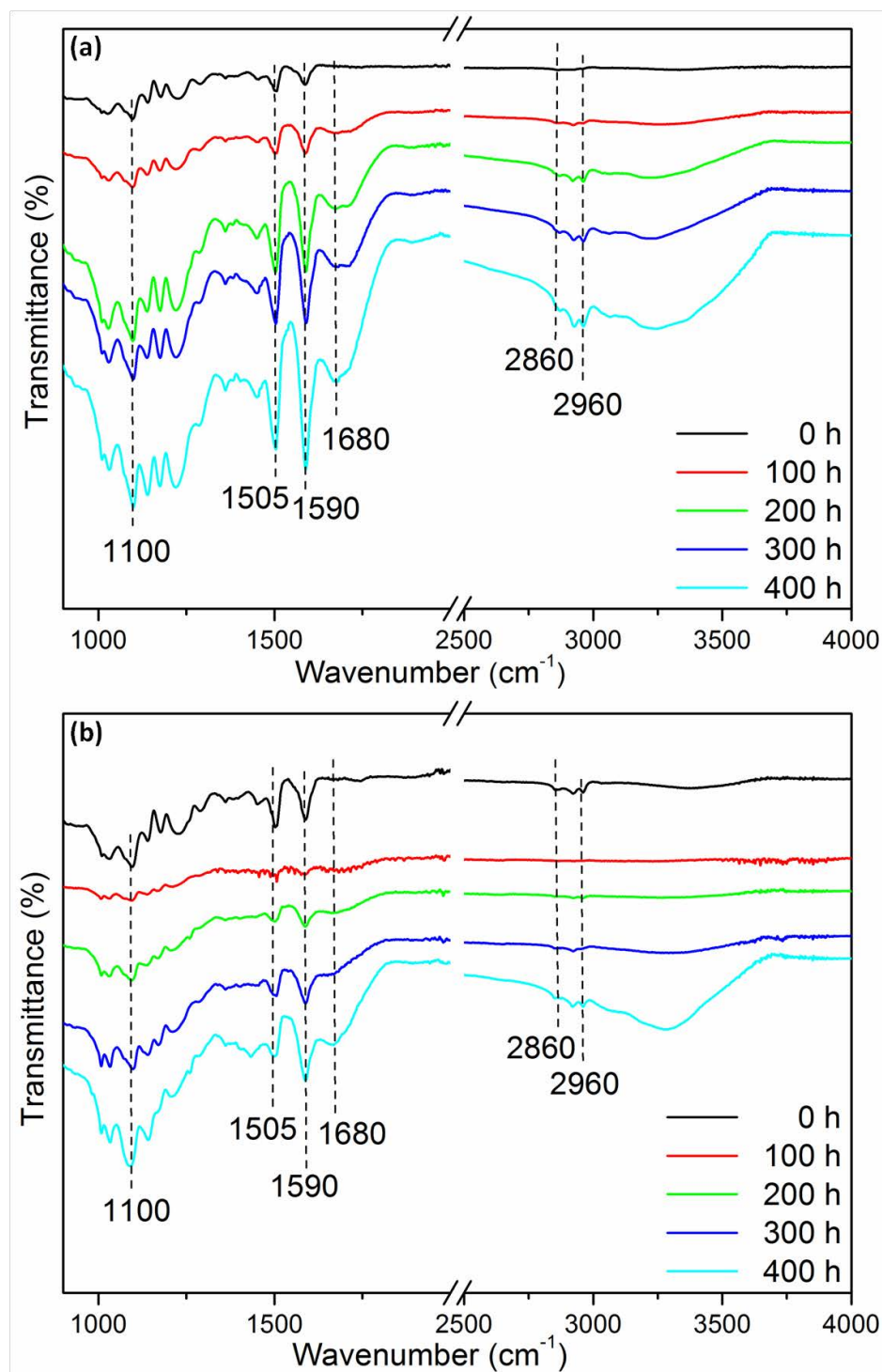
Figure 5-12: ATR-FTIR spectra of (a) pure EP and (b) fCD-DBS-Ph-LDH/EP nanocomposite at different UV irradiation time.

As the UV irradiation time increases, one new peak at 1680 cm^{-1} appears

corresponding to the formation of C=O that is originated from the oxidation induced by UV irradiation (see Scheme 5-1) [25]. Meanwhile, the intensity of all the bands increases with the increase of the UV irradiation time, implying that UV irradiation accelerates the oxidation of epoxy matrix. The ATR-FTIR spectra of fCD-DBS-Ph-LDH/EP nanocomposite exhibits similar trend to that of pure EP; however, the intensity ratio of before and after UV irradiation for fCD-DBS-Ph-LDH/EP nanocomposite is much lower than that of pure EP, meaning the enhanced anti-UV property due to the presence of chalcone species.

5-4 Conclusions

In conclusion, we have prepared a multi-modifiers' system for functionalized LDHs and the resultant LDHs based epoxy composites by sophisticatedly utilizing hydroxypropyl-sulfobutyl-beta-cyclodextrin, SDBS and phytic acid as functional modifiers. TEM and WAXS results revealed that fCD-DBS-Ph-LDH/EP showed better dispersion state than other epoxy nanocomposites containing un-modified LDH and/or single modifier's system. A striking phenomenon was observed: with only 7 wt% of sCD-DBS-Ph-LDH or fCD-DBS-Ph-LDH, the resultant epoxy composite could pass UL-94 V0 rating. Also, significant reduction in the pHRR, THR, TSP and smoke temperature was achieved for fCD-DBS-Ph-LDH/EP composite in the cone calorimeter tests compared to those of other samples, implying the high fire retardant efficiency of fCD-DBS-Ph-LDH for epoxy material. This improved fire retardancy was attributed to the formation of good-quality char layer during the burning which

effectively inhibited the heat and mass transfer and generated low amount of organic degradation volatiles into gas phase.

The fCD-SDBS-Ph-LDH/EP nanocomposites exhibited the enhanced impact properties compared to its counterparts due to the good dispersion state of LDH and the strong interaction between epoxy matrix and LDHs. Furthermore, fCD-SDBS-Ph-LDH/EP nanocomposite showed excellent anti-UV properties owing to the presence of chalcone species that served as UV absorber. This multi-modifiers' LDH nano-material developed in this work will offer a promising solution for developing multifunctional high performance polymer nanocomposite.

6 Fe₃O₄ decorated CD based multimodiers modified LDH/Epoxy nanocompoisites: preparation, characterization, fire behaviors and mechanical properties

6-1 Introduction

As far as the environmental friendliness is concerned, bio-based resources are preferable. Taking these factors into consideration, phytic acid (Ph), a natural resource compound, with abundant flame retardant element and water-soluble cyclodextrin derivative can be selected as modifiers for LDHs. Phytic acid is abundant in phosphorus content that can catalyze the polymer matrix to form intumescent chars, while cyclodextrin derivative with many rigid structures and large number of hydroxyl group may lead to the formation of rich char residues. Furthermore, transition metal oxides are usually used to improve the thermal resistance of char residues. It has been observed that transition metal ions promoted the char formation, leading to enhance flame retardant efficiency. Transition metals serves as a catalyst for the cross-linking of macromolecules, leading to increased char yield, and consequently suppresses the release of flammable volatile products during the combustion of polymers.

In this work, the surface of pristine LDH layers was firstly modified with Ph and hydroxypropyl-sulfobutyl-beta-cyclodextrin sodium (CDBS), and then decorated with the iron oxide nano-particles. The multi-modified iron oxide nanoparticle decorated LDH hybrid (Fe_3O_4@Ph-CDBS-LDH) was characterized by transmission electron microscopy (TEM), wide angle X-ray scattering (WAXS) and thermogravimetric analysis (TGA). Afterwards, Fe_3O_4@Ph-CDBS-LDH was incorporated into epoxy resins using a multi-stage mixing and curing process. The morphology, mechanical properties and flammability behaviors of the resultant epoxy

nanocomposites were investigated, and the flame retardant mechanism was also proposed and discussed.

6-2 Preparation of LDH/epoxy nanocomposite

LDH/epoxy nanocomposites were prepared by using fixed percentage content of nano-fillers (8 wt%). A refined three-roll mill (EXAKT 80E, Germany) was used to blend nano-fillers to the epoxy matrix for 30 min. Then, the mixture diluted with acetone and exposed to ultrasonication for 20 min and 60 °C. Then, acetone was removed by vacuuming at 110 °C to obtain a viscous blend. Subsequently, the mixture heated up to 120 °C followed by adding DDS and stirred for 15 min until DDS completely dissolved, and then immediately poured into the pre-heated PTFE moulds. The curing temperature was set up to 150 °C for 1 hour, 180 °C for 2 hours and 200 °C for 2 hours.

6-3 Charactrization

6-3-1 Structural characterization of LDH-epoxy nanocomposites

X-ray diffraction analysis

X-ray scattering patterns were utilized to characterize the morphology and structure of epoxy nanocomposite and to determine the interlayer spacing of the LDH in the polymer/LDH nanocomposite. Figure 5 shows the XRD patterns of pure EP, LDH/EP,

Ph-CDBS-LDH/EP and Fe$_3$O$_4$@Ph-CDBS-LDH/EP nanocomposites. Pure EP displays a broad and weak reflection peak centered at 2θ value of 18.0 , indicating a typical amorphous of polymer materials.
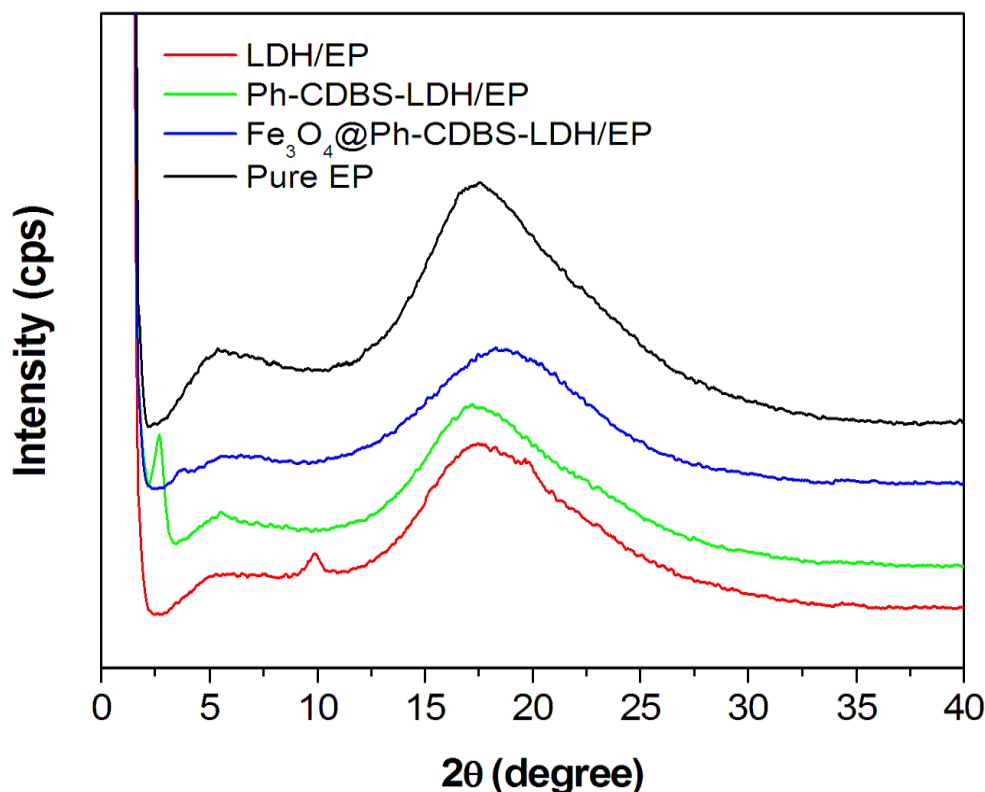
Figure 6-1: WXRD patterns of pure EP, NO$_3$-LDH/EP, Ph-CDBS-LDH/EP and Fe3O4@Ph-CDBS-LDH/EP nanocomposites.

In the case of the LDH/EP composite, there is a visible reflection peak at 2θ = 9.95 (d = 0.88 nm), suggesting the existence of the unmodified LDH agglomerates. For the Ph-CDBS-LDH/EP composite, a weak diffraction peak at 2θ value of 2.8º was observed corresponding to an inter-gallery spacing of 3.18 nm. This increment in the interlayer gallery distance compared to LDH/EP might be caused by partly swollen upon the mixing with epoxy resins. In the case of the Fe$_3$O$_4$@Ph-CDBS-LDH/EP, no visible reflection peaks were observed in the XRD pattern, implying highly

disordered and/or well intercalated LDH platelets within epoxy matrix.

Transmission electron microscopy (TEM)

TEM analysis was conducted to provide direct and perspicuous vision of the microstructures and morphology of the epoxy composites, as shown in Figure 6. It can be observed that large agglomerates with the average size of more than 500 nm exist in the LDH/EP composites (Figure 6a), demonstrating the high difficulty of destroying the ordered structure of the unmodified LDH just using mechanical shearing force.
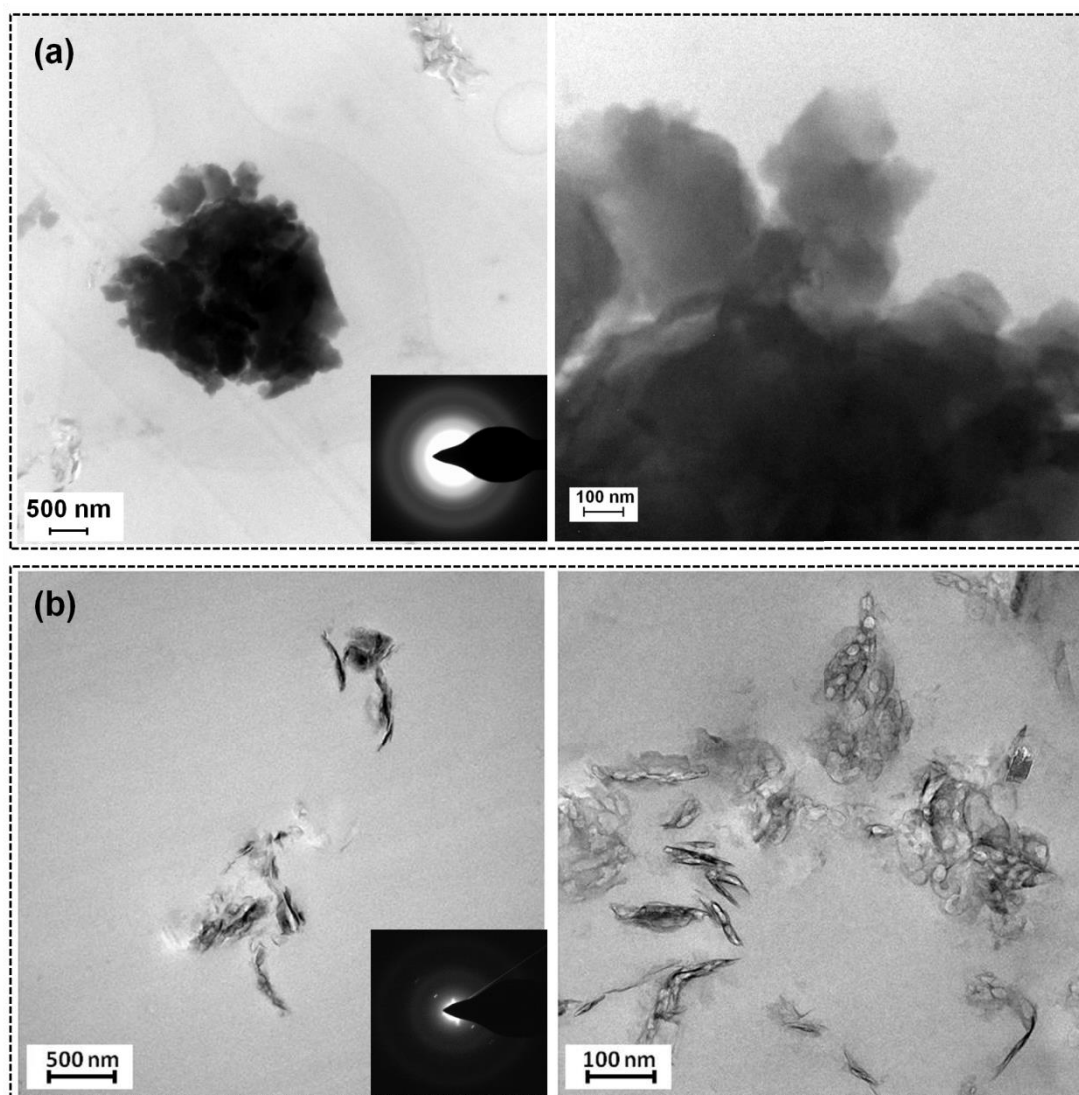
Figure 6-2: TEM images and SAED patterns of (a) NO_3-LDH/EP and (b) Ph-CDBS-LDH/Fe_3O_4/EP with high and low magnification in epoxy matrix.

In contrast, the TEM image of Fe_3O_4@Ph-CDBS-LDH/EP composites (Figure 6b) reveals a typical feature for epoxy-based nanocomposites, a simultaneous presence of intercalated LDH plates as well as small tactoids and stacks. Compared with the unmodified LDH, the Fe_3O_4@Ph-CDBS-LDH distribution in EP matrix is more disordered and the average size of the hybrids is much smaller, which is in good agreement with XRD results (Figure 6-1). The selected area electron diffraction (SAED) patterns of LDH/EP (inset of Figure 6-2a) represent the transition from the hexagonal LDH to a face-centered cubic platelet, indicating the existence of large crystalline structure. As a comparison, there are few dotes around the pointer in the SAED patterns of the Fe_3O_4@Ph-CDBS-LDH/EP composite (inset of Figure 6-2b), implying extremely small crystallites or totally disordered dispersion of the hybrids.

As a comparison, there are few dotes around the pointer in the SAED patterns of the Ph-CDBS-LDH/Fe_3O_4/EP nanocomposite, implying extremely small crystallites or totally disordered dispersion of the hybrids.

6-3-2 Thermal properties

The thermal degradation behaviors of various LDH nanoparticles and their resultant epoxy nanocomposites were studied by thermogravimetric analysis. Table 6-1 lists the main parameters of TGA, including the temperature at which the mass loss is 5% ($T_{5\%}$), the maximum mass loss temperature (T_{max}) and the residual mass percentage at

700 °C. The Ph-CDBS-LDH and Fe₃O₄@Ph-CDBS-LDH hybrid show similar thermal decomposition behavior to the NO3-LDH. However, the thermal stability of the Ph-CDBS-LDH and Fe₃O₄@Ph-CDBS-LDH hybrid is lowered in terms of reduced T5% (Table 6-1) compared to the NO_3-LDH, which is attributed to the intercalation of the thermaly instable organo-modifiers (CDBS and Ph).

Figure 6-3 presents the TGA curves of pure EP and epoxy nanocomposites under nitrogen atmosphere. Neat EP reveals a single thermal degradation stage in the temperature range from 380 to 500 °C, with the $T_{5\%}$ of 397 ºC. The incorporation of nano-fillers reduces the thermal stability compared to pure EP, accompanying with a decreased $T_{5\%}$s of epoxy nanocomposites. This reduced thermal stability can be attributed to the decomposition of modified LDH that causes the earlier initial decomposition of nanocomposites. The earlier initial decomposition of nanocomposites is beneficial to char formation so that the fire spread can be inhibited. The maximal thermal decomposition temperature (T_{max}) of epoxy nanocomposites shows a similar trend to the $T_{5\%}$, which is in good agreement with the thermal stability of nano-fillers. The char residue of epoxy resin at 700 ºC is 14.7 %, whereas NO_3-LDH/EP has 13.8% residues, demonstrating the poor thermal resistance of the char of un-modified LDH filled epoxy nanocomposites. In contrast, the Ph-CDBS-LDH/EP and Fe₃O₄@Ph-CDBS-LDH/EP nanocomposites exhibit 19.7% and 21.1% residues, respectively, both of which are higher than the calculated values. These results indicate that the modifiers play the synergistic role with LDH on the char formation of epoxy matrix.

Figure 6-3: TGA curves of pure EP and epoxy nanocomposites under N_2 at heating rate of 10°C/min.

Table 6-1: TGA data of nano-fillers, pure EP and epoxy nanocomposites

Sample	$T_{5\%}$ (°C)	T_{max} (°C)	Residue yield at 700°C (wt%)	
			Experimental	Calculated
NO_3-LDH	305	413	50.1	-
Ph-CDBS-LDH	224	338	42.3	-
Ph-CDBS-LDH/Fe_3O_4	240	400	74.4	-
EP	397	425	14.7	-
NO3-LDH/EP	386	413	13.8	17.1
Ph-CDBS-LDH/ EP	396	425	19.7	16.6
Fe3O4@Ph-CDBS-LDH/EP	365	391	21.1	19.4

6-3-3 Thermal conductivity analysis

Thermal conductivity, thermal diffusivity and specific heat conveniently measured by the Hot Disk Thermal Constants analysis system. In this study, pure EP, NO_3-LDH/EP, Ph-CDBS-LDH/EP and Ph-CDBS-LDH/Fe_3O_4/EP samples are measured and the anisotropic module was considered. During measurement, a current passes through

the Nickel spiral in order to create and increase the temperature. The heat generated

dissipates through the sample on either side at a rate dependent on the thermal

transport characteristics of the material. With the Hot Disk method, both thermal

conductivity and thermal diffusivity values are measured simultaneously. The results

for the thermal conductivity/diffusivity measurements are listed in Table 6-2. The

axial direction is the direction perpendicular to the plane of the sensor and the radial

direction is the direction in the plane of the sensor (see Scheme 6-1).

Table 6-2: Thermal analysis results of anisotropic measurements

Sample	Thermal conductivity (W/mK)	Thermal diffusivity (mm^2/s)	Specific heat (Cp) (MJ/m^{3}K)
EP	0.220	0.158	1.43
NO$_3$-LDH/EP	0.192	0.154	1.22
Ph-CDBS-LDH/EP	0.220	0.167	1.41
Fe$_3$O$_4$@Ph-CDBS-LDH /EP	0.270	0.180	1.58
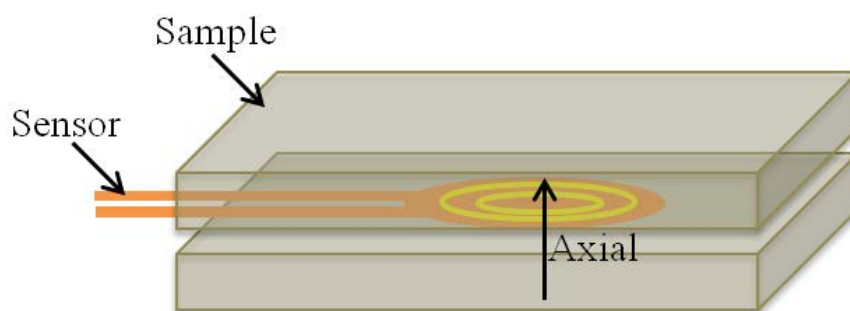
Scheme 6-1: The sample set-up for an anisotropic measurement.

From the results, it can be realized that the thermal conductivity and specific heat

capacity of Ph-CDBS-LDH/Fe$_3$O$_4$/EP are obviously increased as compare to those of

Ph-CDBS-LDH/EP and NO$_3$-LDH/EP, which might be due to the presence of the

Fe$_3$O$_4$ nano-particles and their synergy in transferring and dissipation of the heat

through the specimen.

6-3-4 Flame retardancy

Limiting oxygen index (LOI) and vertical burning test (UL-94) of the cured EP and epoxy nanocomposites were measured to examine the flame retardant properties, and the results are summarized in Table 6-3. Pure epoxy shows the LOI value of 23.0% and no classification in the UL-94 vertical burning test

Table 6-3: LOI and UL94 test results of the cured EP and epoxy nanocomposites

Sample	LOI (%)	UL-94	Observation
pure EP	23	No rating	Fire with Sooty flame
NO$_3$-LDH/EP	25.2	No rating	Fire with Sooty flame
Ph-CDBS-LDH/EP	23.5	V-2	Fire with Sooty flame
Fe3O4@Ph-CDBS-LDH /EP	26.8	V-0	Extinguished immediately

The LOI value of NO$_3$-LDH/EP nanocomposite is increased to 25.2%, but still no rating in the UL-94 test. For CDBS-Ph-LDH/EP nanocomposite, neither the improved LOI value nor the UL-94 V0 rating is observed. In contrast, the addition of Ph-CDBS-LDH/Fe$_3$O$_4$ hybrid into epoxy exhibits an obvious improvement in LOI to 26.8% and the UL-94 V0 rating is achieved in vertical burning test.

Cone calorimeter has been widely used to simulate the flammability behavior of materials in real fire accidents. Figure 6-4 shows the curves of the heat release rate (HRR) versus time of pure EP and epoxy nanocomposites. The detailed data obtained from the cone calorimeter tests is listed in Table 6-4. Pure EP is highly flammable, showing a sharp single PHRR value of 919 kW/m^2. Compared with pure EP, the PHRR value of NO$_3$-LDH/EP and Ph-CDBS-LDH/EP nanocomposite is decreased to 536 kW/m^2 and 701 kW/m^2, respectively, corresponding to a 42% and 24% reduction.

The Fe_3O_4@Ph-CDBS-LDH/EP nanocomposite shows the lowest pHRR value of 411

kW/m^2, corresponding to a striking 55% reduction in PHRR. Furthermore, the value

of time to PHRR also increases after adding nano-fillers.
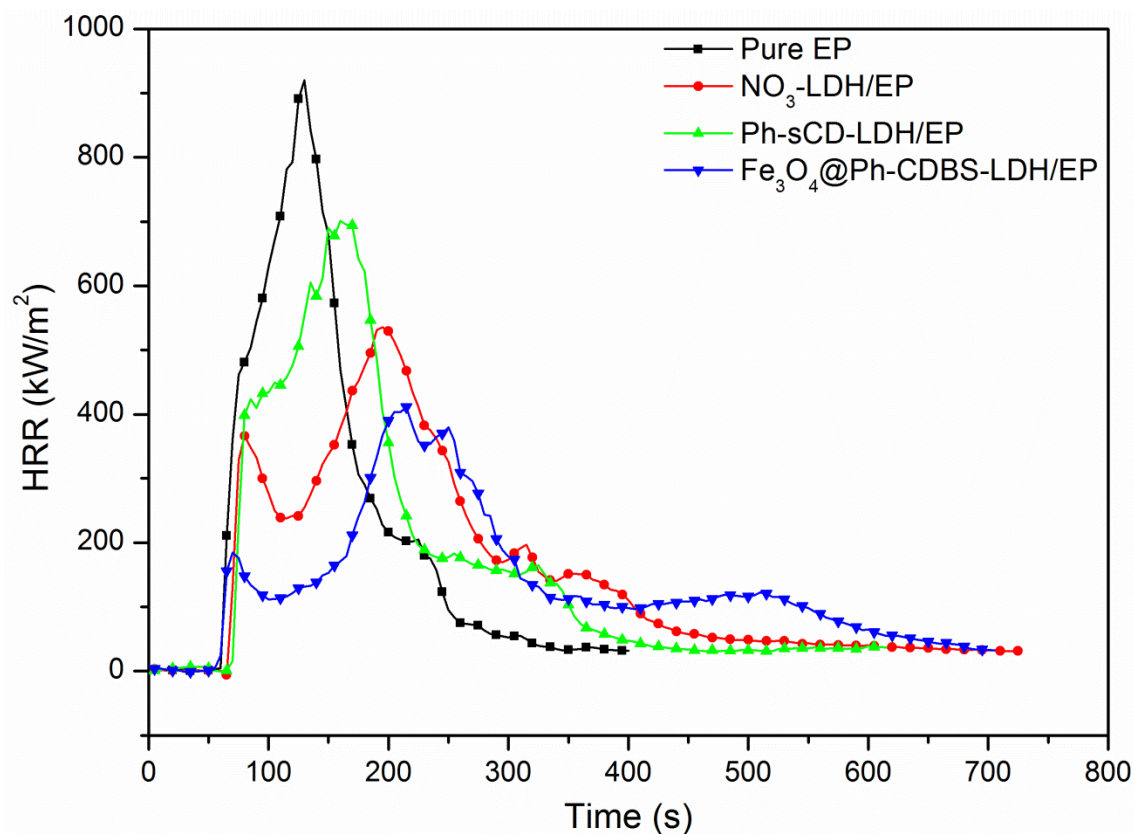
Figure 6-4: Heat release rate (HRR) curves of epoxy and its nanocomposites obtained from cone calorimeter.

The curves of the total heat release (THR) versus time of pure EP and epoxy

nanocomposites are displayed in Figure 6-5. As can be seen, the incorporation of

nano-fillers slows down the total heat release compared to pure EP. At 400 s, pure EP

releases a total heat of 90 MJ/m^2, and the NO$_3$-LDH/EP nanocomposite releases the

THR of 93 MJ/m^2, meaning that unmodified LDH just slows down the heat release

rate rather than reducing the total heat release. The Ph-CDBS-LDH/EP shows a THR

value of 97 MJ/m^2, since the organic Ph and CDBS can serve as fuels to increase the total heat release. In contrast, the Fe$_3$O$_4$@Ph-CDBS-LDH/EP just releases the total heat of 69 MJ/m^2 at 400 s, suggesting the most effective suppression in total heat release. The lower THR indicates more epoxy matrix is maintained in the condensed phase which might be due to the catalytic effect of Ph-CDBS-LDH/Fe$_3$O$_4$ hybrid, and thus the amount of organic volatiles is reduced. The increased residual mass percentage (Table 6-4) well supports the effect of Fe$_3$O$_4$@Ph-CDBS-LDH hybrid.
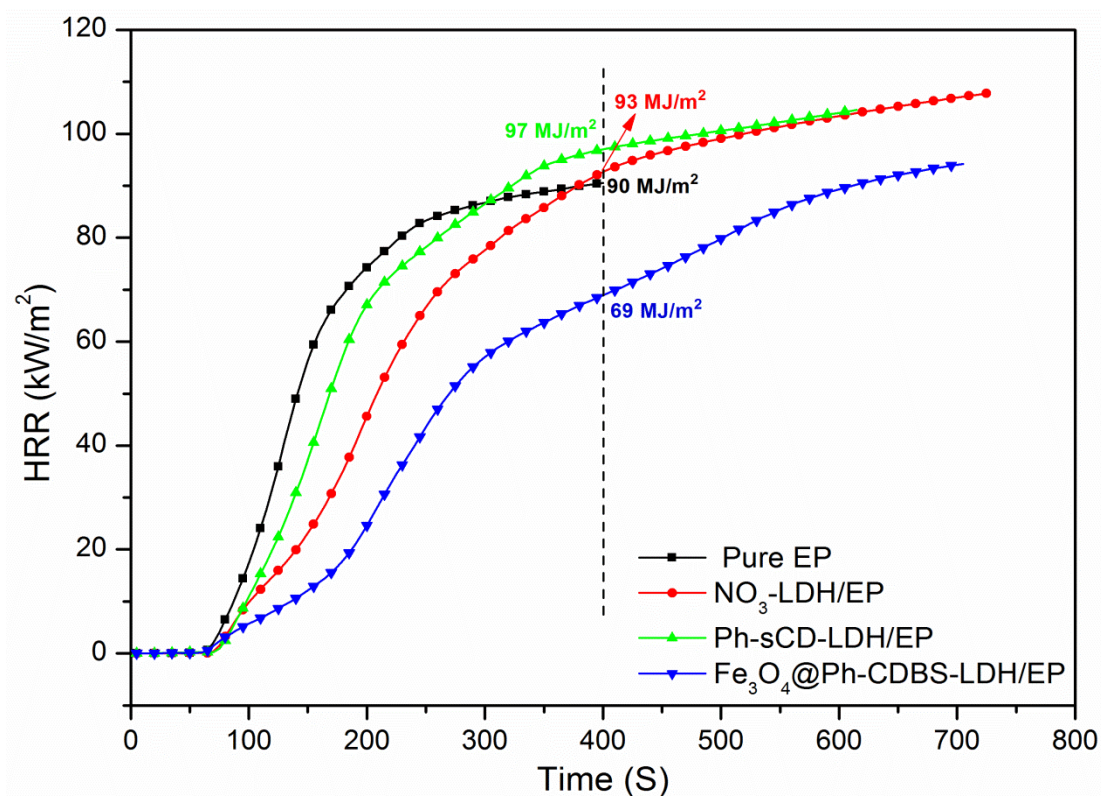
Figure 6-5: Total heat release (THR) of samples from cone calorimeter

Besides the heat hazards, the smoke production is another important aspect of the non-heat hazard of polymeric materials. Figure 6-6 gives the curves of the total smoke production (TSP) versus time of pure EP and epoxy nanocomposites. Pure EP exhibits a TSP of 27.9 m^2, and the addition of NO$_3$-LDH shows little effect on the

smoke suppression. Reversely, the incorporation of organo-modified LDH (Ph-CDBS-LDH/EP) increases the TSP. In contrast, the Fe_3O_4@Ph-CDBS-LDH/EP nanocomposite shows the lowest TSP value of 18.3 m^2. The influence of nano-fillers on the TSP displays the similar trend to that of THR. The decreased amount of the organic volatiles not only inhibits the fuel feedback to flame, but also reduces the major source of smoke particles [28].
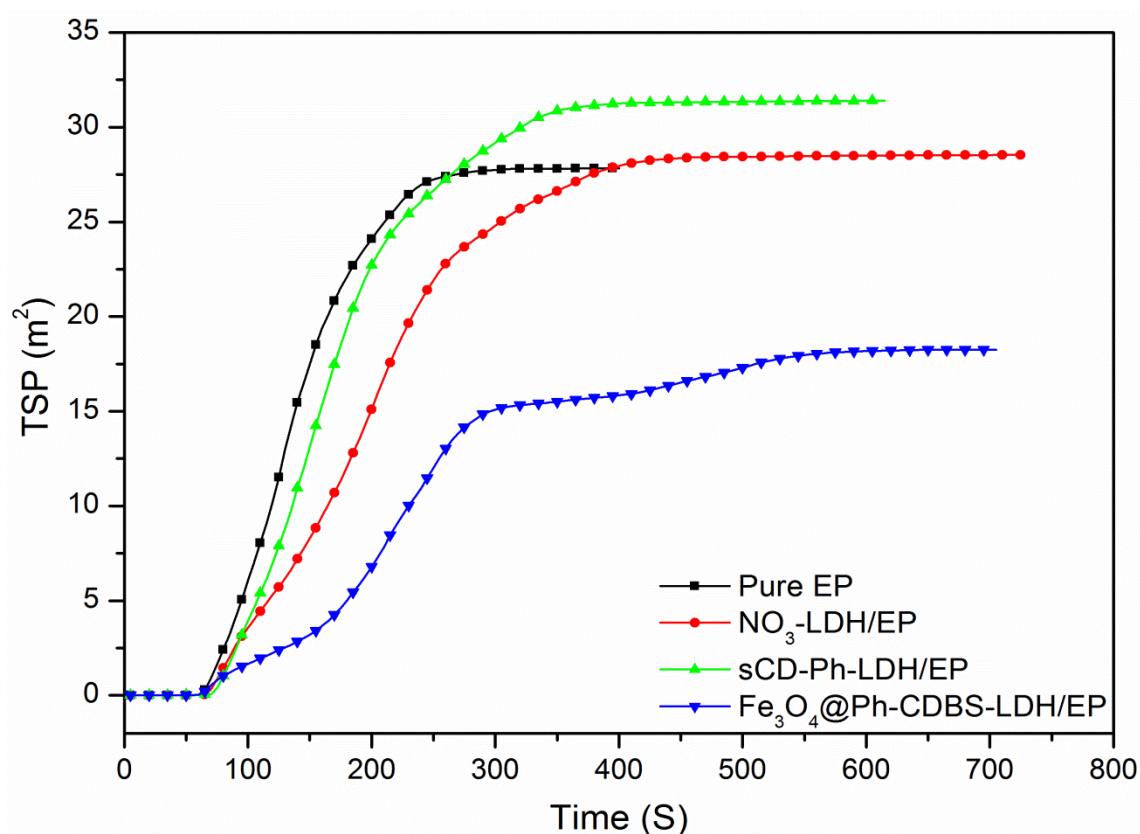
Figure 6-6: Total smoke production (TSP) of pure EP and its nanocomposites obtained from the cone calorimeter tests.

The fire growth rate index (FIGRA), which is defined as the PHRR/time to PHRR ratio, is another important derivative parameter related to fire hazard. As listed in Table 6-4, the FIGRA value of the neat EP is 7.1 $kWm^{-2}s^{-1}$, whereas that for the NO_3-LDH/EP nanocomposite is 2.7 $kWm^{-2}s^{-1}$, respectively. Compared to the

NO$_3$-LDH/EP nanocomposite, the FIGRA value of the Ph-CDBS-LDH/EP nanocomposite is increased to 4.4 kWm^{-2}s^{-1}, which is attributed to that incorporating organic CDBS and Ph species might increase the fire hazard of materials. The dramatically reduced FIGRA value (1.9 kWm^{-2}s^{-1}) is observed for the Fe$_3$O$_4$@Ph-CDBS-LDH/EP nanocomposite, meaning a high fire safety material.

Table 6-4: Combustion parameters obtained from cone calorimeter.

Sample	TTI (s)	PHRR (kW/m^2)	Time to PHRR (s)	FIGRA (kW/m^{2}s)	Residual mass (%)
EP	60	919	129	7.1	10
NO$_3$-LDH/EP	65	536	198	2.7	17
Ph-CDBS-LDH/EP	70	701	160	4.4	16
Fe3O4@Ph-CDBS-LDH /EP	60	411	216	1.9	25

The morphology and microstructure of the char residues could provide direct evidences to understand the flame retardant mechanism. SEM was employed to observe the morphology of the char residues after the cone calorimeter tests. Figure 6-7 illustrates the SEM images and the proposed flame retardant mechanism. In the case of the NO$_3$-LDH/EP nanocomposite, low char yield is obtained after burning. Moreover, a fluffy and cracked char residue was observed by SEM. In contrast, an intumescent and thick char layer was observed for the Fe$_3$O$_4$@Ph-CDBS-LDH/EP. Under high magnification, the char layer is continual and compact. Such a high quality char layer can well serve as an effective barrier that significantly reduces heat transfer and invasion of air and thus inhibit fire spread.
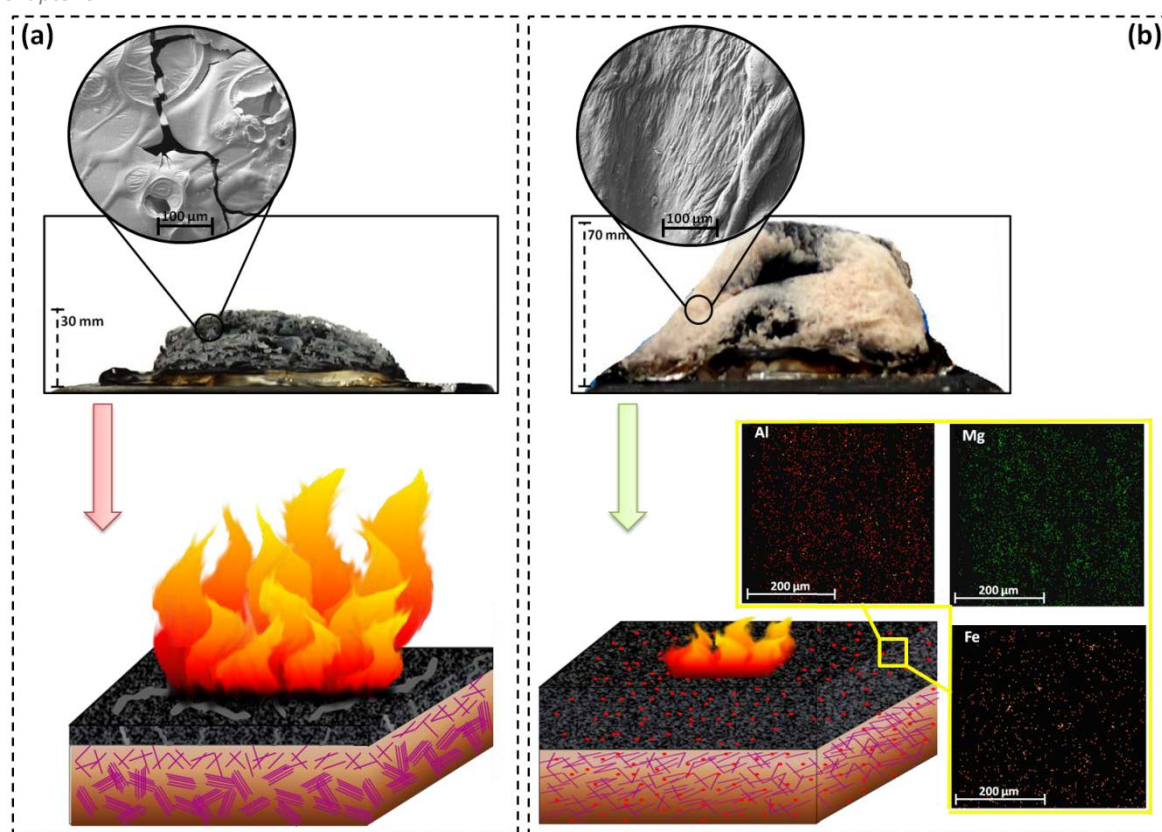
Figure 6-7: Schematic illustration of the flame retardant mechanism of (a) NO$_3$-LDH/EP and (b) Fe$_3$O$_4$@Ph-CDBS-LDH/EP.

6-3-5 Mechanical properties

Impact and tensile tests were performed on the epoxy and its nanocomposites, as summarized in Table 6-5. The results show that the addition of either unmodified LDH or Ph-CDBS-LDH reduces the impact strength of the EP-based composites compared to the control EP. In contrast, the Fe$_3$O$_4$@Ph-CDBS-LDH/EP composite does not show the obvious deterioration in the impact strength of the EP-based composites. A similar trend exhibited in the results for tensile strength and Young's modulus is that the Fe$_3$O$_4$@Ph-CDBS-LDH hybrid is superior in terms of mechanical behaviors over both the unmodified LDH and Ph-CDBS-LDH. As indicated in XRD (Figure 6-1) and TEM results (Figure 6-2a), the existence of substantial agglomeration and clustering of the unmodified LDH and Ph-CDBS-LDH within

epoxy matrix results in demolition of impact and tensile behaviors. Filler agglomeration usually leads to the reduced interfacial contact area at the filler/matrix interface and thus diminishes the ability of the LDH to reinforce the composite. Severe agglomeration can also serve as defect centers, resulting in poor compatibility between the nanoparticles and the polymer matrix, which is detrimental to mechanical properties. Regarding the $Fe_3O_4@Ph$-CDBS-LDH/EP composite, besides the better dispersion of the nanoparticles, the presence of Fe_3O_4 can also act as the physical cross-linking points through the interaction between the hydroxyl groups on the surface of Fe_3O_4 and epoxy chains, which is favorable to the tensile and impact behaviors' enhancements. The elongation at break changes little with the addition of either the unmodified LDH or the modified LDH hybrids.

Table 6-5: Data of impact and tensile tests

Sample	Impact strength (kJ/m^2)	Tensile strength (MPa)	Young's modulus (GPa)	Elongation at break (%)
EP	11.2±0.5	56.4±8.6	3.2±0.1	4.2
NO$_3$-LDH/EP	7.6±0.4	33.8±1.7	1.6±0.5	3.6
Ph-CDBS-LDH/EP	9.4±0.6	35.3±5.7	1.8±0.1	2.7
Fe3O4@Ph-CDBS-LDH /EP	10.1±0.5	61.8±7.3	2.5±0.6	3.6

6-4 Conclusions

In conclusion, we prepared a multi-functional LDH hybrid consisting of phytic acid, hydroxypropyl-sulfobutyl-beta-cyclodextrin sodium and Fe_3O_4 nano-particles. This $Fe_3O_4@Ph$-CDBS-LDH hybrid was incorporated into epoxy resins to develop multi-functional epoxy nanocomposites. It is interesting to note that the

multi-modifier system on LDH can not only improve the flame retardant and mechanical properties of EP resin, but also endow it with special functionalities, such as increased thermal conductivity. Specifically, the incorporation of 8 wt% Fe_3O_4@Ph-CDBS-LDH hybrid into epoxy resin not only reduces the PHRR, THR and TSP during combustion, but also passes the UL-94 V0 rating. These attractive performances can be attributed to the unique structure and the uniform dispersion state of the hybrids as well as the synergistic effect between LDH and multi-modifiers system.

7 Recommendation for the future work

- Layered double hydroxide (LDH) is a general name for a large variety of combination of metal hydroxides with M^{II} and M^{III} atomic configuration. This thesis was focused only on Mg-Al-LDH, but it has the potential to be extended to other types of LDHs.

- High flexibility in selection of organic species provides due to the cationic nature of the metal hydroxide layers in LDH. Organic species containing functional groups -OH, -COOH, -SO3H, -PO$_4$H, etc shows favorable anion exchange with LDH clays. Therefore, LDH can be modified with wide range of organic species. Such flexibility in selecting anionic modifiers makes LDH a suitable candidate for designing multifunctional nanohybrid fillers for polymers.

- Environmental friendliness and bio-based resources are considered as the most preferable topics in the recent years. Taking these factors into consideration can provide a great motivation to utilize metal oxides nanoparticles to decorate/anchor the LDH layers in order to obtain tailored the functionality of the final product such as thermal resistance, self-cleaning, anti-microbial, catalysts, bio-sensors, anti-UV, super capacitors etc. Also, non-chemical preparation methods such as micro-wave treatment, plasma treatment, radiation, etc, would be valuable subjects to be investigated.

- Also, in the current thesis, one type of epoxy resin which is belonging to small group of the thermosetting polymers has been used and discussed.

These aforementioned functionalized LDHs have the capability to be used in other types of thermosetting polymers as well as many different types of thermoplastics.

8 Publications

Journals:

- **Ehsan Naderi Kalali**, Xin Wang and De-Yi Wang, "Functionalized layered double hydroxide-based epoxy nanocomposites with improved flame retardancy and mechanical properties", **J. Mater. Chem. A**, 2015,3, 6819-6826

- **Ehsan Naderi Kalali**, Sergio De Juan, Xin Wang, Shibin Nie, Rui Wang, De-Yi Wang, "Comparative study on synergistic effect of LDH and zirconium phosphate with aluminum trihydroxide on flame retardancy of EVA composites", **Journal of Thermal Analysis and Calorimetry** Aug 2015, Volume 121, Issue 2, pp 619-626

- **Ehsan Naderi Kalali**, Xin Wang and De-Yi Wang, "Functional Intercalation in Layered Double Hydroxide: Toward Multifunctional Hybrid Nanomaterial for Epoxy Resin, **J. Mater. Chem. A. (Submitted)**

- Cheng Li, Jintao Wan, **Ehsan Naderi Kalali**, Hong Fan and De-Yi Wang, "Synthesis and characterization of functional eugenol derivative based layered double hydroxide and its use as a nanoflame-retardant in epoxy resin" **J. Mater. Chem. A**, 2015,**3**, 3471-3479

- **Ehsan Naderi Kalali**, Xin Wang , Anabelen Montes and De-Yi Wang, "Fe$_3$O$_4$ decorated layered double hydroxide hybride as an eco-friend and effective flame retardant for epoxy composites", **ACS Appl. Mater. Interfaces. (Submitted)**

- **Ehsan Naderi Kalali**, Xin Wang and De-Yi Wang, "Synergistic effect of intercalated layered double hydroxide on flame retardant and mechanical properties of wood-flour/polypropylene composites", **(In preparation)**

- **Ehsan Naderi Kalali**, Xin Wang , Jeremy Croyal and De-Yi Wang, "Flame-Retardant Effect of modified layered double hydroxide on an Intumescent Flame-Retardant Polypropylene System", **(In preparation)**

- **Ehsan Naderi Kalali**, Mohammad Marvi Mashhadi, Xin Wang and De-Yi Wang, "Influence of U.V. irradiation on the structural and nano-mechanical properties of functionalized layered double hydroxide-based epoxy nanocomposites", **(In preparation)**

- Xin Wang, **Ehsan Naderi Kalali** and De-Yi Wang, "In situ polymerization approach to MoS2/nylon-6 nanocomposites with enhanced mechanical properties and thermal stability", **J. Mater. Chem. A,**   DOI: 10.1039/c5ta06071k

- Xin Wang, **Ehsan Naderi Kalali** and De-Yi Wang, "Renewable cardanol-based surfactant modified layered double Hydroxide as a highly efficient flame retardant nano-additive for epoxy resins", **ACS Sustain. Chem. Eng., DOI: 10.1021/ acssuschemeng.5b00871**

- Xin Wang, **Ehsan Naderi Kalali,** Jintao Wan and De-Yi Wang, "Carbon-family materials for flame retardant polymeric materials: Current-state-of-the-art", **Submitted**

- Jintao Wan, Bin Gan, Cheng Li, Jon Molina-Aldareguia, **Ehsan Naderi Kalali**, Xin Wanga, and De-Yi Wang, "A sustainable, eugenol-derived epoxy resin with high biobased content, modulus, hardness and low flammability: Synthesis, curing kinetics and structure-property relationship", **Accepted at Chem. Eng. J.,** doi:10.1016/j.cej.2015.09.031

Conferences:

- Ehsan N. Kalali, De-Yi Wang, Multifunctional Layered double hydroxide (LDH)-based polymer nanocomposite and its properties, EUROMAT 2013, Spain, Seville 9-13 September, 2013. (Oral)

- Ehsan N. Kalali, Jeremy Croyal, De-Yi Wang, Fire retardant wood polymer composites: preparation, flammability and mechanical properties, COST FP 1404, Berlin 6-7 October, Germany, 2015. (Poster)

- Ehsan Naderi Kalali, DeYi Wang, Functionalized layered double hydroxide (LDH)-based epoxy nanocomposite and its properties, 7th Asia-Europe Symposium on Processing and Properties of Reinforced Polymers & Advances in Flame Retardancy of Polymeric Materials Workshop (AESP 7), Spain, Madrid 4-6 Febraury, 2015. (Oral)

Patent:

- De-Yi Wang, Nian-Jun Kang, Ehsan Kalali, Cheng Li, Xiao-Min Zhao, "A halogen free flame retardant polymeric composition comprising a modified layered double hydroxide Nanofiller".

Type: International Patent Application

Application/patent number: PCT 2917.4, 2013

9 References

1 Liang, J.; Huang, Y.; Zhang, L.; Wang, Y.; Ma, Y.; Guo, T.; Chen, Y. Molecular-level dispersion of graphene into poly (vinyl alcohol) and effective reinforcement of their nanocomposites. *Advanced Functional Materials* **2009**, *19*, 2297-2302.

2 Kang, N.-J.; Wang, D.-Y. A green functional nanohybrid: preparation, characterization and properties of a β-cyclodextrin based functional layered double hydroxide. *Journal of Materials Chemistry A* **2013**, *1*, 11376-11383.

3 Matusinovic, Z.; Wilkie, C. A. Fire retardancy and morphology of layered double hydroxide nanocomposites: a review. *Journal of Materials Chemistry* **2012**, *22*, 18701-18704.

4 Wang, D.-Y.; Leuteritz, A.; Kutlu, B.; der Landwehr, M. A.; Jehnichen, D.; Wagenknecht, U.; Heinrich, G. Preparation and investigation of the combustion behavior of polypropylene/organomodified MgAl-LDH micro-nanocomposite. *Journal of Alloys and Compounds* **2011**, *509*, 3497-3501.

5 Wang, D.-Y.; Das, A.; Leuteritz, A.; Boldt, R.; Häußler, L.; Wagenknecht, U.; Heinrich, G. Thermal degradation behaviors of a novel nanocomposite based on polypropylene and Co−Al layered double hydroxide. *Polymer Degradation and Stability* **2011**, 96, 285-290.

6 Wang, X.; Rathore, R.; Songtipya, P.; del Mar Jimenez-Gasco, M.; Manias, E.; Wilkie, C. A. EVA-layered double hydroxide (nano) composites: Mechanism of fire retardancy. *Polymer Degradation and Stability* **2011**, 96, 301-313.

7 Manzi-Nshuti, C.; Songtipya, P.; Manias, E.; Jimenez-Gasco, M. M.; Hossenlopp, J. M.; Wilkie, C. A. Polymer nanocomposites using zinc aluminum and magnesium aluminum oleate layered double hydroxides: effects of LDH divalent metals on dispersion, thermal, mechanical and fire performance in various polymers. *Polymer* **2009**, 50, 3564-3574.

8 Manzi-Nshuti, C.; Hossenlopp, J. M.; Wilkie, C. A. Fire retardancy of melamine and zinc aluminum layered double hydroxide in poly (methyl methacrylate). *Polymer Degradation and Stability* **2008**, 93, 1855-1863.

9 Huang, G.; Zhuo, A.; Wang, L.; Wang, X. Preparation and flammability properties of intumescent flame retardant-functionalized layered double hydroxides/polymethyl methacrylate nanocomposites. *Materials Chemistry*

and Physics **2011**, 130, 714-720.

10 Wang, L.; Su, S.; Chen, D.; Wilkie, C. A. Fire retardancy of bis [2-(methacryloyloxy) ethyl] phosphate modified poly (methyl methacrylate) nanocomposites containing layered double hydroxide and montmorillonite. *Polymer Degradation and Stability* **2009**, 94, 1110-1118.

11 Wang, X.; Hu, Y.; Song, L.; Xing, W.; Lu, H.; Lv, P.; Jie, G. Flame retardancy and thermal degradation mechanism of epoxy resin composites based on a DOPO substituted organophosphorus oligomer. *Polymer* **2010**, 51, 2435-2445.

12 Chen, Z.-K.; Yang, G.; Yang, J.-P.; Fu, S.-Y.; Ye, L.; Huang, Y.-G. Simultaneously increasing cryogenic strength, ductility and impact resistance of epoxy resins modified by n-butyl glycidyl ether. *Polymer* **2009**, 50, 1316-1323.

13 Morell, M.; Ramis, X.; Ferrando, F.; Yu, Y.; Serra, A. New improved thermosets obtained from DGEBA and a hyperbranched poly (ester-amide). *Polymer* **2009**, 50, 5374-5383.

14 Wang, X.; Xing, W.; Feng, X.; Yu, B.; Song, L.; Hu, Y. Functionalization of graphene with grafted polyphosphamide for flame retardant epoxy composites: synthesis, flammability and mechanism. *Polymer Chemistry* **2014**, 5, 1145-1154.

15 Kandola, B. K.; Horrocks, A. R.; Myler, P.; Blair, D. New developments in flame retardancy of glass-reinforced epoxy composites. *Journal of applied polymer science* **2003**, 88, 2511-2521.

16 Vogt, J. Thermal analysis of epoxy-resins: identification of decomposition products. *Thermochimica Acta* **1985**, 85, 411-414.

17. Paterson-Jones, J. The mechanism of the thermal degradation of aromatic amine-cured glycidyl ether-type epoxide resins. *Journal of applied polymer science* **1975**, 19, 1539-1547.

18 Bishop, D.; Smith, D. Combined pyrolysis and radiochemical gas chromatography for studying the thermal degradation of epoxy resins and polyimides. I. The degradation of epoxy resins in nitrogen between 400 C and 700 C. *Journal of applied polymer science* **1970**, 14, 205-223.

19 Rakotomalala, M.; Wagner, S.; Dˆring, M. Recent developments in halogen free flame retardants for epoxy resins for electrical and electronic applications. *Materials* **2010**, 3, 4300-4327.

20 Lewin, M.; Weil, E. Mechanisms and modes of action in flame retardancy of polymers. *Fire retardant materials* **2001**, 31-68.

21 Price, D.; Bullett, K.; Cunliffe, L. K.; Hull, T. R.; Milnes, G. J.; Ebdon, J. R.; Hunt, B. J.; Joseph, P. Cone calorimetry studies of polymer systems flame retarded by chemically bonded phosphorus. *Polymer Degradation and Stability* **2005**, 88, 74-79.

22 Burreau, S.; Zebühr, Y.; Broman, D.; Ishaq, R. Biomagnification of PBDEs and PCBs in food webs from the Baltic Sea and the northern Atlantic Ocean. *Science of the Total Environment* **2006**, 366, 659-672.

23 Costa, L. G.; Giordano, G. Developmental neurotoxicity of polybrominated diphenyl ether (PBDE) flame retardants. *Neurotoxicology* **2007**, 28, 1047-1067.

24 Bourbigot, S.; Le Bras, M.; Leeuwendal, R.; Shen, K. K.; Schubert, D. Recent advances in the use of zinc borates in flame retardancy of EVA. *Polymer Degradation and Stability* **1999**, 64, 419-425.

25 Lu, S.-Y.; Hamerton, I. Recent developments in the chemistry of halogen-free flame retardant polymers. *Progress in Polymer Science* **2002**, 27, 1661-1712.

26 Liu, Y. L.; Hsiue, G. H.; Chiu, Y. S. Synthesis, characterization, thermal, and flame retardant properties of phosphate-based epoxy resins. *Journal of Polymer Science Part A*: Polymer Chemistry **1997**, 35, 565-574.

27 Wang, C.-S.; Lee, M.-C. Synthesis and properties of epoxy resins containing 2-(6-oxid-6H-dibenz (c, e)(1, 2) oxaphosphorin-6-yl) 1, 4-benzenediol (II). *Polymer* **2000**, 41, 3631-3638.

28 Wang, C.-S.; Shieh, J.-Y. Synthesis and properties of epoxy resins containing 2-(6-oxid-6H-dibenz (c, e) (1,2) oxaphosphorin-6-yl) 1, 4-benzenediol. *Polymer* **1998**, 39, 5819-5826.

29 Shieh, J. Y.; Wang, C. S. Effect of the organophosphate structure on the physical and flame-retardant properties of an epoxy resin. *Journal of Polymer Science Part A: Polymer Chemistry* **2002**, 40, 369-378.

30 Lin, C.-H.; Wu, C.; Wang, C.-S. Synthesis and properties of phosphorus-containing advanced epoxy resins. II. *Journal of applied polymer science* **2000**, 78, 228-235.

31 Cai, S. X.; Lin, C. H. Flame-retardant epoxy resins with high glass-transition temperatures from a novel trifunctional curing agent: Dopotriol. *Journal of Polymer Science Part A: Polymer Chemistry* **2005**, 43, 2862-2873.

32 Lin, C. H.; Cai, S. X.; Lin, C. H. Flame-retardant epoxy resins with high glass-transition temperatures. II. Using a novel hexafunctional curing agent: 9,

10-dihydro-9-oxa-10-phosphaphenanthrene 10-yl-tris (4-aminophenyl) methane. *Journal of Polymer Science Part A: Polymer Chemistry* **2005**, 43, 5971-5986.

33 Liu, Y. L.; Wu, C. S.; Hsu, K. Y.; Chang, T. C. Flame-retardant epoxy resins from o-cresol novolac epoxy cured with a phosphorus-containing aralkyl novolac. *Journal of Polymer Science Part A: Polymer Chemistry* **2002**, 40, 2329-2339.

34 Lin, C. H. Synthesis of novel phosphorus-containing cyanate esters and their curing reaction with epoxy resin. *Polymer* **2004**, 45, 7911-7926.

35 Shau, M. D.; Wang, T. S. Syntheses, structure, reactivity, and thermal properties of new cyclic phosphine oxide epoxy resins cured by diamines. *Journal of Polymer Science Part A*: Polymer Chemistry **1996**, 34, 387-396.

36 Tchatchoua, C.; Ji, Q.; Srinivasan, S.; Ghassemi, H.; Yoon, T.; Martinez-Nunez, M.; Kashiwagi, T.; McGrath, J. Flame resistant epoxy networks based on aryl phosphine oxide containing diamines. *ACS Polymer Preprints, Division of Polymer Chememistry* **1997**, 38, 113-114.

37 Wang, T. S.; Yeh, J. F.; Shau, M. D. Syntheses, structure, reactivity, and thermal properties of epoxy–imide resin cured by phosphorylated triamine. *Journal of applied polymer science* **1996**, 59, 215-225.

38 Levchik, S.; Piotrowski, A.; Weil, E.; Yao, Q. New developments in flame retardancy of epoxy resins. *Polymer Degradation and Stability* **2005**, 88, 57-62.

39 Braun, U.; Balabanovich, A. I.; Schartel, B.; Knoll, U.; Artner, J.; Ciesielski, M.; Döring, M.; Perez, R.; Sandler, J. K.; Altstädt, V. Influence of the oxidation state of phosphorus on the decomposition and fire behaviour of flame-retarded epoxy resin composites. *Polymer* **2006**, 47, 8495-8508.

40 Bourbigot, S.; Le Bras, M.; Delobel, R.; Gengembre, L. XPS study of an intumescent coating: II. Application to the ammonium polyphosphate/pentaerythritol/ethylenic terpolymer fire retardant system with and without synergistic agent. *Applied surface science* **1997**, 120, 15-29.

41 Liu, Y.-L.; Chen, Y.-J.; Wei, W.-L. Novel thermosetting resins based on 4-(N-maleimidophenyl) glycidylether I. Preparation and characterization of monomer and cured resins. *Polymer* **2003**, 44, 6465-6473.

42 Wu, C. S.; Liu, Y. L.; Chiu, Y. S. Epoxy resins possessing flame retardant elements from silicon incorporated epoxy compounds cured with phosphorus or nitrogen containing curing agents. *Polymer* **2002**, 43, 4277-4284.

43 Gu, L.; Chen, G.; Yao, Y. Two novel phosphorus–nitrogen-containing halogen-free flame retardants of high performance for epoxy resin. *Polymer Degradation and Stability* **2014**, 108, 68-75.

44 You, G.; Cheng, Z.; Peng, H.; He, H. The synthesis and characterization of a novel phosphorus–nitrogen containing flame retardant and its application in epoxy resins. *Journal of applied polymer science* **2014**, 131, DOI: 10.1002/APP.41079.

45 Mercado, L.; Galia, M.; Reina, J. Silicon-containing flame retardant epoxy resins: Synthesis, characterization and properties. *Polymer Degradation and Stability* **2006**, 91, 2588-2594.

46 Hsiue, G.-H.; Wang, W.-J.; Chang, F.-C. Synthesis, characterization, thermal and flame-retardant properties of silicon-based epoxy resins. *Journal of applied polymer science* **1999**, 73, 1231-1238.

47 Wang, W.; Perng, L.; Hsiue, G.; Chang, F. Characterization and properties of new silicone-containing epoxy resin. *Polymer* **2000**, 41, 6113-6122.

48 Martin, C.; Lligadas, G.; Ronda, J.; Galia, M.; Cadiz, V. Synthesis of novel boron-containing epoxy–novolac resins and properties of cured products. *Journal of Polymer Science Part A: Polymer Chemistry* **2006**, 44, 6332-6344.

49 Zhou, Y.; Feng, J.; Peng, H.; Qu, H.; Hao, J. Catalytic pyrolysis and flame retardancy of epoxy resins with solid acid boron phosphate. *Polymer Degradation and Stability* **201**4, 110, 395-404.

50 Unlu, S. M.; Dogan, S. D.; Dogan, M. Comparative study of boron compounds and aluminum trihydroxide as flame retardant additives in epoxy resin. *Polymers for Advanced Technologies* **2014**, 25, 769-776.

51 Dogan, M.; Unlu, S. M. Flame retardant effect of boron compounds on red phosphorus containing epoxy resins. *Polymer Degradation and Stability* **2014**, 99, 12-17.

52 Wang, X.; Hu, Y.; Song, L.; Xuan, S.; Xing, W.; Bai, Z.; Lu, H. Flame retardancy and thermal degradation of intumescent flame retardant poly (lactic acid)/starch biocomposites. *Industrial & Engineering Chemistry Research* **2010**, 50, 713-720.

53 Gu, J.-w.; Zhang, G.-c.; Dong, S.-l.; Zhang, Q.-y.; Kong, J. Study on preparation and fire-retardant mechanism analysis of intumescent flame-retardant coatings. *Surface and coatings technology* **2007**, 201, 7835-7841.

54 Wang, J.-S.; Liu, Y.; Zhao, H.-B.; Liu, J.; Wang, D.-Y.; Song, Y.-P.; Wang, Y.-Z.

Metal compound-enhanced flame retardancy of intumescent epoxy resins containing ammonium polyphosphate. *Polymer Degradation and Stability* **2009**, 94, 625-631.

55 Yang, S.; Wang, J.; Huo, S.; Cheng, L.; Wang, M. Preparation and flame retardancy of an intumescent flame-retardant epoxy resin system constructed by multiple flame-retardant compositions containing phosphorus and nitrogen heterocycle. *Polymer Degradation and Stability* **2015**, 119, 251-259.

56 Gao, M.; Yang, S. A novel intumescent flame-retardant epoxy resins system. *Journal of applied polymer science* **2010**, 115, 2346-2351.

57 Alexandre, M.; Dubois, P. Polymer-layered silicate nanocomposites: preparation, properties and uses of a new class of materials. *Materials Science and Engineering: R: Repor*ts **2000**, 28, 1-63.

58 Wang, S.; Hu, Y.; Zong, R.; Tang, Y.; Chen, Z.; Fan, W. Preparation and characterization of flame retardant ABS/montmorillonite nanocomposite. *Applied Clay Science* **2004**, 25, 49-55.

59 Wang, D.-Y.; Wang, Y.-Z.; Wang, J.-S.; Chen, D.-Q.; Zhou, Q.; Yang, B.; Li, W.-Y. Thermal oxidative degradation behaviours of flame-retardant copolyesters containing phosphorous linked pendent group/montmorillonite nanocomposites. *Polymer Degradation and Stability* **2005**, 87, 171-176.

60 Hong, N.; Song, L.; Hu, W.; Hu, Y. Combination effect of organically modified montmorillonite and layered nickel hydroxide on the fire retardancy of poly (lactic acid). *Procedia Engineering* **2013**, 62, 366-370.

61 Hartwig, A.; Pütz, D.; Schartel, B.; Bartholmai, M.; Wendschuh-Josties, M. Combustion behaviour of epoxide based nanocomposites with ammonium and phosphonium bentonites. *Macromolecular Chemistry and Physics* **2003**, 204, 2247-2257.

62 Camino, G.; Tartaglione, G.; Frache, A.; Manferti, C.; Costa, G. Thermal and combustion behaviour of layered silicate–epoxy nanocomposites. *Polymer Degradation and Stability* **2005**, 90, 354-362.

63 Hussain, M.; Varley, R.; Mathys, Z.; Cheng, Y.; Simon, G. Effect of organo-phosphorus and nano-clay materials on the thermal and fire performance of epoxy resins. *Journal of applied polymer science* **2004**, 91, 1233-1253.

64 Zhang, W.; Li, X.; Guo, X.; Yang, R. Mechanical and thermal properties and flame retardancy of phosphorus-containing polyhedral oligomeric silsesquioxane (DOPO-POSS)/polycarbonate composites. *Polymer*

Degradation and Stability **2010**, 95, 2541-2546.

65 Fina, A.; Abbenhuis, H. C.; Tabuani, D.; Camino, G. Metal functionalized POSS as fire retardants in polypropylene. *Polymer Degradation and Stability* **2006**, 91, 2275-2281.

66 Bourbigot, S.; Turf, T.; Bellayer, S.; Duquesne, S. Polyhedral oligomeric silsesquioxane as flame retardant for thermoplastic polyurethane. *Polymer Degradation and Stability* **2009**, 94, 1230-1237.

67 Lu, T.; Liang, G.; Peng, Y.; Chen, T. Blended hybrids based on silsesquioxane–OH and epoxy resins. *Journal of applied polymer science* **2007**, 106, 4117-4123.

68 Franchini, E.; Galy, J.; Gérard, J.-F.; Tabuani, D.; Medici, A. Influence of POSS structure on the fire retardant properties of epoxy hybrid networks. *Polymer Degradation and Stability* **2009**, 94, 1728-1736.

69 Choi, J.; Kim, S. G.; Laine, R. M. Organic/inorganic hybrid epoxy nanocomposites from aminophenylsilsesquioxanes. *Macromolecules* **2004**, 37, 99-109.

70 Chiu, Y. C.; Tsai, H. C.; Imae, T. Thermal degradation analysis of the isocyanate polyhedral oligomeric silsequioxanes (POSS)/sulfone epoxy nanocomposite. *Journal of applied polymer science* **2012**, 124, 1234-1240.

71 Wang, X.; Hu, Y.; Song, L.; Xing, W.; Lu, H. Thermal degradation behaviors of epoxy resin/POSS hybrids and phosphorus–silicon synergism of flame retardancy. *Journal of Polymer Science Part B: Polymer Physics* **2010**, 48, 693-705.

72 Wu, K.; Song, L.; Hu, Y.; Lu, H.; Kandola, B. K.; Kandare, E. Synthesis and characterization of a functional polyhedral oligomeric silsesquioxane and its flame retardancy in epoxy resin. *Progress in Organic Coatings* **2009**, 65, 490-497.

73 Zhang, W.; Li, X.; Yang, R. Study on flame retardancy of TGDDM epoxy resins loaded with DOPO-POSS compound and OPS/DOPO mixture. *Polymer Degradation and Stability* **2014**, 99, 118-126.

74 Zhang, W.; Li, X.; Yang, R. Novel flame retardancy effects of DOPO-POSS on epoxy resins. *Polymer Degradation and Stability* **2011**, 96, 2167-2173.

75 Iijima, S. Helical microtubules of graphitic carbon. *nature* **1991**, 354, 56-58.

76 Rahatekar, S. S.; Zammarano, M.; Matko, S.; Koziol, K. K.; Windle, A. H.;

Nyden, M.; Kashiwagi, T.; Gilman, J. W. Effect of carbon nanotubes and montmorillonite on the flammability of epoxy nanocomposites. *Polymer Degradation and Stability* **2010**, 95, 870-879.

77 Gong, X.; Liu, J.; Baskaran, S.; Voise, R. D.; Young, J. S. Surfactant-assisted processing of carbon nanotube/polymer composites. *Chemistry of materials* **2000**, 12, 1049-1052.

78 Wang, J.; Fang, Z.; Gu, A.; Xu, L.; Liu, F. Effect of amino-functionalization of multi-walled carbon nanotubes on the dispersion with epoxy resin matrix. *Journal of applied polymer science* **2006**, 100, 97-104.

79 Kuan, C.-F.; Chen, W.-J.; Li, Y.-L.; Chen, C.-H.; Kuan, H.-C.; Chiang, C.-L. Flame retardance and thermal stability of carbon nanotube epoxy composite prepared from sol–gel method. *Journal of Physics and Chemistry of Solids* **2010**, 71, 539-543.

80 Yu, H.; Liu, J.; Wen, X.; Jiang, Z.; Wang, Y.; Wang, L.; Zheng, J.; Fu, S.; Tang, T. Charing polymer wrapped carbon nanotubes for simultaneously improving the flame retardancy and mechanical properties of epoxy resin. *Polymer* **2011**, 52, 4891-4898.

81 Lee, S. K.; Bai, B. C.; Im, J. S.; In, S. J.; Lee, Y.-S. Flame retardant epoxy complex produced by addition of montmorillonite and carbon nanotube. *Journal of Industrial and Engineering Chemistry* **2010**, 16, 891-895.

82 Ma, H.; Zhao, L.; Liu, J.; Wang, J.; Xu, J. Functionalizing carbon nanotubes by grafting cyclotriphosphazene derivative to improve both mechanical strength and flame retardancy. *Polymer Composites* **2014**, 35, 2187-2193.

83 Novoselov, K. S.; Geim, A. K.; Morozov, S.; Jiang, D.; Zhang, Y.; Dubonos, S. a.; Grigorieva, I.; Firsov, A. Electric field effect in atomically thin carbon films. *Science* **2004**, 306, 666-669.

84 Stoller, M. D.; Park, S.; Zhu, Y.; An, J.; Ruoff, R. S. Graphene-based ultracapacitors. *Nano letters* **2008**, 8, 3498-3502.

85 Lee, C.; Wei, X.; Kysar, J. W.; Hone, J. Measurement of the elastic properties and intrinsic strength of monolayer graphene. *Science* **2008**, 321, 385-388.

86 Bolotin, K. I.; Sikes, K.; Jiang, Z.; Klima, M.; Fudenberg, G.; Hone, J.; Kim, P.; Stormer, H. Ultrahigh electron mobility in suspended graphene. *Solid State Communications* **2008**, 146, 351-355.

87 Balandin, A. A.; Ghosh, S.; Bao, W.; Calizo, I.; Teweldebrhan, D.; Miao, F.; Lau, C. N. Superior thermal conductivity of single-layer graphene. *Nano letters*

2008, 8, 902-907.

88 Shi, Y.; Li, L.-J. Chemically modified graphene: flame retardant or fuel for combustion? *Journal of Materials Chemistry* **2011**, 21, 3277-3279.

89 Liu, S.; Yan, H.; Fang, Z.; Wang, H. Effect of graphene nanosheets on morphology, thermal stability and flame retardancy of epoxy resin. *Composites Science and Technology* **2014**, 90, 40-47.

90 Stankovich, S.; Piner, R. D.; Nguyen, S. T.; Ruoff, R. S. Synthesis and exfoliation of isocyanate-treated graphene oxide nanoplatelets. *Carbon* **2006**, 44, 3342-3347.

91 Liao, S.-H.; Liu, P.-L.; Hsiao, M.-C.; Teng, C.-C.; Wang, C.-A.; Ger, M.-D.; Chiang, C.-L. One-step reduction and functionalization of graphene oxide with phosphorus-based compound to produce flame-retardant epoxy nanocomposite. *Industrial & Engineering Chemistry Research* **2012**, 51, 4573-4581.

92 Li, K.-Y.; Kuan, C.-F.; Kuan, H.-C.; Chen, C.-H.; Shen, M.-Y.; Yang, J.-M.; Chiang, C.-L. Preparation and properties of novel epoxy/graphene oxide nanosheets (GON) composites functionalized with flame retardant containing phosphorus and silicon. *Materials Chemistry and Physics* **2014**, 146, 354-362.

93 Wang, X.; Xing, W.; Feng, X.; Yu, B.; Lu, H.; Song, L.; Hu, Y. The effect of metal oxide decorated graphene hybrids on the improved thermal stability and the reduced smoke toxicity in epoxy resins. *Chemical Engineering Journal* **2014**, 250, 214-221.

94 Hong, N.; Song, L.; Wang, B.; Stec, A. A.; Hull, T. R.; Zhan, J.; Hu, Y. Co-precipitation synthesis of reduced graphene oxide/NiAl-layered double hydroxide hybrid and its application in flame retarding poly (methyl methacrylate). *Materials Research Bulletin* **2014**, 49, 657-664.

95 Wang, X.; Song, L.; Yang, H.; Xing, W.; Lu, H.; Hu, Y. Cobalt oxide/graphene composite for highly efficient CO oxidation and its application in reducing the fire hazards of aliphatic polyesters. *Journal of Materials Chemistry* **2012**, 22, 3426-3431.

96 Wang, D.; Zhou, K.; Yang, W.; Xing, W.; Hu, Y.; Gong, X. Surface modification of graphene with layered molybdenum disulfide and their synergistic reinforcement on reducing fire hazards of epoxy resins. *Industrial & Engineering Chemistry Research* **2013**, 52, 17882-17890.

97 Wang, X.; Zhou, S.; Xing, W.; Yu, B.; Feng, X.; Song, L.; Hu, Y. Self-assembly of Ni–Fe layered double hydroxide/graphene hybrids for reducing fire hazard in

epoxy composites. *Journal of Materials Chemistry A* **2013**, 1, 4383-4390.

98 Dong, Y.; Gui, Z.; Hu, Y.; Wu, Y.; Jiang, S. The influence of titanate nanotube on the improved thermal properties and the smoke suppression in poly (methyl methacrylate). *Journal of hazardous materials* **2012**, 209, 34-39.

99 Kang, N.-J.; Wang, D.-Y.; Kutlu, B.; Zhao, P.-C.; Leuteritz, A.; Wagenknecht, U.; Heinrich, G. A new approach to reducing the flammability of layered double hydroxide (LDH)-based polymer composites: Preparation and characterization of dye structure-intercalated LDH and its effect on the flammability of polypropylene-grafted maleic anhydride/d-LDH composites. *ACS applied materials & interfaces* **2013**, 5, 8991-8997.

100 Camino, G.; Maffezzoli, A.; Braglia, M.; De Lazzaro, M.; Zammarano, M. Effect of hydroxides and hydroxycarbonate structure on fire retardant effectiveness and mechanical properties in ethylene-vinyl acetate copolymer. *Polymer Degradation and Stability* **2001**, 74, 457-464.

101 Zammarano, M.; Franceschi, M.; Bellayer, S.; Gilman, J. W.; Meriani, S. Preparation and flame resistance properties of revolutionary self-extinguishing epoxy nanocomposites based on layered double hydroxides. *Polymer* **2005**, 46, 9314-9328.

102 Becker, C. M.; Gabbardo, A. D.; Wypych, F.; Amico, S. C. Mechanical and flame-retardant properties of epoxy/Mg–Al LDH composites. *Composites Part A: Applied Science and Manufacturing* **2011**, 42, 196-202.

103 Becker, C. M.; Dick, T. A.; Ramos, J. T.; Wypych, F.; Amico, S. C. The Effect of the Addition of Mg-Al LDH Intercalated with Dodecyl Sulfate on the Fire Retardancy Properties of Epoxy. *Macromolecular Symposia.* **2012**: Wiley Online Library.

104 Jiang, S.-D.; Bai, Z.-M.; Tang, G.; Song, L.; Stec, A. A.; Hull, T. R.; Hu, Y.; Hu, W.-Z. Synthesis of Mesoporous Silica@ Co–Al Layered Double Hydroxide Spheres: Layer-by-Layer Method and Their Effects on the Flame Retardancy of Epoxy Resins. *ACS applied materials & interfaces* **2014**, 6, 14076-14086.

105 Nhlapo, N.; Motumi, T.; Landman, E.; Verryn, S. M.; Focke, W. W. Surfactant-assisted fatty acid intercalation of layered double hydroxides. *Journal of Materials Science* **2008**, 43, 1033-1043.

106 Iyi, N.; Ebina, Y.; Sasaki, T. Synthesis and characterization of water-swellable LDH (layered double hydroxide) hybrids containing sulfonate-type intercalant. *Journal of Materials Chemistry* **2011**, 21, 8085-8095.

107 Woo, M. A.; Kim, T. W.; Paek, M.-J.; Ha, H.-W.; Choy, J.-H.; Hwang, S.-J.

Phosphate-intercalated Ca–Fe-layered double hydroxides: crystal structure, bonding character, and release kinetics of phosphate. *Journal of solid state chemistry* **2011**, 184, 171-176.

108 Moujahid, E. M.; Besse, J. P.; Leroux, F. J. Poly(styrene sulfonate) layered double hydroxide nanocomposites. Stability and subsequent structural transformation with changes in temperature, *Journal of Material Chemistry* **2003**, 13, 258-264.

109 Woo, M. A.;, T. W. Kim, M. J. Paek, H. W. Ha, J. H. Choy, S. J. J. Hwang, Phosphate-intercalated Ca‐Fe-layered double hydroxides: Crystal structure, bonding character, and release kinetics of phosphate, *Journal of Solid State Chemistry* **2011**, 184, 171−176.

110 Akhavan, J.; Koh, E.; Waring, S.; Kronfli, E., Effect of UV and thermal radiation on polyNIMMO, *Polymer*, **2001**, 42, 7711-7718.

111 Kumar, B. G.; Singh, R. P.; Nakamura, T., Degradation of Carbon Fiber-reinforced Epoxy Composites by Ultraviolet Radiation and Condensation. *Journal of Composite Materials* **2002**, 24, 2713-2721.

112 Si, Z. K.; Zhang, Q.; Xue, M. Z.; Sheng, Q. R.; Liu, Y. G., Novel UV-sensitive bis-chalcone derivatives: synthesis and photocrosslinking properties in solution and solid PMMA film, *Research on Chemical Intermediate* **2011**, 37, 635-646.

113 Muller B W, Brauns U. Hydroxypropyl-B-cyclodextrin derivatives: influence of average degree of substitution on complexing ability and surface activity. *Journal of Pharmaceutical Science* **1986**, 75, 571-572.

114 B. Qi, Q.X. Zhang, M. Bannister, Y.-W. Mai Invertigation of the mechanical properties of DGEBA-based epoxy resin with nanoclay additives. *Composite Structure* **2006**, 75, 514–519

115 S. Lingaiah, R. Sadler, C. Ibeh, K. Shivakumar A method of visualization of inorganic nanoparticles dispersion in nanocomposites. *Composites Part B*, **2008**, 39, 196–201

116 D. Ratna, O. Becker, R. Krishnamurthy, G.P. Simon, R.J. Varley Nanocomposites based on a combination of epoxy resin, hyperbranched epoxy and a layered silicate. *Polymer*, **2003**, 44, 7449–7457

117 A.P. Mouritz, Z. Mathys, A.G. Gibson Heat release of polymer composites in fire Composites Part A, **2006**, 37, 1040–1054

118 P.B. Messersmith, E. Giannelis Synthesis and characterization of layered silicate-epoxy nanocomposites. *Chemistry of Materials*, **1994**, 6, 1719–1725

119 F. Wypych, G.A. Bubniak, M. Halma, S. Nakagaki Functionalization of single layers and nanofibers: a new strategy to produce polymer nanocomposites with optimized properties. *Journal of Colloid and Interface Science*, **2003**, 264, 203–207

120 C.M.C. Pereira, M. Herrero, F.M. Labajos, A.T. Marques, V. Rives Preparation and properties of new flame retardant unsaturated polyester nanocomposites based on layered double hydroxides. *Polymer Degradation and Stability*, **2009**, 94, 939–946

121 R.F. Costa, U. Wagenknecht, G. Heinrich LDPE/Mg‒Al layered double hydroxide nanocompósito: thermal and flammability properties. *Polymer Degradation and Stability*, **2007**, 92, 1813‒1823.

122 E. N. Kalali , X. Wang , D. Y. Wang multifunctional intercalation in layered double hydroxide: toward multifunctional nanohybrid for epoxy resin. Under review